

2

# MATERIALS FOR ADAPTIVE STRUCTURAL ACOUSTIC CONTROLS

Period February 1, 1993 to January 31, 1994

Annual Report

VOLUME IV

AD-A279 224



OFFICE OF NAVAL RESEARCH  
Contract No. N00014-92-J-1510

DTIC  
ELECTE  
MAY 17 1994  
S G D

APPROVED FOR PUBLIC RELEASE - DISTRIBUTION UNLIMITED

Reproduction in whole or in part is permitted for any purpose  
of the United States Government

918

94-14589

L. E. Cross



DTIC SOURCE UNCLASSIFIED 5

## PENNSTATE



THE MATERIALS RESEARCH LABORATORY  
UNIVERSITY PARK, PA

94 5 16 068

# REPORT DOCUMENTATION PAGE

Form Approved  
OMB No 0704-0188

Public reporting burden for this collection of information is estimated to average 1 hour per response, including the time for reviewing instructions, searching existing data sources, gathering and maintaining the data needed, and completing and reviewing the collection of information. Send comments regarding this burden estimate or any other aspect of this collection of information, including suggestions for reducing this burden, to Washington Headquarters Services, Directorate for Information Operations and Reports, 1215 Jefferson Davis Highway, Suite 1204, Arlington, VA 22202-4302, and to the Office of Management and Budget, Paperwork Reduction Project (0704-0188), Washington, DC 20503.

|                                  |                                  |   |
|----------------------------------|----------------------------------|---|
| 1. AGENCY USE ONLY (Leave blank) | 2. REPORT DATE<br><b>4/11/94</b> | 3. REPORT TYPE AND DATES COVERED<br><b>ANNUAL REPORT 02/01/93 TO 01/31/94</b> |
|----------------------------------|----------------------------------|---|

|  |                    |
|--|--------------------|
| 4. TITLE AND SUBTITLE<br><br><b>MATERIALS FOR ADAPTIVE STRUCTURAL ACOUSTIC CONTROL</b> | 5. FUNDING NUMBERS |
|--|--------------------|

|  |  |
|--|--|
| 6. AUTHOR(S)<br><br><b>L. ERIC CROSS</b> |  |
|--|--|

|  |  |
|--|--|
| 7. PERFORMING ORGANIZATION NAME(S) AND ADDRESS(ES)<br><b>MATERIALS RESEARCH LABORATORY<br/>THE PENNSYLVANIA STATE UNIVERSITY<br/>UNIVERSITY PARK, PA 16802</b> | 8. PERFORMING ORGANIZATION REPORT NUMBER |
|--|--|

|  |  |
|--|--|
| 9. SPONSORING / MONITORING AGENCY NAME(S) AND ADDRESS(ES)<br><b>OFFICE OF NAVAL RESEARCH      GERALD T. SMITH<br/>CODE 1513:NRJ                      OFFICE NAVAL RESEARCH RES. REP<br/>800 NORTH QUINCY STREET       536 SOUTH CLARK STREET, RM 286<br/>ARLINGTON, VA 22217              CHICAGO, ILLINOIS 60606-1588</b> | 10. SPONSORING / MONITORING AGENCY REPORT NUMBER |
|--|--|

11. SUPPLEMENTARY NOTES

|  |                        |
|--|------------------------|
| 12a. DISTRIBUTION / AVAILABILITY STATEMENT | 12b. DISTRIBUTION CODE |
|--|------------------------|

|  |   |               |  |            |                                     |          |                          |             |                          |                     |  |          |  |                |  |                    |  |      |                         |            |  |
|--|---|---------------|--|------------|-------------------------------------|----------|--------------------------|-------------|--------------------------|---------------------|--|----------|--|----------------|--|--------------------|--|------|-------------------------|------------|--|
| <p>13. ABSTRACT (Maximum 200 words)</p> <p style="text-align: center;"><b>SEE FOLLOWING PAGE</b></p> | <table border="1" style="width: 100%; border-collapse: collapse;"> <tr> <td colspan="2" style="padding: 2px;">Accession For</td> </tr> <tr> <td style="padding: 2px;">NTIS CRA&amp;I</td> <td style="padding: 2px; text-align: center;"><input checked="" type="checkbox"/></td> </tr> <tr> <td style="padding: 2px;">DTIC TAB</td> <td style="padding: 2px; text-align: center;"><input type="checkbox"/></td> </tr> <tr> <td style="padding: 2px;">Unannounced</td> <td style="padding: 2px; text-align: center;"><input type="checkbox"/></td> </tr> <tr> <td colspan="2" style="padding: 2px;">Justification .....</td> </tr> <tr> <td colspan="2" style="padding: 2px;">By .....</td> </tr> <tr> <td colspan="2" style="padding: 2px;">Distribution /</td> </tr> <tr> <td colspan="2" style="padding: 2px; text-align: center;">Availability Codes</td> </tr> <tr> <td style="padding: 2px; text-align: center;">Dist</td> <td style="padding: 2px; text-align: center;">Avail and/or<br/>Special</td> </tr> <tr> <td style="padding: 2px; text-align: center;"><b>A-1</b></td> <td style="padding: 2px;"></td> </tr> </table> | Accession For |  | NTIS CRA&I | <input checked="" type="checkbox"/> | DTIC TAB | <input type="checkbox"/> | Unannounced | <input type="checkbox"/> | Justification ..... |  | By ..... |  | Distribution / |  | Availability Codes |  | Dist | Avail and/or<br>Special | <b>A-1</b> |  |
| Accession For  |   |               |  |            |                                     |          |                          |             |                          |                     |  |          |  |                |  |                    |  |      |                         |            |  |
| NTIS CRA&I   | <input checked="" type="checkbox"/>   |               |  |            |                                     |          |                          |             |                          |                     |  |          |  |                |  |                    |  |      |                         |            |  |
| DTIC TAB   | <input type="checkbox"/>  |               |  |            |                                     |          |                          |             |                          |                     |  |          |  |                |  |                    |  |      |                         |            |  |
| Unannounced  | <input type="checkbox"/>  |               |  |            |                                     |          |                          |             |                          |                     |  |          |  |                |  |                    |  |      |                         |            |  |
| Justification .....  |   |               |  |            |                                     |          |                          |             |                          |                     |  |          |  |                |  |                    |  |      |                         |            |  |
| By .....   |   |               |  |            |                                     |          |                          |             |                          |                     |  |          |  |                |  |                    |  |      |                         |            |  |
| Distribution /   |   |               |  |            |                                     |          |                          |             |                          |                     |  |          |  |                |  |                    |  |      |                         |            |  |
| Availability Codes   |   |               |  |            |                                     |          |                          |             |                          |                     |  |          |  |                |  |                    |  |      |                         |            |  |
| Dist   | Avail and/or<br>Special   |               |  |            |                                     |          |                          |             |                          |                     |  |          |  |                |  |                    |  |      |                         |            |  |
| <b>A-1</b>   |   |               |  |            |                                     |          |                          |             |                          |                     |  |          |  |                |  |                    |  |      |                         |            |  |

|                   |                     |
|-------------------|---------------------|
| 14. SUBJECT TERMS | 15. NUMBER OF PAGES |
|                   | 16. PRICE CODE      |

|                                       |  |   |                            |
|---------------------------------------|--|---|----------------------------|
| 17. SECURITY CLASSIFICATION OF REPORT | 18. SECURITY CLASSIFICATION OF THIS PAGE | 19. SECURITY CLASSIFICATION OF ABSTRACT | 20. LIMITATION OF ABSTRACT |
|---------------------------------------|--|---|----------------------------|

## ABSTRACT

The research goals of this ONR sponsored University Research Initiative entitled "Materials for Adaptive Structural Acoustics Control" relate directly to the sensing and actuating material which must be integrated to function in adaptive control of acoustic structures. This report documents work in the second year of the program and for convenience the activities are grouped under the headings General Summary Papers, Materials Studies, Composite Sensors, Actuator Studies, Integration Issues, Processing Studies, and Thin Film Ferroelectrics.

The general papers cover a new comprehensive description of ferroelectric ceramics and their applications, analysis of high temperature piezoelectric sensors and the possible application of nonlinearity in enhancing the "smartness" of ceramics and composites. Scale effects on ferroics are of increasing interest and the manner in which nano-scale polar regions control the properties of relaxor ferroelectrics is again emphasized.

For material studies the detailed examination of the evolution of diffuse, then relaxor behavior in lanthanum modified lead titanate has been completed. Interest in the soft PZTs, relaxor and phase switching materials continues, with a new thrust developing towards a more complete description of domain walls and morphotropic phase boundaries in perovskites. Materials issues in the wear out and fatigue effects in polarization switching systems have been subjected to detailed evaluation and the precautions necessary to fabricate long lasting materials which will stand  $10^9$  switches without any fatigue are delineated.

Sensor studies have continued to focus on flextensional composites and have demonstrated both the very high hydrostatic sensitivity and the amplified actuation response of this configuration. Integration of sensors with the "moonie" actuators has been accomplished in individual cells. Actuator studies cover the gamut from highly reproducible micro positioning using electrostrictive compositions to high strain polarization switching shape memory ceramics capable of driving a latching relay device. Studies of the destruct mechanisms in practical MLA systems complement the earlier materials work and show the importance of internal electrodes and consequent stress concentrations for crack initiation. Integration studies have focused upon more detailed evaluation of 1:3, 2:2 and tubular 1:3 composites and upon the influence of the polymer characteristic and of face plates and edge guards upon sensing and actuation capabilities. In processing, the interest in dielectrophoretic forming of composites is continuing and assembly of interesting 1:3 composites is demonstrated. Guidelines for the transducer application of electrostrictive materials have been formulated and a useful classification scheme proposed. In fiber PZTs techniques for fabricating thin ( $30\ \mu$ ) fibers are demonstrated, the first successful technique for poling fibers is described and it is shown that properly poled fibers have electro-elastic characteristics similar to bulk material. Film papers are selected to reflect the transducer capabilities of lead titanate and of phase switching lead zirconate titanate stannate antiferroelectric compositions.

**MATERIALS FOR ADAPTIVE STRUCTURAL ACOUSTIC CONTROLS**

Period February 1, 1993 to January 31, 1994

Annual Report

**VOLUME IV**

**OFFICE OF NAVAL RESEARCH**  
Contract No. N00014-92-J-1510

**APPROVED FOR PUBLIC RELEASE -- DISTRIBUTION UNLIMITED**

Reproduction in whole or in part is permitted for any purpose  
of the United States Government

**L. E. Cross**

**PENNS**STATE



---

**THE MATERIALS RESEARCH LABORATORY**  
UNIVERSITY PARK, PA

## TABLE OF CONTENTS

|   |    |
|---|----|
| ABSTRACT .....  | 6  |
| INTRODUCTION .....  | 7  |
| 1.0 GENERAL SUMMARY PAPERS .....  | 9  |
| 2.0 MATERIALS STUDIES .....   | 10 |
| 3.0 COMPOSITE SENSOR .....  | 11 |
| 4.0 ACTUATOR STUDIES .....  | 11 |
| 5.0 INTEGRATION ISSUES .....  | 12 |
| 6.0 PROCESSING STUDIES .....  | 12 |
| 7.0 THIN FILM FERROELECTRICS .....  | 13 |
| 8.0 HONORS AND AWARDS .....   | 14 |
| 9.0 APPRENTICE PROGRAM .....  | 14 |
| 10.0 GRADUATING STUDENTS IN THE PROGRAM .....   | 15 |
| 11.0 PAPERS PUBLISHED IN REFERRED JOURNAL .....   | 15 |
| 12.0 INVITED PAPERS PRESENTED AT<br>NATIONAL AND INTERNATIONAL MEETINGS .....           | 17 |
| 13.0 INVITED PRESENTATIONS AT UNIVERSITY,<br>INDUSTRY AND GOVERNMENT LABORATORIES ..... | 20 |
| 14.0 CONTRIBUTED PAPERS AT<br>NATIONAL AND INTERNATIONAL MEETINGS .....                 | 22 |
| 15.0 BOOKS (AND SECTIONS THEREOF) .....   | 25 |

## APPENDICES

### *General Summary of Papers*

1. Turner, R. C. , P. A. Fuierer, R. E. Newnham, and T. R. **Materials for High Temperature Acoustic and Vibration Sensors: A Review.** *Applied Acoustics* 41:1-26 (1993).
2. Uchino, K. **Ferroelectric Ceramics.** *Materials Science and Technology*, Edited by R.W. Cahn, P. Haasen, E.J. Kramer, Vol. I, VCH 1994.
3. Newnham, R. E. **Smart, Very Smart and Intelligent Materials,** *MRS Bulletin XVIII(4),* 24-26 (April 1993).

### ***General Summary of Papers (continued)***

4. Newnham, R. E. Size Effects and Nonlinear Phenomena in Ferroic Ceramics. 3rd European Ceramic Society Conference, Madrid (1993).
5. Cross, L. E. Relaxor Ferroelectrics: Useful Electron Nanocomposite Structures, Proc. IUMRS, Iwakura, Tokyo (September 1993).

### ***Materials Studies***

6. Rossetti, G. A., Jr., W. Cao, and C. A. Randall. Microstructural Characterization and Diffuse Phase Transition Behavior of Lanthanum Modified Lead Titanate. *Ferroelectrics: Proceedings of IMF8, Gaithersburg, Maryland (August 1993)*.
7. Cao, W. and L. E. Cross. Distribution Function of Coexisting Phases in a Complete Solid Solution System. *J. Appl. Phys.* 73(7), 3250 (1993).
8. Cao, W. Polarization Gradient Coefficients and the Dispersion Surface of the Soft Mode in Perovskite Ferroelectrics. *J. Phys. Soc. Jpn.* 63, 827 (1994).
9. Cao, W. and L. E. Cross. Nonlinear and Nonlocal Continuum Theory on Domain Walls in Ferroelectrics. *Ferroelectrics: Proceedings of IMF8, Gaithersburg, Maryland (August 1993)*.
10. Cao, W. and C. Randall. Theory on the Fringe Patterns in the Study of Ferroelectric Domain Walls Using Electron Holography. *Solid State Comm.* 86, 435-439 (1993).
11. Zhang, Q. M., H. Wang, N. Kim, and L. E. Cross. Direct Evaluation of Domain Walls and Intrinsic Contributions to the Dielectric and Piezoelectric Constants and Their Temperature Dependence in Lead Zirconate Titanate Ceramics. *J. Appl. Phys.* 75 (1), 454 (1994).
12. Subbarao, E. C., V. Srikanth, W. Cao, and L. E. Cross. Domain Switching and Microcracking during Poling of Lead Zirconate Titanate Ceramics. *Ferroelectrics* 145, 271-281 (1993).
13. Li, S., W. Cao, R. E. Newnham, and L. E. Cross. Electromechanical Nonlinearity of Ferroelectric Ceramic and Related non 180° Domain Wall Motion. *Ferroelectrics* 139, 25-49 (1993).
14. Jiang, Q., W. Cao, and L. E. Cross. Electrical Fatigue in Lead Zirconate Titanate Ceramics. *J. Am. Ceram. Soc.* 77(1), 211-215 (1994).
15. Jiang, Q., E. C. Subbarao, and L. E. Cross. Grain Size Dependence of Electrical Fatigue Behavior in Hot Pressed PLZT Ferroelectric Ceramics. (Submitted to *Acta. Met.*)
16. Jiang, Q., E. C. Subbarao, and L. E. Cross. Effects of Composition and Temperature on electrical Fatigue of La Doped Lead Zirconate Titanate Ceramics. *J. Appl. Phys.* (in press).
17. Jiang, Q. and L. E. Cross. Effect of Porosity on Electrical Fatigue Behavior in PLZT and PZT Ceramics. *J. Mat. Sci.* 28, 4536-4543 (1993).

### **Materials Studies (continued)**

18. Jiang, Q., E. C. Subbarao, and L. E. Cross. Effects of Electrodes and Electroding Methods on Fatigue Behavior in Ferroelectric Materials. *Ferroelectrics: Proceedings of IMF8, Gaithersburg, Maryland (August 1993)*.
19. Jiang, Q., E. C. Subbarao, and L. E. Cross. Fatigue in PLZT: Acoustic Emission as a Discriminator Between Microcracking and Domain Switching. *Ferroelectrics: Proceedings of IMF8, Gaithersburg, Maryland (August 1993)*.
20. Jiang, Q., E. C. Subbarao, and L. E. Cross. Field Induced Stress Concentration and Electrical Fatigue in Ferroelectric Ceramics. *IEEE Trans. on Ultrasonic Ferroelectrics and Frequency Control* (submitted).
21. Jiang, Q., E. C. Subbarao, and L. E. Cross. Dielectric Properties of Single Grain in PLZT Ferroelectric Ceramics. *Ferroelectric Letters* (in press).
22. Li, S., A. S. Bhalla, R. E. Newnham, and L. E. Cross. Quantitative Evaluation of Extrinsic Contribution to Piezoelectric Constant  $d_{33}$  in Ferroelectric PZT Ceramics. *Materials Letters* 17, 21-26 (1993).
23. Wang, H., Q. Zhang, and L. E. Cross. A High Sensitivity Phase Sensitive  $d_{33}$  Meter for Complex Piezoelectric Constant Measurement. *Jpn. J. Appl. Phys.* 32(Pt. 2; No. 9A), L1281-83 (1993).

### **Composite Sensors**

24. Newnham, R. E., Q. C. Xu, and S. Yoshikawa. Metal-Electroactive Ceramic Composite Actuator. U.S. Patent# 5,276, 657.
25. Onitsuka, K., A. Dogan, J. A. Tressler, Q. C. Xu, S. Yoshikawa, and R. E. Newnham. Metal-Ceramic Composite Transducer--The Moonie. *Ferroelectrics: IMF8, Gaithersburg, Maryland (August 1993)*.
26. Tressler, J. F., Q. C. Xu, S. Yoshikawa, K. Uchino, and R. E. Newnham. Composite Flextensional Transducer for Sensing and Actuating. *Ferroelectrics: IMF8, Gaithersburg, Maryland (August 1993)*.
27. Newnham, R. E., A. Dogan, Q. C. Xu, K. Onitsuka, J. Tressler, and S. Yoshikawa. Flextensional "Moonie" Actuators. *IEEE 1993 Ultrasonics Symp. Proc., Baltimore, Maryland; Vol. 2, pp. 509-514 (1993)*.
28. Harshe, G., J. P. Dougherty, and R. E. Newnham. Theoretical Modeling of Multilayer Magnetolectric Composites. *Int. J. of Appl. Mag. in Mtls.* 4, 145-159 (1993).
29. Newnham, R. E. and G. R. Ruschau. Electromechanical Properties of Smart Materials. *J. Intelligent Mtls. Systems and Structures* 4, 289 (1993).
30. Onitsuka, K., A. Dogan, Q. Xu, S. Yoskikawa, and R. E. Newnham. Design Optimization for Metal-Ceramic Composite Actuator, "Moonie." *Ferroelectrics: IMF8, Gaithersburg, Maryland (August 1993)*.

### ***Actuator Studies***

31. Uchino, K. Relaxor Ferroelectric Devices. Ferroelectrics: Proceedings IMF8, Gaithersburg, Maryland (August 1993).
32. Uchino, K. Recent Development of Piezoelectric Actuators for Adaptive Structures. 3rd International Conference on Adaptive Structures (1991).
33. Furuta, A. and K. Uchino. Dynamic Observation of Crack Propagation in Piezoelectric Multilayer Actuators. J. Am. Ceram. Soc. 76(6), 1615 (1993).
34. Uchino, K. Ceramic Actuators Principles and Applications. MRS Bull. (April 1993).
35. Uchino, K. Applications of Piezoelectric Ceramics in Smart Actuator Systems. ADPA/AIAA/ASME/SPIE Cont. on Active Mtls. (1992).
36. Uchino, K. and A. Furuta. Destruction Mechanism of Multilayer Ceramic Actuators. ISAF92, South Carlonia (1992).
37. Furuta, A., K. Y. Oh, and K. Uchino. Shape Memory Ceramics and Their Application to Latching Relays. Sensors and Materials 3, 205 (1992).
38. Uchino, K. Piezoelectric Ceramics in Smart Actuators Systems. 1st European Conference on Smart Structures and Materials, Glasgow (1992).
39. Zhang, Q. M., J. Chen, and L. E. Cross. Electric Field Induced Piezoelectric Response in Ferroelectric Materials Near the Paraelectric-Ferroelectric Transition. Proceedings Ultrasonics Symposium, pp. 525 (1993).

### ***Integration Issues***

40. Zhang, Q. M., W. Cao, J. Zhao, and L. E. Cross. Piezoelectric Performance of Piezoelectric Polymer Composites with 2-2 Connectivity—A Combined Theoretical and Experimental Study. IEEE Transactions UFFC (accepted) (1993).
41. Chen, J., Q. M. Zhang, L. E. Cross, and C. M. Trottier. Modeling and Design of 1-3 Tubular Composites for Smart Transducer Applications. 1994 Proceedings International Conference on Intelligent Materials (submitted) (1994).
42. Wang, H., Zhang, and L. E. Cross. Piezoelectric Relaxation of P(VDF-TrFE) Copolymers. Ferroelectrics: IMF8, Gaithersburg, Maryland (August 1993).
43. Zhao, J., Q. M. Zhang, and W. Cao. Effects of Face Plates and Edge Strips on Hydrostatic Piezoelectric in 1-3 Composites. J. Mat. Sci. (submitted).

### ***Processing Studies***

44. Yoshikawa, S. and T. R. Shrout. Multilayer Piezoelectric Actuator Structures and Reliability. Proceedings Structural Dynamics, Materials Conference AIAA/ASM Adaptive Structures Forum, Pt. 6, 3581-3586 (1993).

### ***Processing Studies (continued)***

45. Bowen, C. P., T. R. ShROUT, R. E. Newnham, and C. Randall. Intelligent Processing of Composite Materials. *J. Intelligent and Smart Materials* (submitted) (1993).
46. ShROUT, T. R., C. A. Randall, B. P. Brodeur, and S. J. Jang. Classification of Electrostrictive Based Materials for Transducers. U.S. Japan Meeting on Dielectrics, Lahaina, Hawaii (November 1994).
47. Yoshikawa, S., U. Selvaraj, P. Moses, Q. Jiang, and T. R. ShROUT.  $\text{Pb}(\text{ZrTi})\text{O}_3$  [PZT] Fibers—Fabrication and Properties. *J. of Intelligent Material Systems and Structures* (submitted) (1994).
48. Miller, D., C. A. Randall, A. S. Bhalla, R. E. Newnham, and J. Adair. Electrorheological Properties of  $\text{BaTiO}_3$  Suspensions. *Ferroelectric Letters* 15, 141-151 (1993).
49. Randall, C. A., C. P. Bowen, T. R. ShROUT, A. S. Bhalla, and R. E. Newnham. Dielectrophoresis: A Means to Assemble Novel Electroceramic Composite Materials. *Proceedings of Electrorheological Fluids*. Feldrick, Austria (1993).

### ***Thin Film Ferroelectrics***

50. Udayakumar, K. R., S. B. Krupanidhi, K. Kushida, and L. E. Cross. Origina of Orientation in Sol-Gel-Derived Lead Titanate Films. *J. Am. Ceram. Soc.* 76, 1345 (1993).
51. Brooks, K. G., J. Chen, K. R. Udayakumar, and L. E. Cross. Electric Field Forced Phase Switching in La Modified Lead Zirconate Titanate Stannate Films. *J. Appl. Phys.* 75, 1399 (1994).
52. Sheen, J., R. Guo, A. S. Bhalla, and L. E. Cross. Measurements of Dielectric Constant and Quality Factor of  $\text{Ba}(\text{Mg}_{1/3}\text{Ta}_{2/3})\text{O}_3$  at X Band Frequencies. *Ferroelectric Letters* 16, 33 (1993).

### ***Graduating Students in the Program***

53. Rossetti, George A., Jr. PhD Thesis (Abstract), Solid State Science. Structural and Thermodynamic Investigation of the Ferroelectric Phase Transition in Lanthona-Substitued Lead Titanate. May 1993.
54. Chen, Jaiyu. PhD Thesis (Abstract), Electrical Engineering. Electrical and Electromechanical Properties of Ferroelectric Thin Films for Microelectromechanical Applications. August 1993.
55. Alberta, Edward. MS Thesis (Abstract), Solid State Science. The Dielectric, Piezoelectric and Pyroelectric Properties of Lead Zirconate-Lead Zinc Niobate-Lead Titanate Ceramics. October 1993.

# **PROCESSING STUDIES**

**APPENDIX 44**

# MULTILAYER PIEZOELECTRIC ACTUATORS-- STRUCTURES AND RELIABILITY

Shoko Yoshikawa and Thomas Shrout

Materials Research Laboratory  
The Pennsylvania State University  
University Park, PA 16802

## Abstract

Piezoelectric and electrostrictive ceramic multilayer actuators (MLAs) offer a combination of large generative force, quick response time, high volumetric efficiency, and low cost while utilizing relatively simple E-field control. A stack of ceramic disks is one form of multilayer actuator which provides a relatively reliable device, while limitations of disk thickness restrict driving voltages. Co-fired MLAs fabricated using conventional multilayer ceramic capacitor processing are essential for ultimate large scale production and low cost. Four types of internal electrode configurations for co-fired MLAs have been developed in the course of time in reference to performance and reliability. MLC type electrode configurations offer layer thicknesses less than 25  $\mu\text{m}$  and thus driving voltage of only  $\sim 20\text{V}$ , but high stresses developed as a result of inactive regions may lead to failure. Plate-through multilayer actuators eliminate internal stress concentration but introduce difficulties in controlling electrode silver migration. Consequently, MLC electrode structures with slits or gaps have been introduced to overcome the above problems, though adding complexity to the process. A new interdigital line electrode configuration offers large displacement through excitation of gaps between fine electrode lines, though reintroducing non-uniform field strength in a system. In addition to the structural differences, materials choice is an important issue for each application and improvement of reliability.

## Introduction

The realization of "Adaptive Structures with Active Materials" greatly depends on the ultimate reliability of the integral components. Among the three components, sensors, actuators, and structural matrix, the functionality of actuators is foreseen to be the limiting factor governing the life of the active structure. Of the various types of actuators, including piezoelectric ceramics, magnetostrictors, and shape memory alloys, only piezoelectric actuators offer the combination of large generative forces, sub-millisecond response time, high volumetric efficiency and low cost while utilizing relatively simple E-field control. Multilayer piezoelectric actuators offer additional performance features, i.e. semiconductor drive voltage capability and large displacements on the order of several tens of microns.

Categorically, there are two types of multilayer actuators, hereafter designated MLAs; (1) stacked-disk and (2) co-fired. Co-fired MLAs can be divided into four types based on their electrode configuration, each offering specific advantages, particularly in terms of reliability.\*

\* Reliability is defined as the probability of which an actuator will perform its specified function under a set of external conditions for a specified period of time.

Similar to multilayer ceramic capacitors (MLCs), recent strides have been made to reduce the overall cost of MLAs, utilizing established multilayer fabrication techniques and low cost internal electrodes. Since both MLCs and MLAs consist of layered ceramics with interconnected electrodes, many of the same issues determining reliability must be addressed. Specifically, electrode migration and internal stresses are of greater concern as a result of higher operating E-fields and displacements, i.e. strains, associated with actuators. In addition, actuators are required to function under high loads for large numbers of cycles, further limiting their life.

The purpose of this paper is to review fabrication and structural differences of present day MLAs and their interrelationship with performance and reliability.

## Multilayer Actuator Structure

### Stacked-Disk Actuators

With all multilayer actuator structures, the goal is to reduce the required driving voltage without sacrificing displacement. The first multilayers were fabricated simply by stacking a number of piezoelectric ceramic plates, as presented in Figure 1. Key to the performance of the actuators is the bonding interface. Uneven or excessive polymeric adhesives lead to reduced response time and poor displacement reproducibility.

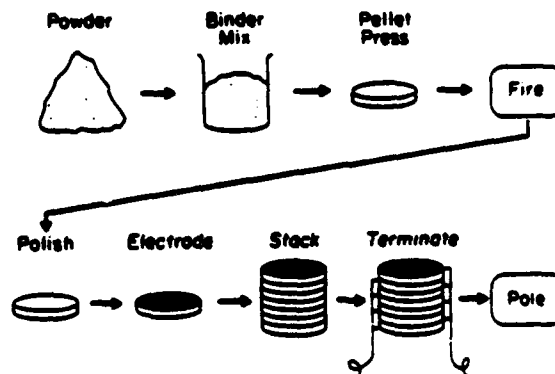


Figure 1. Processing flow chart of a stacked-disk actuator.

Generally, a pre-stress is required to provide plate-to-plate electrical and physical intimacy, insuring maximum piezoelectric strain response. The application of a compressive pre-stress offers the added advantage of enhancing mechanical integrity and hence operating life. Naturally, the pre-stress level must lie within the range of the piezoelectric's generative load line. Representative load-lines for commonly used barium titanate (BT), lead zirconate titanate (PZT) and lead magnesium niobate family (PMN-PT) are given in Figure 2. Please note that most of piezoelectric or electrostrictive ceramics have a maximum generative stress of approximately  $35 \times 10^6 \text{ N/m}^2$ .

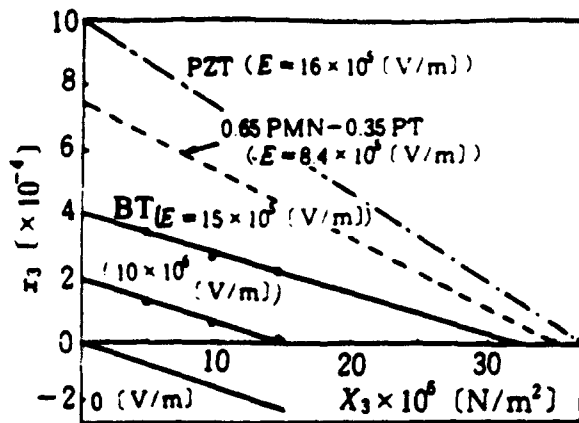


Figure 2. Stress and strain requirements for barium titanate (BT) family, lead magnesium niobate-lead titanate (PMN) family and lead zirconate titanate (PZT) family of ceramics under specific electric field (E). Note: the slope is equivalent to the elastic compliance.

The electrode structure in stacked-disk actuators is referred to as the plate-through type, which utilizes all the piezoelectric ceramic, generally in the thickness or longitudinal direction. The electrode material is commonly comprised of a thin conductive foil, requiring the ceramic surface to be polished and pre-electroded prior to stacking. Ohnishi and Morohashi found that ultra-thin ( $\sim 10 \mu\text{m}$ ) silver (Ag) foil could be bonded between the ceramic plates by the application of pressure while heating at  $900^\circ\text{C}$  to produce high performance, stacked-disk actuators.<sup>(1)</sup>

Multilayer stacked-disk actuators offer good performance and longer life relative to co-fired ones, owing to the nearly defect-free ceramics by firing each disk under optimum conditions. In addition, the post application of electrodes and plate-through design eliminates metallic diffusion and undesired stress concentration due to inactive regions, as found for co-fired actuators (to be discussed), thus reducing mechanical and electrical breakdown. Their intrinsic high reliability makes them the candidate of choice for actuators used in applications such as automobile suspension control.<sup>(2)</sup> Disadvantages associated with stacked-disk actuators are their relatively high costs owing to the number of ceramic finishing steps, difficulty in mass production, and limitations in plate thickness, typically no less than  $0.5 \text{ mm}$ , thus requiring higher ( $500 \text{ V}$  or more) driving voltages.

### Co-fired Multilayer Actuators

A flow chart for the fabrication of co-fired multilayer actuators is presented in Figure 3. Based on MLC technology, most of the steps have been automated, offering the potential of low cost and reproducibility on a large scale. Layer thicknesses for MLCs are obtainable on the level of  $\sim 10 \mu\text{m}$ , being several orders of magnitude less than that achievable for ceramic disks.

In conjunction with automation, great strides have been made to reduce the firing temperature of MLCs allowing the use of low cost internal electrodes. Fluxed BT-based dielectrics can be readily processed at temperatures below  $1100^\circ\text{C}$ . The significance of this temperature limit is the elimination of precious metal electrodes, such as

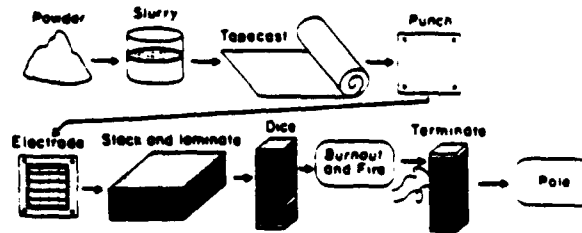


Figure 3. Processing flow chart of a co-fired multilayer actuator.

platinum (Pt) or gold (Au), while permitting the use of silver (Ag):palladium (Pd) alloys, e.g. 70Ag:30Pd.

Advantages of Ag:Pd alloys are its raised melting temperature over that of pure silver, while alloying minimizes silver migration as well as undesirable Pd oxidation reactions, all of which can lead to device failure. In contrast to BT-based ceramics, Pb-based piezoelectrics generally require higher sintering temperatures than  $1100^\circ\text{C}$ . In addition, lead can be highly reactive, forming unwanted reactions such as Pb:Pd compound formation, leading to changes in ceramic stoichiometry.<sup>(3)</sup> For these reasons, Pt electrodes are widely used, resulting in substantial cost per actuator. As with the drive for lower cost MLCs, significant advances have been made by means of sintering aids to reduce the firing temperature to below  $1100^\circ\text{C}$ , allowing the use of 70Ag:30Pd electrodes. Problems associated with the reduction of sintering temperature are underdeveloped microstructures and excessive grain boundary phases, which lead to degraded piezoelectric performance. Elimination of voids can be made by hot isostatic pressing (HIP),<sup>(4)</sup> though adding high processing cost. Poor electrode-ceramic adhesion as associated with reduced firing temperatures is also a concern. Improvements in this regard have been realized using small additions of ceramic particulates within the electrode paste.<sup>(5)</sup> Particulates of the same composition to that of the ceramic offer strong ceramic-ceramic bonding between layers while minimizing thermal expansion mismatch.

It is important to point out that only "soft" piezoelectric ceramics (DOD Type II & IV) actuators have successfully integrated low-cost Ag:Pd electrodes.

### Electrode Configurations of MLAs

Various electrode configurations have been examined in the course of MLA development. Basically, there are four types of electrode configurations currently available and/or are under investigation: (1) MLC, (2) plate-through, (3) slit or internal gap, and (4) line interdigital. The natural progression of their development will become evident, particularly in reference to reliability and performance.

#### (1) MLC Electrode Structure

As discussed above, the electrode configuration used in MLCs was the original choice put forth for MLAs. Early investigations by Bowen et al.<sup>(6)</sup> used tape cast PZT ceramics while incorporating Pt electrodes. As shown in Figure 4(A), each layer is oppositely polarized (parallel connectivity). Drawbacks of this structure are piezoelectrically inactive regions as depicted in region (a), which not only leads to clamping of the displacement, but contributes to large stress concentration at around region (c)

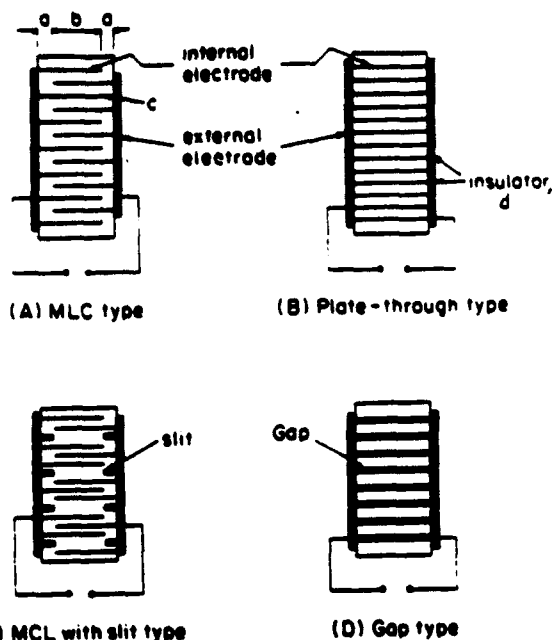


Figure 4. Cross section view of various internal electrode configurations for co-fired multilayer actuators: (A) MLC type; (B) Plate-through type; (C) MLC with slit type; and (D) MLC with gap type.

and eventual fracture. For thin layers ( $<80 \mu\text{m}$ ), however, the MLC electrode structure is still viable since it allows a simple means to electrically isolate the alternating electrodes.

The MLC electrode structure has been further improved by minimizing the inactive area by utilizing small protruding electrodes referred to as tabs on the same or close neighbor, as described in reference 7. This structure is considered as a compromise between MLC and plate-through electrode structure described in the following section.

### (2) Plate-Through Electrode Design

Based on elemental analysis of MLC-type actuators,<sup>(8)</sup> the obvious solution of using plate-through electrodes was confirmed, as presented in Figure 4(B). As shown, this design eliminates internal stress problems related to inactive regions and E-field concentration at the tip of internal electrodes (area (c) of Figure 4(A)). However, the manufacturing issue of electrically isolating alternating electrodes had to be established as evident in Figure 4(B), region (d). NEC Corporation developed<sup>(9)</sup> a method of insulation using glass passivation methods often used in IC technology allowing ultimate commercialization of MLAs for applications such as dot matrix printer heads.

Owing to the technical limits in the application of glass insulators, the layer thickness of plate-through actuators is limited to approximately  $100 \mu\text{m}$ . In addition, the exposed electrodes have to be hermetically sealed as a result of electrode breakdown due to water condensation, as well as silver migration. Insulator glass bonding on the dissimilar materials may also lead to failure. As a result, even though internal stress concentration was eliminated, new sets of problems are introduced which govern their reliability.

### (3) Slit or Internal Gap Electrode Design

To further minimize internal stresses in the conventional MLC structure, allowing both the ease of fabrication and thin-layer capability, the slit electrode design for multilayer actuators was proposed by Takahashi<sup>(10)</sup>. As presented in Figure 4(C), internal stresses due to inactive regions are relieved through the advent of slits formed via the use of a fugitive phase, typically carbon, applied during the screen printing process. The carbon is removed along with the other organic materials, binders, plasticizer, etc., during the burn-out processing step. MLAs with ceramic layer thicknesses of only  $25 \mu\text{m}$  have been reported using this method. Similar to the slit design, Kanayama et al.<sup>(11)</sup> developed an internal gap structure as presented in Figure 4(D), providing electrical isolation. Both the gap and slit structures provide performance similar to plate-through MLAs with improved reliability, particularly in ambient environments of high humidity, as a result of the elimination of exposed electrodes.

### (4) Interdigital Electrode Design

Fine line interdigital electrodes have long been used in surface acoustic wave (SAW) transducers.<sup>(12)</sup> More recently, Hirose et al.<sup>(13)</sup> investigated piezoelectric length-expansion-mode resonators incorporating interdigital electrodes while Shimizu and Yoshida explored their potential in a torsional actuator.<sup>(14)</sup> Interdigital electrodes offer ease of longitudinal excitation of long, thin piezoelectric plates.

The implementation of interdigital electrodes in MLAs arises from limitations in longitudinal displacement ( $\sim 15 \mu\text{m}$ ) for the actuators previously described. This limitation is caused by the impracticality in fabricating conventional co-fired multilayer structures with greater than 100 layers. A green ceramic sample with more than 100 layers tends to cause delaminations after firing. Though stacked MLAs can be employed, problems in response time due to adhesion and alignment are difficult to overcome. In order to achieve displacements significantly greater than  $15 \mu\text{m}$ , the transverse configuration is desired, in which relatively long structures ( $> 5 \text{cm}$ ) can be made. To achieve expansion in the transverse direction, interdigital electrodes, as schematically shown in Figure 5, offer a solution. As presented, numerous electrode lines with the same polarity are shifted one-half pitch relative to the opposing layer. Application of an electric field results in a longitudinal displacement in the transverse direction being proportional to the  $\cos\theta$ , i.e. angle between staggered electrodes, and the number of gaps between opposite polarity electrodes is the multiplier of the displacement. MLAs of this type have been fabricated up to 74 mm in length with displacements greater than  $50 \mu\text{m}$ .<sup>(15)</sup> Drawbacks of this structure include limitations in line width and internal-stresses due to non-uniform E-field as shown in a fundamental unit, Figure 6. However, reliability based on DC degradation in high temperature, high humidity tests showed superior performance over the plate-through type MLAs, both comprised of the same soft-PZT and Ag/Pd electrode.

In addition to large displacements and improved reliability, the interdigital design offers simple fabrication processing, being similar to MLC processing, thus lower cost.

A rough comparison of the above various structured MLAs are summarized in Table 1.

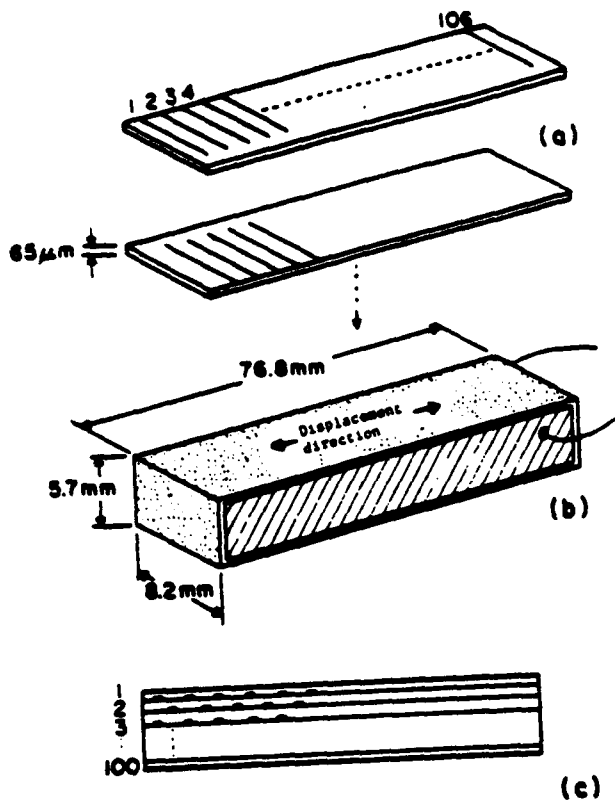


Figure 5. Schematic diagram of an interdigital line electrode actuator:  
 (a) Green sheet configuration  
 (b) Fired and electroded sample  
 (c) Section view of (b)

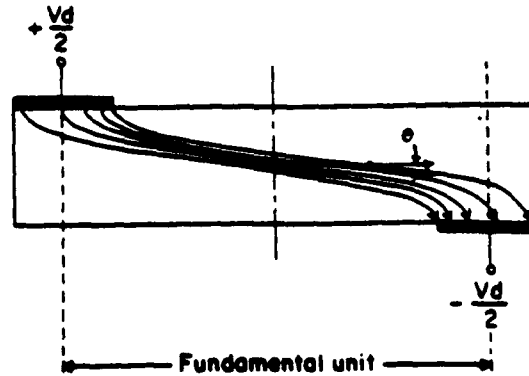


Figure 6. Cross section of fundamental unit of interdigital line electrode actuator with electric force lines.

### Materials Issues

Although Table I provides a rough comparison among various MLA structures, the complexities involved in the fabrication of various MLAs makes it difficult to accurately evaluate them in terms of reliability and performance. What is clear in the natural development of MLAs, however, is cost per performance being evident in the usage of low-cost 70Ag:30Pd electrodes and established MLC fabrication technology. However, the necessity of post-HIP processing, and soft-PZT-based ceramics as the primary materials choice leaves room for much improvement. The need for non-Ag, low-cost electrodes and ceramics with minimal strain-E-field hysteresis while providing high displacement are of particular concern.

To eliminate problems associated with Ag-based electrodes, i.e. migration, investigators are exploring the possibility of base-metal systems, including both copper (Cu) and nickel (Ni). As clearly developed for MLCs, the use of Cu and Ni internal electrodes places new constraints on the dielectric or piezoelectric in this case, whereby processing must be performed in a non-oxidizing atmosphere. Recently, Nagata et al.<sup>(16)</sup> and Kim et al.<sup>(17)</sup> have reported the development of PZT-based ceramics capable of N<sub>2</sub> atmosphere firing. However, actual MLAs with base metal electrodes have yet to be evaluated.

Table 1.

Performance Comparisons for Various Multilayer Actuators

| Electrode Configuration   | Stacked disk  | Co-fired |               |                    |                   |
|---------------------------|---------------|----------|---------------|--------------------|-------------------|
|                           | Plate-through | MLC type | Plate-through | MLC w/allts & gaps | Interdigital line |
| Max. Displacement a) (μm) | ~50           | ~10      | ~15           | ~15                | ≥50               |
| Driving Voltage           | High          | Low      | Medium        | Low                | Low               |
| Cost b)                   | High          | Low      | Moderate      | Moderate           | Low               |
| Reliability c)            | High          | Poor     | Poor          | Moderate           | Moderate          |

- a) Values reported in literatures  
 b) Assuming mass production  
 c) Assuming use of Ag:Pd internal electrode

As presented in Figure 7, the PZT-based materials widely used offer large displacements for a given E-field, but yield non-negligible hysteresis during E-field cycling. Okada et al. have demonstrated that hysteresis can be minimized through microstructural control, i.e. grain size. PZT ceramics with grain sizes  $\sim 1 \mu\text{m}$  were shown to decrease the hysteresis in half with little sacrifice in performance.<sup>(18)</sup> This improvement in microstructure should also lead to improved mechanical integrity. Along these lines, novel powder synthesis methods are being employed to produce highly reactive materials. Specifically, PZT powders prepared by hydrothermal synthesis have yielded soft and hard PZTs capable of firing temperatures less than  $1100^\circ\text{C}$  with improved performance both piezoelectrically and microstructurally.<sup>(19,20)</sup>

In terms of new materials, the use of electrostrictive based materials for MLAs such as lead magnesium niobate (PMN), which offers virtually no hysteresis while providing strains greater than 0.1%, is particularly attractive for active optical systems. Applications for the use of PMN, soft and hard PZT actuators have been summarized by Uchino.<sup>(21)</sup>

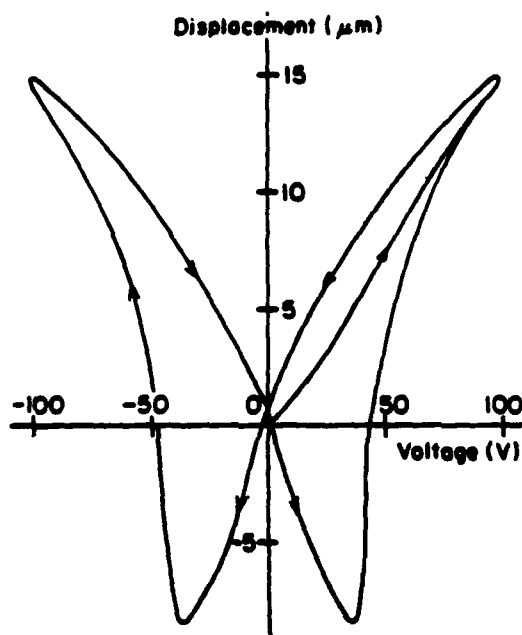


Figure 7. Displacement vs. voltage of typical co-fired MLAs using soft PZT ceramics.

An additional group of ceramics that has a large potential for several applications is field-forced antiferroelectric-to-ferroelectric switching material and shape memory ceramics. They are the stannate addition in PZT family and their modified forms. The first systematic study was in the 1960s, done by D. Berlincourt et al.<sup>(22)</sup> The studies carried out since then have shown their large strain capability (up to 0.85%) and quick switching time (less than  $1 \mu\text{s}$ )<sup>(23)</sup> in addition to some applications of these types of ceramics.<sup>(24)</sup>

## Summary

As presented above, the development of MLAs has paralleled that for MLCs. Requirements of E-fields more than  $1 \text{ kV/mm}$  and long cycling times ( $> 10^8$ ) while under high load conditions have placed performance limitations well above that required for MLCs, hence the disparity in cents vs. dollars. As the number of applications continues to grow through better understanding of structure-property relationships, the cost gap should close, making MLAs the actuators of choice.

## Acknowledgement

One of the authors (S.Y.) would like to thank Mr. T. Ohno and Mr. Y. Fuda of Tokin Corporation for their helpful discussion. This work was partially supported by ONR Grant No. N00014-92-J-1059.

## References

1. K. Ohnishi and T. Morohashi, *Jpn. J. Ceram. Soc.* 98, 895-99 (1990).
2. H. Tsuka and A. Fukami, *IEEE Workshop on Electronic Application in Transportation* (1990).
3. S.F. Wang, W. Huebner, and C.-Y. Huang, *J. Am. Ceram. Soc.* 75, 2232-39 (1992).
4. Tokin Corporation, *Multilayer Piezoelectric Actuator, Brochure 2nd ed.* (1989).
5. S. Yoshikawa, personal communication.
6. L.J. Bowen, T. ShROUT, W.A. Schulze, and J.V. Biggers, *Ferroelectrics*, 27, 59-62 (1980).
7. S.R. Winzer, N. Shankar, A.P. Ritter, *J. Am. Cer. Soc.* 72, 2246-57 (1989).
8. W. Carlson, R.E. Newnham, and L.E. Cross, *Ferroelectrics*, 88, 17-25 (1988).
9. A. Ochi, K. Ustumi, T. Mori, M. Yonezawa, J. Moroshita, and T. Yoshimoto, *Ceram. Trans.*, 8 (1990) 45-53.
10. S. Takahashi, *Ferroelectrics*, 91, 293-302 (1989).
11. K. Kanayama, H. Mase, H. Saigo and others, *Proceedings of 8th Symposium of Application of Ferroelectrics*, p. 137-8, Kyoto, Japan, May 29-31, 1991.
12. R.M. White and R.W. Voltmer, *Appl. Phys. Lett.*, 7, 314-316 (1965).
13. S. Hirose, H. Nakamura, H. Shimizu, *J. Inst. Elec. Info. Comm. Eng. J71-A*, 2093-2101 (1988) (in Japanese).
14. H. Shimizu and T. Yoshida, *5th U.S.-Japan Seminar on Dielec. Piezoelec. Ceram.*, Kyoto, Japan, Abstract III-17, p. 250-252 (1990).
15. Y. Fuda, T. Yoshida, T. Ohno, and S. Yoshikawa, *Proceeding, IEEE, International Ferroelectric Symposium on Application of Ferroelectrics*, Aug. 31-Sept. 3, 1992, Greenville, SC.

16. K. Nagata, *Jpn. J. Appl. Phys.* 30, 2224-7 (1991).
17. N. Kim, T. Shroul, and S.J. Jang, in *Annual Report on "Materials Studies for the Industrial Sensor Applications."* Sponsor, Research Institute of Industrial Science and Technology (RIST), The Pennsylvania State University (1991).
18. N. Okada, K. Ishikawa, T. Nomura, K. Murakami, S. Fukuoka, N. Nishino, and U. Kihara, *Jpn. J. Appl. Phys.* 30, 9B, 2267-2270 (1991).
19. T. Yamamoto, *Ceramic Bulletin*, 71, 978-985 (1992).
20. W. Dawson and S. Swartz. U.S. Patent # 5112433.
21. K. Uchino, *Am. Ceram. Soc. Bulln.*, 65, 647 (1986).
22. D. Berlincourt, H.H.A. Krueger, and B. Jaffe, *J. Phys. Chem. Solids*, 25, 659-674 (1964).
23. W. Pan, Q. Zhang, A. Bhalla, and L.E. Cross, *J. Am. Ceram. Soc.* 72, 571-78 (1989).
24. K. Oh, A. Furata, and K. Uchino, *Proceedings IEE 7th International Symposium on Applications of Ferroelectrics*, 525-529 (1990).

**APPENDIX 45**

# INTELLIGENT PROCESSING OF COMPOSITE MATERIALS

Christopher P. Bowen, Thomas R. ShROUT, Robert E. Newnham, Clive A. Randall

Intercollege Materials Research Laboratory  
The Pennsylvania State University  
University Park, PA, USA 16802

## ABSTRACT

Using the dielectrophoretic effect, it is possible to fabricate polymer/ceramic composite materials in which the filler phase can be manipulated to form a desired microstructure. This is performed via the application of an electric field to a colloidal suspension consisting of a filler material dispersed in a fluid polymer medium. Field induced dipole-dipole interactions cause particles to experience a mutual interaction potential resulting in distinct particle chains which align parallel to the applied electric field direction. This chained microstructure can then be "frozen in" by crosslinking the polymer matrix. The chaining phenomena is dependent on both the magnitude and the frequency of the applied field. Optimum assembly conditions for this process are determined via optical microscopy and electrorheological measurements. The dielectrophoretic assembly process also has the advantage of "in-situ" quality control through dielectric measurements. Both the degree of alignment and the batch uniformity can be confirmed via dielectric measurements. The dielectrophoretic assembly process is projected to be utilized for electrical, structural, and thermal composite applications.

**KEY WORDS :** Dielectrophoretic assembly, composite, composite processing, intelligent manufacturing.

## INTRODUCTION

Many of today's adaptive materials are based on composite systems (Newnham, 1989, 1986a, 1986b). A composite is a multiphase material which exhibits properties unattainable in any of the isolated constituent phases. The properties of composite materials are controlled through materials selection, volume fraction of filler, percolation behavior, and connectivity. For the typical case of a polymer matrix-ceramic filler composite, we introduce a novel assembly technique which allows manipulation of the ceramic filler phase during the manufacturing process. This assembly involves the induction of dipole-dipole interactions between the second

phase filler particulates under both alternating and direct current electric fields, a phenomena known as dielectrophoresis (Pohl, 1978). The result is a unidirectional alignment of the filler material in the polymer matrix.

The dielectrophoretic assembly is suited to a variety of thermoset polymers and filler materials. Optimum assembly conditions have been determined via electrorheological behavior and in-situ microscopy (Bowen et al., 1993). Dielectric property and impedance changes (suitable for quality control monitoring of the composite assembly process) are also projected to be a useful means to determine the optimum assembly conditions. The potential of this processing methodology is not yet fully realized. Target applications include electronic, structural, and thermally conductive composite materials. This paper will discuss the background, theory, and important parameters of the dielectrophoretic processing technique with emphasis on electrical composites.

## BACKGROUND

Before beginning the discussion of dielectrophoretic processing, it is useful to clarify some basic definitions and terms that will be used in the characterization this class of composite.

### Connectivity

In composite materials, there exists a classification system to describe the architecture of the component phases. This classification system is designated as the connectivity of the composite material. Connectivity is a system that describes the number of dimensions a phase in a composite material is continuous in. Newnham (1986b) developed a self-consistent nomenclature to describe the connectivity of composite materials. He showed that for a given number of components ( $n$ ), there is a finite set of connectivity patterns given by the expression:

$$\frac{(n+3)!}{3! n!} \quad (1)$$

For example, with a diphasic composite material (a matrix phase and a single filler phase),  $n = 2$ , resulting in a possible 10 connectivity patterns (Newnham, Skinner and Cross, 1978). The convention is to make the first term of the connectivity pattern description equal to the number of dimensions in which the filler is continuous while the second term refers to the number of dimensions in which the matrix is continuous. For a 0-3 connectivity, the filler phase is completely discontinuous while the matrix phase is continuous in all three directions (e.g. a well dispersed powder in a polymer matrix). This differs from a 1-3 connectivity

where the filler is continuous in one dimension and the matrix is continuous in all three dimensions (e.g. parallel rods in a polymer matrix). By carefully choosing a process to give a desired connectivity, the directional anisotropy and magnitude of properties in a composite can be precisely engineered.

### Percolation Theory

Percolation theory is the means used to explain how the properties of a composite material are altered by changing the volume fraction of the filler phase (Zallen, 1983). For simplicity in describing percolation theory, a metal powder will be considered and the composite property of conductivity will be examined. Intuitively, at low volume fractions of filler, the conductivity of the composite material will be low, approximately equal to that of the polymer matrix. A schematic of a low volume fraction composite material is given in Figure 1a. As more and more metal particles are added, they begin to crowd together and come in contact with each other until, at high volume fractions, conducting pathways exist through the polymer matrix. The conducting microstructure is shown schematically in Figure 1b. This results in a composite conductivity that is approximately equal to that of the metal filler.

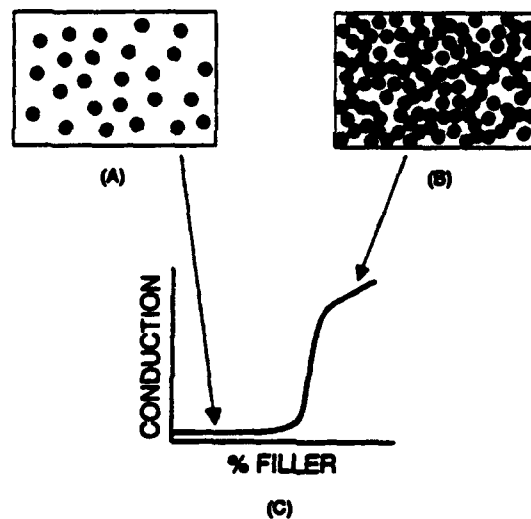


**FIGURE 1. (A) SCHEMATIC OF COMPOSITE MICROSTRUCTURE AT LOW VOLUME FRACTION FILLER. (B) SCHEMATIC OF COMPOSITE MICROSTRUCTURE AT HIGH VOLUME FRACTION FILLER. (C) SCHEMATIC OF THE PERCOLATION CURVE FOR A METAL FILLED POLYMER COMPOSITE.**

The change in conductivity as a function of increasing volume fraction metallic filler is schematically plotted in Figure 1c. The volume fraction of filler at the inflection point in the curve is defined as the percolation limit. This inflection point exists at a

volume fraction approximately equal to the tap density of the powder ( $\approx 30$  volume %) but it is also variable with particle size, size distribution, morphology, and composite thickness. By changing the volume fraction of the filler material in the composite, properties can be altered and effectively tuned to meet certain design parameters. This tuning effect is utilized in applications such as piezoresistors and both positive and negative temperature coefficient resistors (Newnham, 1989).

## **PROCESSING TECHNIQUES UTILIZED FOR COMPOSITE MATERIALS**

Because the electronics industry is driven to obtain increasingly higher volumetric efficiencies from devices, smaller filler materials must be manufactured. Fabrication of functional composites on a micron-submicron scale makes processing very difficult and is the driving force in the search for more sophisticated processing techniques. This section is intended to give a brief look at relevant processes currently utilized in the fabrication of electronic composite materials.

### **Low Connectivity Processing Techniques (0-3 Connectivity)**

One of the most common architectures in electronic composite materials is the 0-3 connectivity. This type of composite is generally used for piezoelectric transducer applications (electrical to mechanical energy conversion and vice versa) such as those used in pressure sensors. The 0-3 composite is attractive not only for its property enhancement advantages (decoupling of the transverse piezoelectric effect and acoustical impedance matching) but for its ease in processing as well.

Composites of the 0-3 type are usually fabricated through a high-shear mixing process that disperses a ceramic or metal powder uniformly into an uncured polymer matrix. Typical means of high shear mixing range from an automated, large scale mixer (such as a 3-roll mill) to laboratory scale mortar and pestle mixing. Usually, 0-3 composite materials are processed as sheets which are easily mass produced (Baker, Moore and Petroff, 1991). However, these sheets can contain large density gradients and heterogeneities due to segregation effects of incomplete mixing.

### **Electric Field Processing**

Electric fields have been used in the processing of composite materials mainly for producing specific orientations of filler materials within a polymer matrix. Electric fields can be used to orient polar crystals and fibers (via induced dipolar interactions), to deposit thin coatings (via electrophoretic effects), and to induce particulate chaining within a matrix polymer (via the dielectrophoretic effect) (Bowen et al., 1993; Tada et al., 1993; Sarkar, Haug and Nicholson, 1992).

Orientation of fibers and polar crystals into a quasi 1-3 connectivity can be accomplished through dipolar interactions with an applied electric field. When an electric field is applied to a fiber, charge on the filler surface will migrate to the region nearest the opposite charged electrode. The fiber will rotate and align its long axis parallel to the applied field direction as a result of the redistribution of charge. This phenomena is shown schematically in Figure 2.

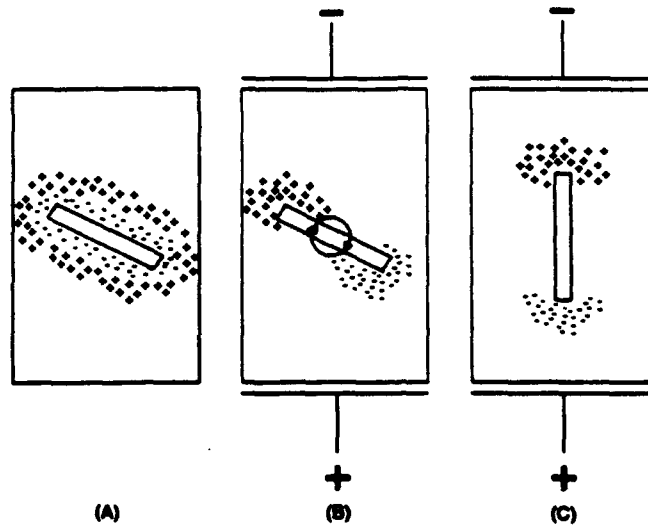


**FIGURE 2. (A) SCHEMATIC SHOWING CHARGE DOUBLE LAYER IN THE ABSENCE OF AN APPLIED ELECTRIC FIELD. (B) ON THE APPLICATION OF AN ELECTRIC FIELD, THE CHARGE WILL SEPARATE AND MIGRATE TOWARDS THE ELECTRODE OF OPPOSITE CHARGE, EFFECTIVELY FORMING A MACROSCOPIC DIPOLE. (C) AS THE CHARGE IS PULLED BY THE ELECTRODES, IT ACTS TO ROTATE THE FIBER INTO AN ORIENTATION WHERE THE CHARGES CAN BE CLOSEST TO THE ELECTRODES, I.E. ALIGNED PARALLEL TO THE APPLIED FIELD DIRECTION.**

The electrophoretic effect involves the migration of charged particles in an electric field. If a particle obtains a positive charge in a suspension and an electric field is applied, the particle will migrate toward the negatively charged electrode. In a colloidal system, a thin coating of particles can be deposited on the surface of an electrode utilizing the electrophoretic concept (Sarkar, Haung and Nicholson, 1992). By depositing alternating layers of particles (alumina and zinc, for example), laminate composite structures (2-2 connectivity) can be produced. The variables affecting electrophoretic deposition include the magnitude of the applied electric field, the surface charge on the particles (variable by altering pH when using aqueous systems), viscosity of the suspension medium, and the duration of the applied field (longer times will facilitate the deposition of a greater number of particles and hence, thicker films).

The dielectrophoretic effect can be used to induce an attractive potential between particles in a suspension resulting in a quasi 1-3 connectivity. This effect is currently being researched as an assembly technique for composite materials and will be exclusively

addressed in the remainder of this paper.

## THE DIELECTROPHORETIC EFFECT AS A COMPOSITE ASSEMBLY TECHNIQUE

While dielectrophoresis has been recognized since 1949, it was generally utilized as a separation technique by mineralogists and biologists (Pohl, 1978; Winslow, 1949). Only recently has the dielectrophoretic effect been recognized as a useful means of assembling composite materials (Randall et al., 1993). Through the mutual dielectrophoretic effect, quasi 1-3 composites can be fabricated such that the separation phenomena is suppressed, yielding a composite material with minimized structural disorder.

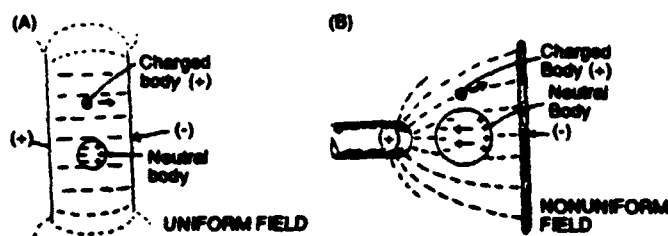


**FIGURE 3.** SCHEMATIC SHOWING THE PHENOMENA OF DIELECTROPHORESIS FOR A SINGLE PARTICLE IN SUSPENSION. FIGURE (A) SHOWS THAT A NEUTRAL BODY WILL BE SIMPLY POLARIZED IN A UNIFORM ELECTRIC FIELD AND NO TRANSLATION WILL OCCUR. FIGURE (B) SHOWS THAT, FOR THE NON-UNIFORM CASE, THE NEUTRAL PARTICLE WILL MIGRATE TO THE REGION OF HIGHER FIELD CONCENTRATION. (AFTER POHL).

### Dielectrophoretic Effect - Background Information

When a single particle suspended in a fluid medium is exposed to an electric field, two phenomena can possibly occur: (1) electrophoresis and (2) dielectrophoresis. Electrophoresis was defined earlier as the translational motion of charged matter within any electric field (uniform or non-uniform). Dielectrophoresis will be defined as translational motion of neutral matter caused by the induction of a polarization in a non-uniform electric field (Pohl, 1978). Both of these effects are shown in Figure 3. The major differences between the electrophoretic and dielectrophoretic effects are given as:

1. The dielectrophoretic effect is not dependent on the sign of the applied electric field whereas the electrophoretic effect is dependent on both the field direction and the sign of the particle charge.
2. The dielectrophoretic effect is proportional to the particle volume and, as such, is more pronounced as particle size increases. However, the electrophoretic effect is relatively independent of particle size.
3. Dielectrophoresis usually requires very divergent non-uniform electric fields for pronounced effects while electrophoresis is

observed in both uniform and non-uniform electric fields.

A special case arises when more than one particle is considered in the suspension. Consider two particles having a higher dielectric constant than the suspension medium (i.e. a higher polarizability) and in close proximity to each other. When a uniform electric field is applied to the suspension, it is perturbed in a manner consistent with that shown in Figure 4a. Hence, a non-uniform electric field is generated in the gap between the two particles. Since the particles are already polarized by the field (Figure 4b), the non-uniform perturbation acts to pull the particles together. A semi-quantitative model for the mutual agglomeration is explained in the next section.

When many particles are present in the suspension, the mutual dielectrophoretic effect acts to cause particles to attract each other and agglomerate unidirectionally to form chains parallel to the applied field direction. This is shown schematically in Figure 5. With this chained microstructure, the composite achieves percolation at a much lower volume fraction filler than the simple dispersion case. However, the percolation of properties is anisotropic, with property enhancement occurring along the chained direction.

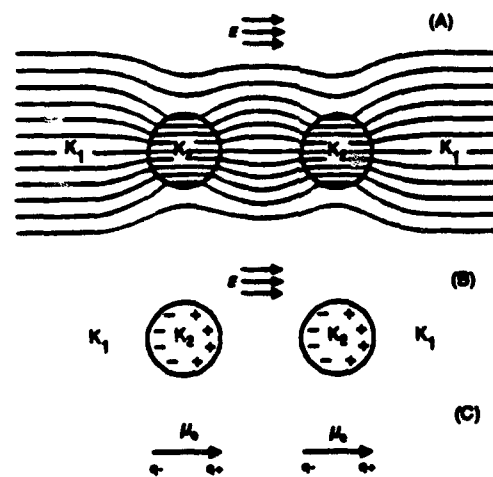


**FIGURE 4.** (A) EFFECT ON FIELD WHEN TWO PARTICLES IN A MEDIUM ARE CLOSE AND THEIR DIELECTRIC CONSTANT,  $K_2$ , EXCEEDS THAT OF THE MEDIUM,  $K_1$ . (B) EXCESS POLARIZATION PRODUCED IN TWO PARTICLES SUBJECT TO AN EXTERNAL ELECTRIC FIELD WHEN  $K_2 > K_1$ . (C) EFFECTIVE DIPOLES, SHOWING THEIR ATTRACTIVE NATURE. (AFTER POHL).

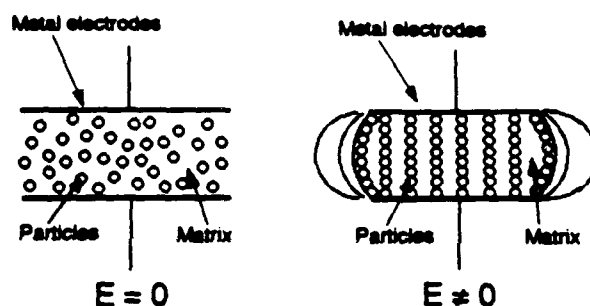


**FIGURE 5.** SCHEMATIC SHOWING THE UNIDIRECTIONAL AGGLOMERATION PHENOMENA. AT ZERO APPLIED FIELD, THE PARTICLES STAY IN A DISPERSED STATE. UPON THE APPLICATION OF AN EXTERNAL ELECTRIC FIELD, DIPOLE-DIPOLE INTERACTION CAUSES PARTICLE CHAINS PARALLEL TO THE APPLIED FIELD DIRECTION.

### Interaction Potential Theory Of Colloidal Suspensions

If a two particle suspension is considered, the interaction potential can be explained by the DLVO colloidal stability expression given as :

$$V(r) = 2\pi\epsilon_0\epsilon_f a\zeta^2 \ln(1 + \exp(-\kappa r)) - \frac{Aa}{12r} \quad (2)$$

where  $V(r)$  = Total interaction potential,  $\epsilon_0$  = Permittivity of free space,  $\epsilon_f$  = Dielectric constant of the medium,  $a$  = Spherical particle radius,  $\zeta$  = Zeta potential,  $\kappa$  = Debye reciprocal length,  $r$  = Interparticle distance and  $A$  = Hamaker constant (Reed, 1988).

The first term in Equation (2) represents a repulsive potential due to the Stern and Gouy-Chapman charge layers surrounding a particle in suspension (Figure 2 schematically shows charge layers around a fiber morphology). The second term is an attractive potential based on van der Waals forces of attraction. When typical values for particles suspended in an uncured polymeric matrix are chosen and input into Equation (2), a plot (Figure 6) showing the interaction potential curves can be generated. Figure 6 shows that there is a critical separation distance at which the two particles must overcome an energy barrier in order for agglomeration to occur.

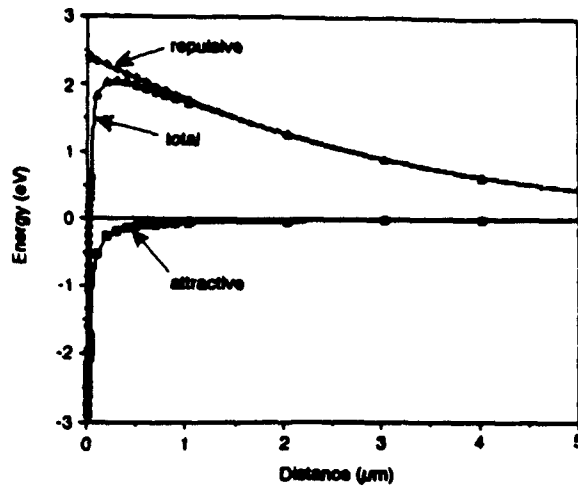


**FIGURE 6.** CALCULATED INTERACTION POTENTIAL VERSUS SEPARATION DISTANCE ACCORDING TO THE CLASSICAL COLLOIDAL STABILITY EQUATION FOR SrTiO<sub>3</sub> IN AN UNCURED POLYMER.

When the effects of an electric field applied to the suspension are considered, a third term is introduced. This term is the quadrupole solution to the Laplace Equation and is included in the interaction potential Equation to yield :

$$V(r) = 2\pi\epsilon_0\epsilon_f a^2 \zeta^2 \ln(1 + \exp(-\kappa r)) - \frac{Aa}{12r} + \frac{v(1 - 3\cos^2 \theta)}{r^3} \quad (3)$$

where:  $v = \frac{(\beta a^3 \epsilon_f E_{loc})^2}{\epsilon_f}$  and  $\beta = \frac{\epsilon_p - \epsilon_f}{\epsilon_p + 2\epsilon_f}$

where  $\theta$  = Orientation angle of particles,  $r$  = Interparticle distance,  $\beta$  = Effective polarizability,  $a$  = Particle radius,  $\epsilon_f$  = Dielectric constant of the suspending fluid,  $\epsilon_p$  = Dielectric constant of the particles, and  $E_{loc} = E_{applied}$  (Halsey, 1992). As can be seen, the Laplace term is dependent on the square of the applied electric field and on the difference between the dielectric constants of the particle and suspending medium. Hence, if the applied field is increased or if higher permittivity filler material is utilized, the attractive potential between the particles will increase.

The modified interaction potential Equation (3) can be solved and plotted for differing field conditions as found in Figure 7. As an applied electric field is increased, the barrier to agglomeration is reduced and particles at larger separation distances will experience an attractive potential. Figure 7 also shows that the equilibrium interparticle spacing varies with the magnitude of the electric field.

Utilizing this calculated dependence of the particle spacing on the magnitude of the applied field, adaptive composite materials can be produced with properties that will depend on the applied processing conditions.

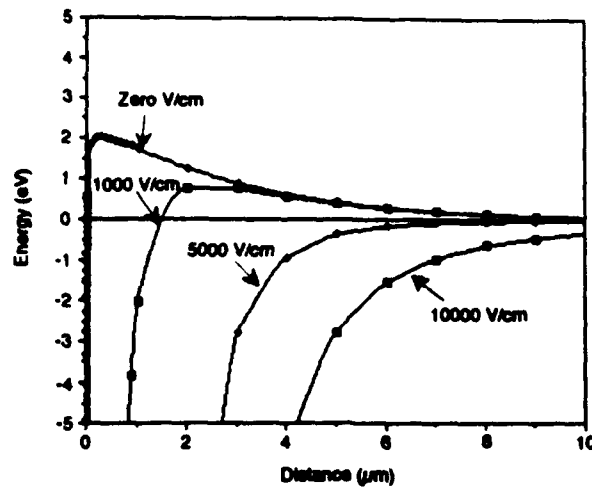


**FIGURE 7. CALCULATED INTERACTION POTENTIAL VERSUS SEPARATION DISTANCE ACCORDING TO THE MODIFIED CLASSICAL COLLOIDAL STABILITY EQUATION FOR  $\text{SrTiO}_3$  IN AN UNCURED POLYMER AT VARYING ELECTRIC FIELD INTENSITIES.**

The orientation angle dependence of Equation (3) shows why, fundamentally, the particles form distinct chains exclusively along the electric field direction. The orientation angle ( $\theta$ ) is defined as the angle formed between a vector parallel to the applied field and a vector connecting the centers of two particles in suspension (see Figure 8). The contribution to the attractive interaction potential is maximized when  $\theta = 0^\circ$ . At a critical angle of approximately  $55^\circ$ , the dipole-dipole potential switches from an attractive to a repulsive potential. Hence, particles existing at an orientation greater than  $55^\circ$  (those particles existing approximately perpendicular to the applied field) will experience a repulsive potential. The result is the formation of distinct chains parallel to the applied field direction. Figure 9 shows the interaction potential at varying orientation angles and it can be seen that an essentially infinite barrier to agglomeration exists at angles greater than  $55^\circ$  to keep particles separated in the direction perpendicular to the applied field.

#### **Materials Issues For Dielectrophoretic Assembly Of Composite Materials**

When choosing materials to fabricate composites, one must consider components that best suit the composite application. Careful considerations must be taken to control properties such as electrical and thermal conductivity, thermal stability, mechanical strength and stiffness, and piezoelectric coefficient. Through the combination of the chosen filler and matrix materials, one can achieve composite properties which are unattainable in the isolated constituent phases.

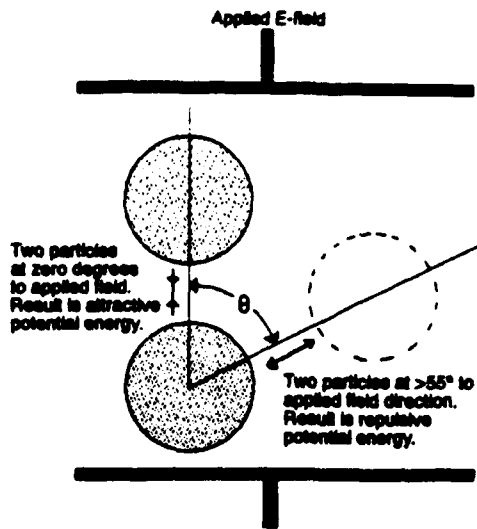


**FIGURE 8. SCHEMATIC OF THE ORIENTATIONAL RELATIONSHIP OF THE INTERACTION POTENTIAL UNDER AN APPLIED ELECTRIC FIELD. AT ANGLES GREATER THAN 55°, A REPULSIVE POTENTIAL EXISTS WHICH AIDS IN THE FORMATION OF THE DISTINCT CHAINED MICROSTRUCTURE.**

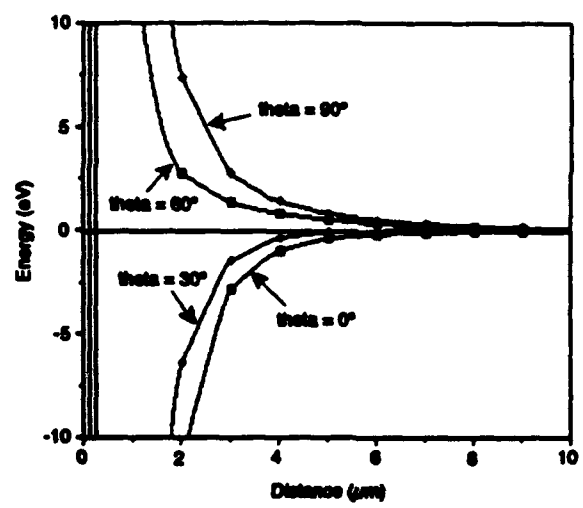


**FIGURE 9. CALCULATED INTERACTION POTENTIAL VERSUS SEPARATION DISTANCE ACCORDING TO THE MODIFIED CLASSICAL COLLOIDAL STABILITY EQUATION FOR  $\text{SiTiO}_3$  IN AN UNCURED POLYMER AT VARYING ORIENTATIONS. THERE IS AN ENORMOUS BARRIER TO AGGLOMERATION FOR THE 60° AND 90° ORIENTATION ANGLES. THIS CAN ESSENTIALLY BE CONSIDERED AS AN INFINITE BARRIER TO AGGLOMERATION RESULTING IN AN EQUILIBRIUM SEPARATION OF PARTICLES PERPENDICULAR TO THE APPLIED FIELD. HENCE, A NUMBER OF PARALLEL CHAINS FORM.**

## Matrix Materials

There are several general requirements necessary for the matrix materials in the dielectrophoretic assembly of composites. The first requirement is that the matrix must be an insulating material of low dielectric constant that can easily transform from a liquid-like to a solid state (crosslinked or vitrified). The liquid-like state is necessary to suspend and align particles while the solid state is required to "freeze in" the oriented structure to produce a useful device. The matrix must be insulating in order to allow the generation of a polarization field (driving force for the chaining phenomena) and the dielectric constant is desired to be low so the attractive interaction potential between particles (recall  $\beta$  in Equation (3)) is maximized. The second requirement is that the polymer matrix should have a high breakdown strength in the uncured state. This will reduce the chance of electric breakdown inhibition of the curing process. Thirdly, the viscosity of the uncured polymer matrix must be such that it is low enough to allow dielectrophoretic migration of particles into the chained microstructure but high enough to prohibit settling of the particles due to gravitational forces. Finally, the matrix should crosslink rapidly and easily to allow for a rapid production rate and lower production costs.

The matrix materials utilized thus far are shown in Table 1. All of these polymers have supported dielectrophoretic assembly. A special note about the Norland optical adhesive (a UV curing polymer) is that it is limited to low volume fractions of filler material ( $\approx 0.05$ ) and small thicknesses due to scattering conditions accompanying these two variables. If the volume fraction filler is too high for the desired thickness, the UV light necessary to cure the polymer will be scattered at the surfaces and will not be able to penetrate and cure the center of the composite sample. Hence, the UV transmission of the composite must be accounted for when utilizing UV curing polymer matrices.

## Filler Materials

Theoretically, any material with a dielectric constant higher than that of the matrix can be aligned and chained through the dielectrophoretic effect. Table 2 shows a list of insulators, semiconductors, and metals which have been successfully aligned in a thermoset polymer matrix. Randall et al. (1992) showed that insulating particles are easily aligned, provided that their dielectric constant is greater than that of the matrix phase used (i.e.  $\beta > 1$  in Equation (3)). Fibrous filler morphologies are also capable of being aligned utilizing the dielectrophoretic assembly technique. Figure 10 shows PZT fibers aligned at approximately 0.1 and 0.005 volume fractions.

**Table 1: Matrix Materials For Dielectrophoretic Assembly**

| <u>Thermosets</u>   | <u>Trade-Name/Supplier</u>                              |
|---------------------|---|
| Silicone Elastomer  | Eccocil (Emerson-Cummings)                              |
| Polyurethane        | Sylgard-184 (Dow Corning)                               |
| Epoxies             | Hysol-Dexter<br>Eccogel-1365-80<br>(Emerson - Cummings) |
|                     | Epon 815 (Shell)  |
| <u>U.V. Curable</u> |   |
| Optical Adhesive    | NOA-65 Norland Co.                                      |

**Table 2: Filler Materials Successfully Aligned Via Dielectrophoretic Assembly**

| <u>Insulators</u>                                | <u>Semiconductors</u>                               | <u>Metals</u>             |
|--|---|---------------------------|
| BaTiO <sub>3</sub>                               | YBa <sub>2</sub> Cu <sub>3</sub> O <sub>6.5+δ</sub> | Aluminum Powder           |
| PbTiO <sub>3</sub>                               | Graphite  | Ag Covered Resin Balls    |
| PZT fibers & particles                           | SiC Fibers  | Ag Covered Acrylic Fibers |
| Ba <sub>2</sub> TiSi <sub>2</sub> O <sub>8</sub> |   |                           |
| ZrO <sub>2</sub> (purified anhydrous)            |   |                           |
| TiO <sub>2</sub>                                 |   |                           |
| Silica Glass Spheres                             |   |                           |

(after Randall, Miller, Adair and Bhatta)

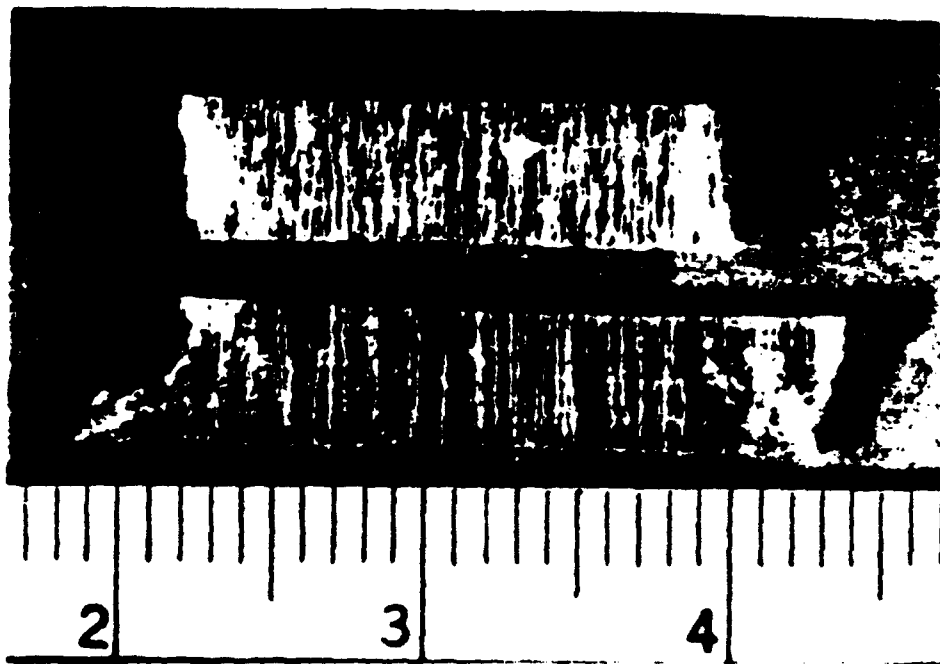


**FIGURE 10. PHOTOGRAPH OF PZT FIBERS ( $30\mu\text{m}$  THICK,  $1\text{cm}$  LONG) ALIGNED IN A POLYMER MATRIX AT APPROXIMATELY 0.1 VOLUME FRACTION (TOP) AND 0.005 VOLUME FRACTION (BOTTOM).**

When conducting fillers are used, limitations associated with composite fabrication arise. The first limitation involves the elimination of the potential drop across the sample once the particles successfully chain. When the particles chain, the composite becomes conducting and the potential voltage drop (polarizing field) across the sample is destroyed. The polarizing field is the driving force for the chaining phenomena and without it, migration of particles to form chains will not occur. Recent studies have revealed that once the composite sample becomes conducting, a few chains will remain intact and keep the polarizing field at zero while the rest of the chains will relax and dissipate due to Brownian motion. Hence, a rapid cure polymer is necessary to freeze in the chained structure before it can drift apart. Recent progress with alignment in UV curable polymers has been promising, but more work is necessary.

The second limitation of using conducting filler materials is that the volume fraction of the filler materials must be less than the percolation limit (recall Background section). If the conducting powder is present in large enough quantities that the particles touch to create a conducting pathway through the material, there will be no chaining phenomena because the polarization field will never be established.

The third limitation of conducting fillers concerns electrical breakdown of the uncured polymer during assembly. As particles begin to form chains, the insulating gap between the particles becomes increasingly smaller. This creates an enormous energy

density between the particles and can result in sparking or electrical discharge. This electric breakdown can slow and even prohibit the curing of the matrix.

### Ideal Dielectrophoretic Assembly Conditions For Composite Materials

Once the constituent materials have been selected, the focus of the assembly shifts to the process parameters. Based on the conditions placed on an individual system, the dielectrophoretically assembled composite can have a number of microstructures. The filler can exist in a dispersed state, well-defined chains, poorly-defined chains, and a turbulent flow state (Bowen et al., 1993).

While it was shown previously that the effects of the applied field magnitude have a great effect on the alignment of the particulate filler material, the frequency of the applied field also has an enormous impact on the microstructure of the final composite material (Bowen et al., 1993). Figure 11 shows a plot of the shear stress versus the square of the applied field for a polyurethane matrix with SrTiO<sub>3</sub> filler. When DC voltages are applied, an initial increase in the shear stress is seen, however it diminishes with increasing field intensity. This is believed to be caused by the domination of the electrophoretic effect at high electric field strengths.

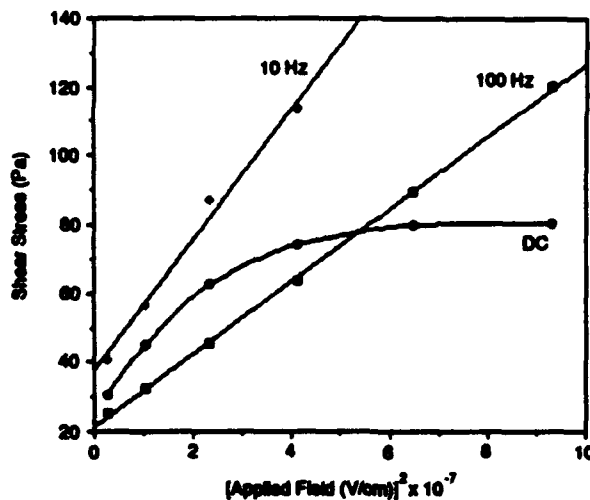


**FIGURE 11. SHEAR STRESS VS. SQUARED APPLIED FIELD FOR POLYURETHANE + 0.2 VOLUME FRACTION SrTiO<sub>3</sub> AT A SHEAR RATE OF 9.6 SEC<sup>-1</sup> (AFTER BOWEN, BHALLA, NEWNHAM, AND RANDALL).**

As can be seen for both the AC frequencies in Figure 11, the electrophoretic effect has been successfully suppressed (the plot has a linear dependence on E<sup>2</sup> as predicted by Equation (3)). Also, Figure 11 clearly shows that the force of attraction between particles is highly frequency dependent. For this system at a given electric field, there is a larger particulate force of attraction at 10 Hz than at

100 Hz. This shows that the composite architecture is adaptive based on the given set of assembly conditions (applied field intensity and frequency). Also, an optimum condition (which differs from system to system) exists to assemble a composite material via the dielectrophoretic technique (Bowen et al., 1993).

### APPLICATIONS FOR DIELECTROPHORETICALLY ASSEMBLED COMPOSITE MATERIALS

Composite materials assembled utilizing the dielectrophoretic effect can be exploited in a number of potential applications. These materials may not only be used as electrical composite materials but as thermally conducting and structural composites as well. They also have the ability to achieve percolation at low volume fractions so less filler material is necessary. A chart showing the potential of dielectrophoretically assembled composites is given in Figure 12.

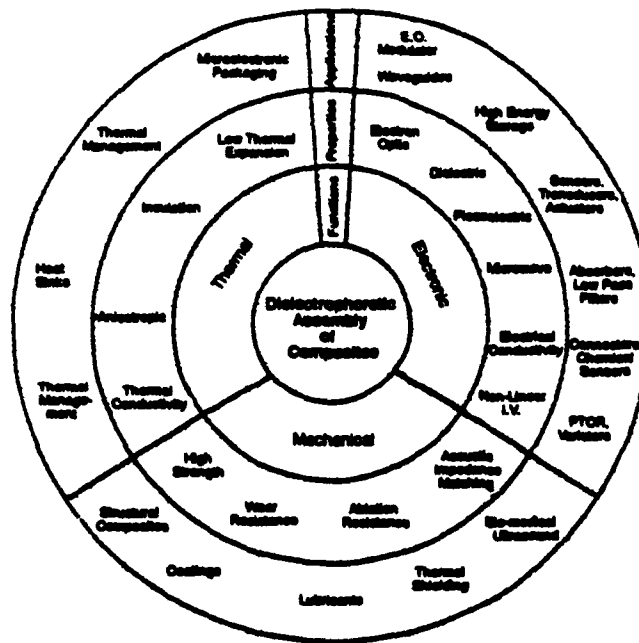


FIGURE 12. POTENTIAL APPLICATIONS FOR DIELECTROPHORETICALLY ASSEMBLED COMPOSITE MATERIALS. THE CIRCLE CHART IS READ FROM THE CENTER RADIALLY OUTWARDS WITH TITLES LOCATED AT THE TOP OF EACH RING.

#### Electronic Composite Applications

As electronic composite applications is our original projected field of use for dielectrophoretically processed composite materials, many devices have been considered as potential candidates for this processing technique. The use of dielectric measurements is foreseen as a type of quality control on this class of materials. Through the use of dielectric measurements, the

degree of alignment as well as the uniformity of the composite architecture across large sample areas can be quantitatively determined.

### Hydrophones

Using the direct piezoelectric effect, piezoelectric ceramics based on  $\text{Pb}(\text{Zr,Ti})\text{O}_3$  can be utilized as pressure sensors. However, the performance of these materials is limited in hydrostatic applications such as underwater acoustic sensing devices (hydrophones) due to transverse piezoelectric contributions. The limitations of the monolithic ceramic sensitivity can be overcome by combining the ceramic with a polymer to form a composite material. In the composite design, higher sensitivity levels are obtainable due to enhancements of the effective  $d_{33}$  coefficient via stress transfer from the polymer to the ceramic (Cao, Zhang, and Cross, 1992). Also, the composite device has an acoustical and capacitive impedance closer to that of the water medium (due to the replacement of most of the ceramic with a polymer) so it will be more sensitive to subtle pressure gradients. The most sensitive hydrophones have been designed with a 1-3 connectivity which has the advantage of large  $d_{33}$ , easy poling conditions, and good impedance matching to the working environment.

Hydrophones have also been utilized as biomedical transducers which allow ultrasonic imaging of internal organs. These biomedical devices require high frequency operation ( $\geq 1$  MHz) in order to provide accurate and distinct images (Smith and Shulov, 1988). To obtain these high frequencies, small scale hydrophone composites are required. The dielectrophoretic assembly technique provides a means to fabricate such devices on a much smaller scale than is currently possible.

### PTC Thermistors

When processing conditions are applied to cause a conducting filler to chain such that the particles are touching, a positive temperature coefficient of resistivity composite material is created. This composite material will be conductive at low temperatures and insulating above a certain critical temperature. When the device is heated, the thermal expansion mismatch between the polymer and the filler material can cause the composite to become insulating (see Figure 13). Since the polymer matrix will have a much larger coefficient of thermal expansion than the filler material, it will, on heating, expand in between the conducting particles and separate them. This results in an insulating composite at high temperatures. Figure 14 shows typical resistivity versus temperature response for such a composite device. A device such as this is useful in applications such as thermostats and temperature sensors.

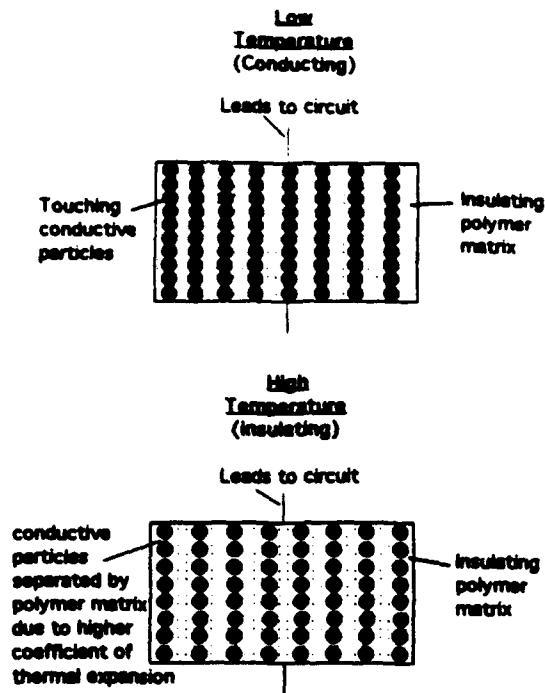


**FIGURE 13.** SCHEMATIC OF THE THERMISTOR APPLICATION.

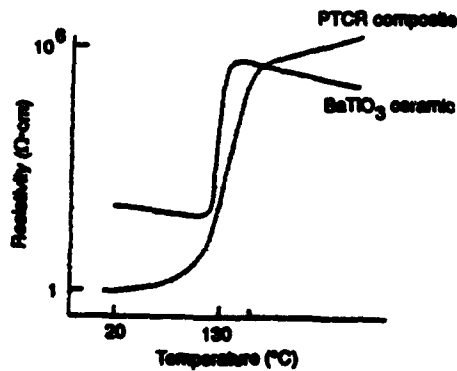


**FIGURE 14.** PLOT OF THE PTC EFFECT IN A COMPOSITE THERMISTOR AS COMPARED TO THAT IN A BaTiO<sub>3</sub> CERAMIC (AFTER NEWNHAM).

### Tunable Compliance Devices

It is anticipated that a device can be fabricated which alters its elastic compliance as a function of the magnitude of an applied electric field. By applying an electric field to a suspension of polarizable particles in an insulating fluid medium, the elastic compliance, and hence, the mechanical resonant frequency of the device can be altered (Newnham and Ruschau, 1991). The resonant

frequency can then be tuned to a specific value by applying an appropriate voltage to the system according to the following expression :

$$f_r = \frac{1}{2t} \sqrt{\frac{c}{\rho}} \quad (4)$$

where  $\rho$  = density,  $c$  = elastic stiffness (voltage dependent), and  $t$  = thickness of the sample. This device is shown schematically in Figure 15.

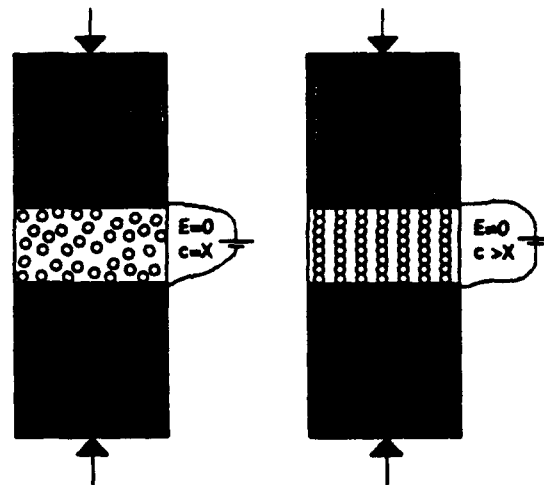


**FIGURE 15. SCHEMATIC OF THE TUNABLE COMPLIANCE APPLICATION. THE ELECTRIC FIELD INDUCED CHAINS (RIGHT) WILL GIVE THE DEVICE A DIFFERENT ELASTIC COMPLIANCE THAN THE DISPERSED CASE (LEFT).**

### Structural Applications

The focus of the dielectrophoretic assembly of composite devices has recently expanded to differing particle morphologies and it has been shown that fibers will align with the electric field (recall Figure 10 where short fibers of PZT were aligned and chained). Hence, it is now anticipated that structural composites will benefit from the dielectrophoretic assembly technique. It is predicted that a bulk short fiber reinforced composite material can be processed such that all the fibers are aligned in the same direction. This would give dramatic increases in composite properties over those attainable in a random chopped fiber system. As mentioned, this effect has only recently been identified and, as such, requires further study before any conclusions can be drawn.

## Thermally Conducting Composites

Dielectrophoretic assembly of composite materials also has the potential of being used to produce composites utilized for their thermal conduction properties. A composite filled with a high thermal conductivity material (such as SiC) aligned using the dielectrophoretic effect will exhibit a high thermal conductivity in the chained directions while the thermal conduction in the transverse directions will be minimal. While the thermal expansion mismatch that is exploited in the composite PTC thermistor must be taken into consideration, it is projected that the working range of these devices can be controlled by the temperature used to cure the device.

Bhattacharya and Chaklader (1983) have shown thermally conductive composites are possible using the percolation effect. By using dielectrophoretic processing, the percolation limit should be able to be shifted so that the same thermal conductivity is possible at lower volume fractions of filler material. In addition, the thermal conductivity of the device will be anisotropic, having a higher thermal conductivity in the chained direction. As is the case with structural composite materials, the applications of dielectrophoretically produced thermal composites have only recently been realized so further study is required in this area.

## SUMMARY

In this paper, a new novel processing technique termed dielectrophoretic assembly has been introduced. It has been shown to be applicable to a wide range of matrix and filler materials, but limitations still exist. Different assembly conditions for composite fabrication were shown to have a dramatic effect on composite architecture, giving the composite its adaptive nature. With optimum assembly conditions applied, the composite consists of a filler material which is aligned unidirectionally in the matrix phase. This type of microstructure can be exploited in terms of its electrical, thermal, and structural advantages. It is believed that once the science behind this processing technique is fully developed, dielectrophoretic assembly will become a powerful processing tool for the fabrication of functional composite materials.

## REFERENCES

- Baker, W.E., E.M. Moore, T.E. Petroff, 1991, "PZT 0-3 Composites Using Acid Based Co-Polymers," IEEE Proceedings 1991, pg. 309.
- Bhattacharya, S.K. and A.C.D. Chaklader, 1983, "Review on Metal-Filled Plastics. Part 2. Thermal Properties," *Polym. Plast. Technol. Eng.*, 20 [1], 35 - 59.
- Bowen, C.P., A. S. Bhalla, R. E. Newnham, C. A. Randall, 1993, "An Investigation of the Assembly Conditions of Dielectric Particles in Uncured Thermoset Polymers," (accepted *J. Mat. Res.* (October (1993))).
- Cao, W., Q.M. Zhang and L.E. Cross, *J. Appl. Phys.*, 72 [12], 15 December (1992).

- Halsey, T.C., 1992, "Electrorheological Fluids," *Science*, **258**, pg. 761 - 764.
- Newnham, R.E., D.P. Skinner, L.E. Cross, 1978, *Mater. Res. Bull.*, **13**, 525.
- Newnham, R.E., 1986a, *Ann. Rev. Mat. Sci.* **16** 47 - 68.
- Newnham, R.E., 1986b, *Ferroelectrics*, **68**, 1 - 32.
- Newnham, R.E., 1989, *Rep. Prog. Phys.*, **52**, 123 - 156.
- Newnham, R.E., and G.R.Ruschau, 1991, *J. Am. Ceram. Soc.*, **74**, 463 - 480.
- Pohl, H.A., 1978, *Dielectrophoresis*, Cambridge University Press, Cambridge, London, New York, and Melbourne, 34 - 47.
- Randall, C.A., S. Miyazaki, K. L. More, A. S. Bhalla, and R. E. Newnham, 1992, "Structural-Property Relationships in Dielectrophoretically Assembled BaTiO<sub>3</sub> Nanocomposites," *Mater. Letters*, **15**, 26 - 30.
- Randall, C.A., D. V. Miller, J. H. Adair, and A. S. Bhalla, 1993, "Processing of Electroceramic-Polymer Composites Using the Electrorheological Effect," *J. Mater. Res.*, **8** [4], 899 - 904.
- Reed, J., 1988, *Introduction to the Principles of Ceramic Processing*, John Wiley & Sons, Inc., New York, Chichester, Brisbane, Toronto, and Singapore, 144.
- Sarkar, P., X.Haung, P.S. Nicholson, 1992, "Structural Ceramic Microlaminates by Electrophoretic Deposition," *J. Am. Ceram. Soc.*, **75** [10] 2907-2909.
- Smith, W.A. and A.A. Shaulov, *Ferroelectrics*, **87**, 309 - 320 (1988).
- Tada, H., Y.Saito, M.Hirata, M.Hyodo, H.Kawahara, 15 January, 1993, "A Novel Switchable Glazing formed by Electrically Induced Chains of Suspensions," *J. Appl. Phys.*, **73** [2], pg. 489 - 493.
- Winslow, W.M., 1949, *J. Appl. Phys.*, **20**, 1137.
- Zallen, R., 1983, *The Physics of Amorphous Solids*, Wiley, New York.

**APPENDIX 46**

## CLASSIFICATION OF ELECTROSTRICTIVE-BASED MATERIALS FOR TRANSDUCERS

T.R. SHROUT, C.A. RANDALL, R.P. BRODEUR, and S.J. JANG

The Pennsylvania State University, Intercollege Materials Research Laboratory, University Park, PA 16802 U.S.A.

**ABSTRACT:** Analogous to PZT-based piezoelectrics and associated applications, four families of perovskite electrostrictors were classified being based on their intrinsic polarization change mechanism and underlying structural origin (where known). The four types include both normal and relaxor ferroelectrics in which large polarizations and electrostrictive strains can be induced with an appropriate electric field. Relaxors Type I and II exhibit broad and dispersive phase transitions with  $\text{Pb}(\text{Mg}_{1/3}\text{Nb}_{2/3})\text{O}_3$  and PLZT, as representative compositions, respectively. Types III and IV include "pinched" and normal ferroelectrics with anomalously high dielectric maximas near room temperature with  $\text{Ba}(\text{Ti},\text{Sn})\text{O}_3$  and  $(\text{Ba},\text{Sr})\text{TiO}_3$  given as examples. Additional classification parameters, in terms of application requirements, include induced electromechanical coupling, elastic constant tunability, and temperature usage regime.

### I. INTRODUCTION

Electrostrictive ceramics are viable alternatives to piezoelectrics for applications where effective and reliable electromechanical actuation is important. The highest performance electrostrictive materials are those ferroelectrics in which a large reversible dielectric polarization can be induced with an appropriate electric field. Applications of the electrostrictive phenomena continue to grow as new families of ferroelectric compositions are explored. For actuation purposes, the strong basic electrostrictive coupling can be used for precision positioning control in adaptive optics and high strain energy density sonar transducers. In addition, other areas include "smart" materials with tunable vibration/strain sensing and combined actuation functions, high frequency medical ultrasound, and nonlinear transducers for fiber optic electric-field sensors.

### II. CLASSIFICATION

The classification of the large family of piezoelectric materials arose from the standpoint of application requirements, based principally on  $\text{Pb}(\text{Zr},\text{Ti})\text{O}_3$ -PZT (e.g. DOD Type I, II, etc., or "hard" and "soft"). The numerous families of perovskite electrostrictors requires a similar form of classification. As presented in Table I, classification of the type of electrostrictor can be readily derived from their intrinsic polarization change mechanism and underlying structural origin (where known)<sup>(1)</sup>. Four ferroelectric material families were chosen in which large polarizations can be induced at the paraelectric→ferroelectric transition, owing to their inherently high dielectric constants ( $K$ ). For the case of relaxor-type ferroelectrics, Type I and II, the materials exhibit broad and frequency-dispersive phase transitions. Furthermore, unlike Type III and IV normal ferroelectrics, relaxors depolarize at a temperature, designated  $T_d$ , well below  $T_m$ , the temperature of maximum dielectric constant, as depicted in Figure 1. The dispersion arises from the breakdown of long range polarization coupling, due to symmetry breaking defects in the form of A-site lattice vacancies (Type II) and nano-scale B-site order-disorder in Type I electrostrictors.<sup>(2,3)</sup> Within the thermal regime  $\Delta T = T_d - T_m$ , large reversible and non-remanent polarizations and strains are achievable owing to micro-macro domain (Regime II) switching, offering a relatively wide temperature range of usage in contrast to the Type III and IV materials, but with increased hysteresis. See Figure 1. As a note, the ferroelectric transitions of Type III and IV materials can be broadened (or made diffuse) through controlled compositional heterogeneity, but at the expense of  $K$ , and thus  $P_{\text{ind}}$  and electrostrictive strain. [Note:  $P_{\text{ind}} \propto KE \rightarrow x \propto K^2$ ]

### III. ELECTROSTRICTOR FAMILIES

As presented in Table I, four material families, having the perovskite crystal structure  $ABO_3$ , were classified based on their polarization change mechanism. In this section, we will contrast the various dielectric and polarization behavior of the four types using representative examples of each class, listed in order of increasing electrostrictive ( $Q$ ) coefficient. Additional classification, relevant to application requirements, includes dielectric behavior, E-field induced polarization ( $P_{ind}$ ), and strain ( $x_{ij}$ ), electro-mechanical coupling ( $k_{ij}$ ) and interrelationships thereof, and temperature regime in which they can operate effectively. See Table II.

**Type I.  $Pb(B_1B_2)O_3$ -Relaxors.** The well known perovskite ferroelectric  $Pb(Mg_{1/3}Nb_{2/3})O_3$  [PMN] typifies the Type I electrostrictor. Representative dielectric and polarization behavior for this type is given in Figure 2a, for a composition modified with the normal ferroelectric  $PbTiO_3$ , allowing the transition to be shifted from  $T_m \sim -10^\circ C$  to that near room temperature. Although the Type I relaxors possess electrostrictive coefficients nearly an order of magnitude smaller than the Type IV normal ferroelectrics, electrostrictive strains  $> 0.1\%$  are achievable owing to their inherently high dielectric maximas (Regime I) with even larger strains and associated polarization levels achievable in the micro-macro domain regime.

Further advantages not readily apparent from Figure 2a include low dielectric loss ( $T > T_m$ ), low E-field K-dependency and low thermal expansion. In addition, a wide range of compositional modifications are possible (A- and B-site); however, their role in the nano-scale order-disorder and subsequent impact on the polarization behavior is not well understood at present.

**Type II. e.g. PLZT-Relaxors.** PLZT-type relaxors also exhibit frequency dispersive phase transitions, although with significantly lower  $K_{max}$ 's, but a wider  $\Delta T = T_m - T_d$  micro-macro region, offering a temperature use range of  $> 100^\circ C$  with only minimal remanent strain. Disadvantages include the compositional invariability to shift  $T_m$  below room temperature, hence limiting operation to Regime II, and the high E-fields required to achieve equivalent  $P_{ind}$  levels to Type I materials.

**Type III and IV. "Pinched" and Normal Ferroelectrics.** The application requirement of high dielectric permittivity is met for compositional families possessing 1st order ferroelectric phase transitions, typified by  $BaTiO_3$ , with  $K_m$ 's on the order of 10,000. Further enhancement is readily achievable through compositional modifications [e.g.  $Ba_{1-x}Sr_xTiO_3$  ( $K_m$ 's  $> 20,000$ )] with increased 2nd order character and minimal dispersion. See Figure 2d. Even higher dielectric maximas are achievable in the Type III "pinched" ferroelectrics, wherein all associated  $BaTiO_3$  phase transitions converge at a single compositional point, e.g.  $BaTi_{1-x}Sn_xO_3, x=0.13$ , as presented in Figure 2c. Despite their larger  $K_m$ 's, induced polarization and strain levels are significantly lower than for Type I and II electrostrictors, with additional performance limitation arising from their narrow dielectric maximas. In contrast, to the Type IV normal ferroelectrics, the polarization temperature behavior for the Type III ceramics did not show the expected  $T_m = T_d$  relation, but instead showed a continuous decrease to  $\approx 100^\circ C$ , well above  $T_m$ . This observed behavior is believed to be due to a "core-shell" structure, in which the core is comprised of nearly pure  $BaTiO_3$ , although this has yet to be confirmed. Furthermore, the induced (electrostrictive) strain levels were virtually temperature-independent in the vicinity of  $T_m$ , with minimal remanent strain and hysteresis, even well below  $T_m$ , again indicative of stress-induced domain reversal owing to a "core-shell" structure.

Table I. Classification of Electrostrictive Perovskites(1)

| Classification  | Dielectric Family       | Temperature Behavior             | Polarization-Structure Relationship  |
|---|-------------------------|----------------------------------|--|
| Type I<br>Pb(B <sub>1</sub> B <sub>2</sub> )O <sub>3</sub><br>e.g. Pb(Mg <sub>1/3</sub> Nb <sub>2/3</sub> )O <sub>3</sub> | Relaxor                 | T <sub>m</sub> > T <sub>d</sub>  | • Micro-polar Domains $\sqrt{P^2} \neq 0$<br>• B-site Nano-scale ordering        |
| Type II<br>Pb <sub>1-y</sub> La <sub>y</sub> (Zr <sub>x</sub> Ti <sub>1-x</sub> )O <sub>3</sub><br>y > 7 x ≥ 0.65         | Relaxor                 | T <sub>m</sub> >> T <sub>d</sub> | • Micro-polar Domains $\sqrt{P^2} \neq 0$<br>• A-site vacancy lattice decoupling |
| Type III<br>e.g. Ba(Ti <sub>1-x</sub> Sn <sub>x</sub> )O <sub>3</sub><br>x = 0.1  | "Pinched Ferroelectric" | T <sub>m</sub> = T <sub>d</sub>  | • Phase Pinching (R,O,T,C)<br>• B-site heterogeneity (diffuse transition)        |
| Type IV<br>e.g. Ba <sub>(1-x)</sub> Sr <sub>(x)</sub> TiO <sub>3</sub>  | Normal Ferroelectric    | T <sub>m</sub> = T <sub>d</sub>  | • Paraelectric $\sqrt{P^2} = 0$<br>• A-site heterogeneity (diffuse transitions)  |

#### IV. SUMMARY

Tables I and II summarize the dielectric-polarization strain behavior for the four types of electrostrictors. As seen in these Tables, the largest achievable strains are not observed for materials with the largest electrostrictive coefficients, but those in which a micro-macro domain polarization change mechanism occurs.

Relative to actuator/transducer application requirements, the four Types of electrostrictors can be ranked accordingly:

- Large Induced Strain - Type II ≥ I > III > IV.
- Operating Temp Range - Type II > I > III > IV
- Hysteresis Level - Type I > III > IV > II
- Strain Energy Density - Type I > II > III > IV

For high frequency and adaptive transducer applications, the four types are ranked as follows:

- Induced Piezoelectric Coupling
  - k<sub>p</sub> - Type I > II > III = IV
  - k<sub>t</sub> - Type II = IV = I > III
- Elastic Constant, e.g. C<sub>33</sub><sup>D</sup> - Type IV > III > II > I

Further classification/comparison is made difficult due to electrostrictor's inherent non-linear and frequency dependent behavior, particularly for relaxors.

#### V. REFERENCES

1. L.E. Cross, "Piezoelectric and Electrostrictive Sensors and Actuators for Adaptive Structures and Smart Materials," Proc. AME 110th Annual Mtg., San Francisco (Dec. 1989).
2. George Rossetti, Ph.D. Thesis, The Pennsylvania State University (1993).
3. C.A. Randall, A.S. Bhalla, T.R. Shrout, and L.E. Cross, "Relationship Between B-site Order and Properties in Pb(B'B'')O<sub>3</sub> Perovskites," Ferroelectric Letters, 11, 1, 103-106 (1990).

#### VI. ACKNOWLEDGEMENTS

The authors would like to thank Mr. Joseph Fielding and Dr. Dean McHenry for their research assistance and Dr. L.E. Cross for his inspiration. The authors also wish to acknowledge the Office of Naval Research for funding this area of work.

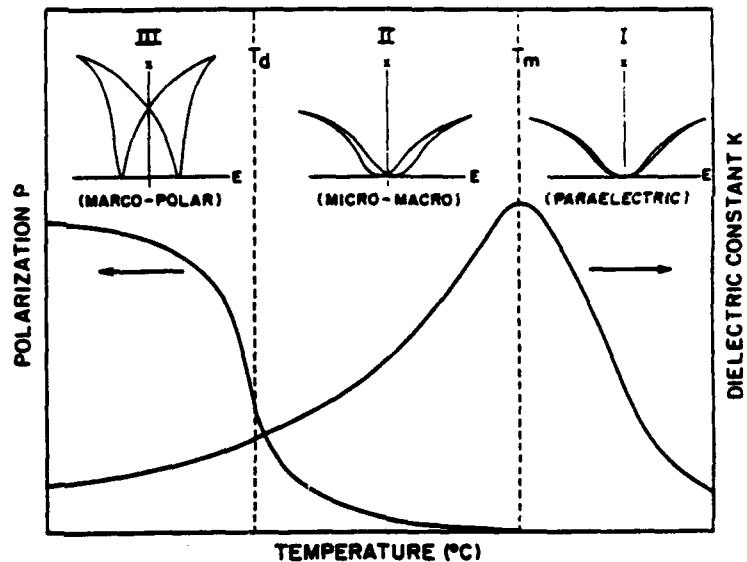


Figure 1. Representation of dielectric, polarization, and strain-E-field regimes for electrostrictive-based ferroelectrics.

Table II. Summary of Polarization-Strain and Related Parameters\* for Type I-IV Electrostrictors

| Material Type      | †Electrostriction Coefficient ( $Q_{12} \text{ m}^4/\text{C}^2$ ) | †† $K_{max}$ (Temp/freq behavior) | $P_{ind} \text{ (C/m}^2\text{)}$<br>{ 10 KV/cm }<br>{ 20 KV/cm } | †††Transverse Micro-strain<br>{ 10KV/cm }<br>{ 20 KV/cm } | ‡Anisotropy <sup>oo</sup> Piezo-coupling |       | Elastic Constant $C_{33}^D$<br>( $\times 10^{12} \text{ N/m}^2$ ) |
|--------------------|---|-----------------------------------|--|---|--|-------|---|
|                    |   |                                   |  |   | $k_p$                                    | $k_t$ |   |
| Type I (Relaxor)   | ~ .004  | $\leq 30,000$ (dispersive)        | ~ 0.1-0.2<br>~ 0.2-0.3   | ~ 100-300<br>~ 300-500                                    | ~40%                                     | ~50%  | ~ 17-18   |
| Type II (Relaxor)  | ~ .007  | 6,000-9,000 (dispersive)          | ~ 0.1-0.15<br>~ 0.2-0.3  | ~ 100-250<br>~ 300-700                                    | ~ 45%                                    | ~50%  | ~ 16-19   |
| Type III "Pinched" | ~ .01   | $\leq 35,000$ (normal)            | ~ 0.08-0.15 (saturated)  | ~ 200   | ~ 20%                                    | ~ 40% | ~ 21-23   |
| Type IV Normal     | ~ .013  | $\leq 20,000$ (normal)            | ~ 0.02-0.1 (saturated)<br>@ 0.14                                 | ~ 10-150<br>~ 200   | ~ 10%                                    | ~ 40% | ~ 16-20   |

\* Data presented based on room temperature usage.

\*\* Maximum induced electromechanical coupling, also reflecting percent change of E-field tunability.

† Transverse strain polarization electrostriction coefficients.  
Note:  $Q_{11} = -3.5 Q_{12}$

†† Dielectric maxima ( $K_m$ ) for relaxors @ 1 KHz.

††† Transverse strain: non-remnant.

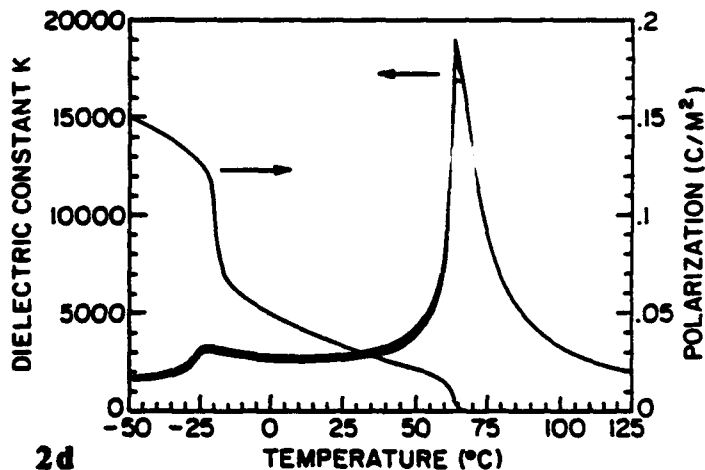
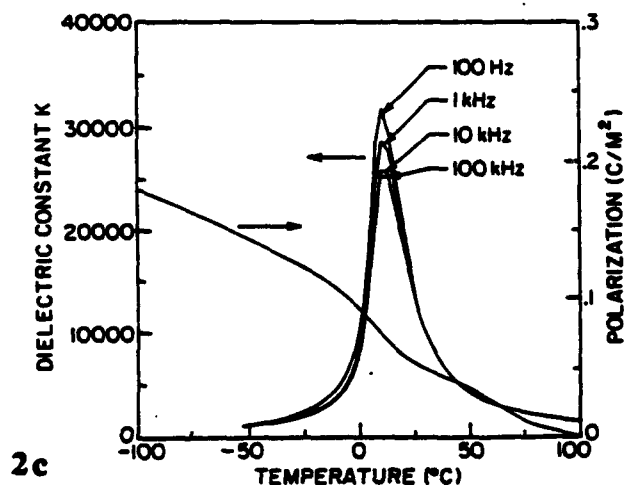
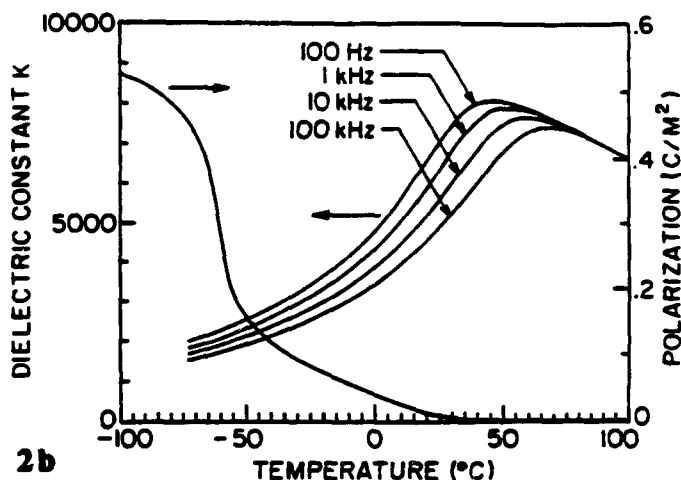
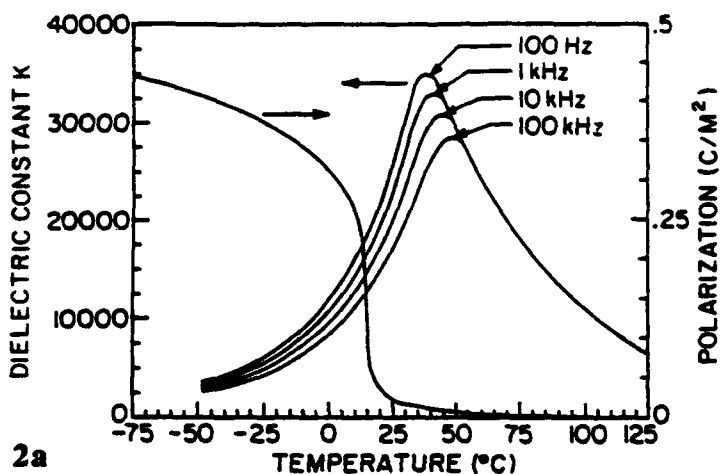


Figure 2. Dielectric and polarization behavior for various types of electrostrictors; (a) Type I— $0.9\text{Pb}(\text{Mg}_{1/3}\text{Nb}_{2/3})\text{O}_3-0.1 \text{PbTiO}_3$ , (b) Type II— $\text{Pb}_{0.91}\text{La}_{0.09}(\text{Zr}_{0.65}\text{Ti}_{0.35})\text{O}_3$ , (c) Type III— $\text{Ba}(\text{Ti}_{1-x}\text{Sn}_x)\text{O}_3$   $x=0.13$ , and (d) Type IV— $\text{Ba}_{1-x}\text{Sr}_x\text{TiO}_3$   $x=0.3$  (Note: the tetragonal to orthorhombic transition @  $T \approx -25^\circ\text{C}$ ).

**APPENDIX 47**

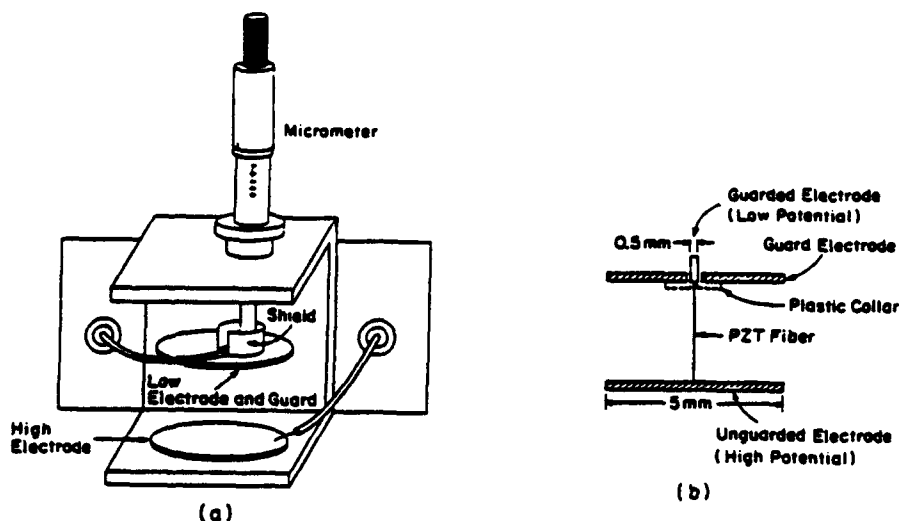


FIGURE 2. Fixture for fiber permittivity and polarization (a), and section view of electrode configuration (b).

The polarization hysteresis was measured using a specially-built automated system which applies the excitation field and collects the charges while maintaining a virtual-ground state, thus assuming control of the stray field. To avoid electrical breakdown, the entire fixture was immersed in a fluorocarbon fluid. Fields of  $> 3$  MV/m, typically of 10 Hz were used.

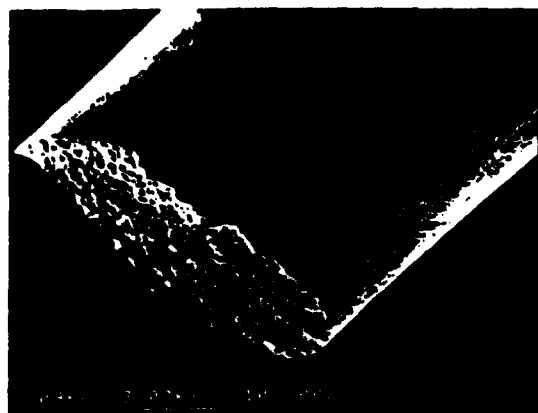
In addition to chemical and electrical characterization, the mechanical integrity of the PZT fibers was also investigated. The tensile strength was determined for selected fibers at the Nagasaki University of Japan, using a technique described by Iwanaga et al.<sup>10</sup> Specimens 1 to 2 mm in length, diameter range between 26 to 36  $\mu\text{m}$ , were glued to carbon fiber and the direct tensile strength was measured with a load range of 1 to 10g.

## RESULTS AND DISCUSSION

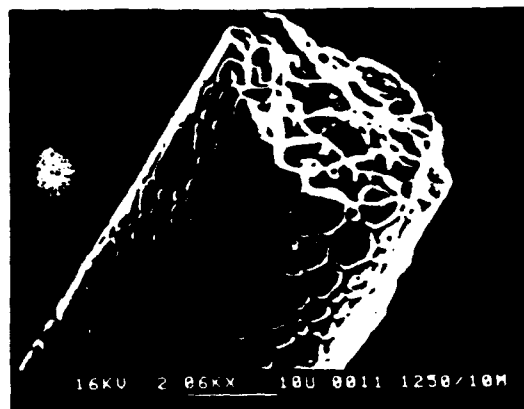
### Microstructural Analysis

As spun amorphous fibers corrected on the take-up drum were continuous and flexible with gold color. All of the XRD spectra of PZT and Nb-PZT fibers fired at 750°C and 1250°C revealed the presence of well-crystallized perovskite phase. Figure 3 presents SEM micrographs of PZT and Nb-PZT fibers after heat treatments. As presented, the diameter of the fibers were in the range of 20 to 50  $\mu\text{m}$ , showing little evidence of porosity on the surface of the fiber. SEM examination of the cross section of the PZT fibers fired at 750°C revealed 10 to 20% fine porosity uniformly distributed across the fibers, except near the dense surface, with grain sizes on the order of 0.2 - 0.3  $\mu\text{m}$ . Fibers processed at 1250°C possessed dense microstructures with grain sizes into the range of 2 to 8  $\mu\text{m}$ . A small amount of closed porosity ( $\sim 0.3$   $\mu\text{m}$  in diameter), both in grains and at grain boundaries were evident in the cross sectional view of the fiber after the pull test. Fracture surface was intergranular. The fibers with Nb-PZT composition fired at 1250°C showed uniform and finer grain size, 1 to 3  $\mu\text{m}$ , and little porosity. The reason for the smaller grain size is due to the niobium substitution, which tends to inhibit grain growth of PZT in addition to many other characteristics governed by this "A-site vacancy additive".

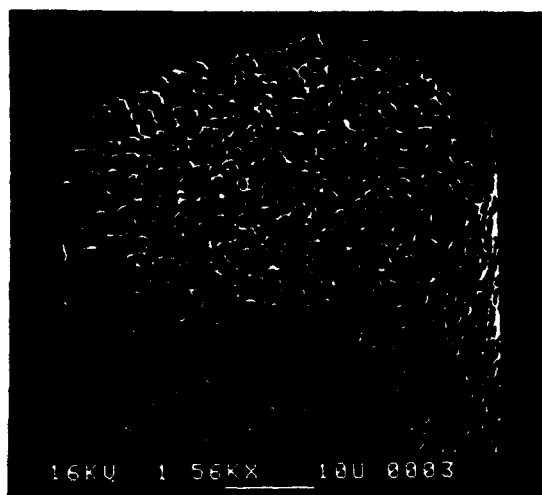
## PZT FIBERS--FABRICATION AND PROPERTIES



(a)



(b)



(c)

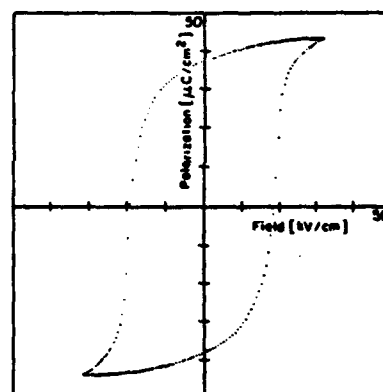


**FIGURE 3. SEM micrograph of:**  
(a) PZT fired at 750°C for 10 min.  
(b) PZT fired at 1250°C for 10 min.  
(c) Nb-PZT fired at 1250°C for 10 min.

**FIGURE 4. Polarization hysteresis of Nb-PZT fiber (diameter 30 μm).**

### Electrical Properties

The dielectric constant values of the various fibers processed are summarized in Table I. Due to the small input signals, dielectric loss values for the PZT fibers were not measured. The PZT fibers showed comparable dielectric values to that of the bulk ceramics disk samples made from the same solution. The dielectric constant of the samples fired at 750°C gave lower values which were probably due to the combination of porosity and smaller grain size. Representative room temperature hysteresis polarization E-field behavior for Nb-PZT fired at 1250°C are shown in Figure 4. The ferroelectric nature of the single piezoelectric fiber has not been reported before. The polarization hysteresis provides direct evidence that these fibers can be polarized to induce the desired

## **Pb(Zr,Ti)O<sub>3</sub> [PZT] FIBERS--FABRICATION AND PROPERTIES**

SHOKO YOSHIKAWA, ULAGARAJ SELVARAJ, PAUL MOSES,  
QIYUE JIANG, AND THOMAS SHROUT  
Materials Research Laboratory, The Pennsylvania State University,  
University Park, PA 16802

**Abstract** Fine scale lead zirconate titanate (PZT) and niobium substituted PZT (Nb-PZT) piezoelectric fibers were fabricated from sol-gel processed viscous "sol" using the "spinning" methodology developed for the continuous production of glass fibers. Subsequent drying and firing at above 750°C gave pure perovskite PZT and Nb-PZT fibers of 30 μm in average diameter. Further densification and grain growth were evident for fibers fired at 1250°C. Experimental methods for the determination of dielectric and polarization properties were developed to overcome inherent electric field difficulty relevant to fine scale fibers. The dielectric constant and polarization hysteresis values of the fibers were comparable with that of bulk ceramics. Preliminary single fiber mechanical pull tests indicated that the tensile strength of 30 μm diameter PZT fibers were similar to that of bulk ceramics, being in the range of 35-55 MPa.

### **INTRODUCTION**

Lead zirconate titanate (PZT) piezoelectric ceramics' ability to efficiently convert electrical energy to mechanical and vice versa has made them attractive for both actuators and sensors in active control systems.<sup>1</sup> This reversible transformation ability also makes piezoceramics viable candidates for passive vibration damping.<sup>2</sup> For structural materials comprised of various fibers, i.e. glass and carbon, the incorporation of piezoelectric fibers is, therefore, inherently desired.<sup>3</sup>

For fibers with diameters less than 100 μm, non-conventional methods have been employed, including the impregnation of host fibers with a precursor solution<sup>4</sup> and hand drawing from a viscous sol.<sup>5-7</sup> Single strand fibers fabricated thus far have been limited to lengths of a few centimeters, being for demonstration purposes only. Furthermore, little information regarding electrical and mechanical properties has yet to be reported.

It was the objective of this work to fabricate fine-scale PZT fibers using a "spinning" methodology developed for the continuous production of carbon and/or glass fibers. A further objective was to determine the electrical and mechanical properties of individual fibers prepared above.

### **EXPERIMENTAL PROCEDURE**

#### **PZT Fiber Fabrication**

The advantages of sol-gel processing in the fabrication of ferroelectric thin films; i.e., compositional control, low-temperature densification and overall simplicity makes it the ideal methodology for the fabrication of fine-scale fibers. Detail processing of PZT sol-gel precursor for fiber formation was reported previously.<sup>3,7</sup>

## PZT FIBERS--FABRICATION AND PROPERTIES

Stoichiometric quantities of each chemical was weighed out in accordance with the PZT formulations  $Pb(Zr_{0.48}Ti_{0.52})O_3$  and  $Pb_{0.988}(Ti_{0.48}Zr_{0.52})_{0.976}Nb_{0.024}O_3$ , as reported in Jaffe, Cook, and Jaffe<sup>8</sup>.

The precursor solution was transferred to a vessel consisting of a spinneret and a plunger as shown schematically in Figure 1(a)<sup>9</sup>. Fibers were extruded through the spinneret with twelve  $100\ \mu\text{m}$  diameter holes at  $\sim 7\ \text{kPa}$  of pressure. The spun-drawn fibers were collected on a rotation drum with a variable speed control, as described in Figure 1(b). Factors involved in controlling the diameter of the fibers are: (i) viscosity of the sol, i.e. control of hydrolysis and condensation reaction, (ii) spinneret diameter, and (iii) speed of the take-up drum.

Fibers with diameters ranging from  $10$  to  $80\ \mu\text{m}$  were fabricated. The fibers were dried at room temperature for approximately 12 hours, cut into lengths of  $\sim 10\ \text{cm}$  and fired at temperatures from  $750^\circ\text{C}$  to  $1250^\circ\text{C}$  for 10 minutes. For samples fired at temperatures  $>1200^\circ\text{C}$ , a lead atmosphere was created to minimize lead loss. The sintering condition of  $750^\circ\text{C}$  for 10 minutes was chosen based on a previous study<sup>7</sup> which was high enough to enable the formation of the desired perovskite structure, yet low enough to fire in open air without lead loss. This may be an important factor in the future when continuous fiber spinning and subsequent firing are desired. Firing temperatures at  $1250^\circ\text{C}$  were used to examine densification behavior and grain growth, being similar to that used for conventionally processed PZT ceramics.

### Characterization

Crystallinity and phase analysis of the fibers as a function of thermal treatment were determined using x-ray diffraction (XRD) analysis. The microstructure, i.e. grain size and degree of porosity, and diameter of the fibers were examined using scanning electron microscopy (SEM).

Dielectric constant and polarization of heat treated individual fibers were measured at room temperature using the holder described in Figure 2. A small amount of air-dried silver was applied to both ends of the fiber prior to both measurements. For the capacitance measurement, 1 to 2 cm length samples were used, whereas specimens  $\sim 3\ \text{mm}$  in length were prepared for polarization measurement.

Dielectric measurements were made, using a low frequency Impedance Analyzer at 10 kHz with an external amplifier/divider circuit which increased the sensitivity of the meter by a factor of 100 by increasing the applied voltage to approximately  $150\ \text{V}_{\text{rms}}$ . After the capacitance of the fiber was measured, the fiber was removed and the capacitance of the fixture was measured. This capacitance represents both stray and the direct (air gap) capacitance, but dominated by the direct capacitance, was then subtracted from the previous measurement yielding the sample's capacitance.

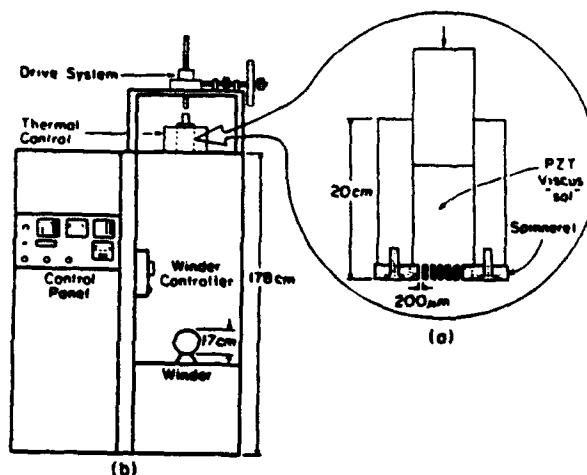


FIGURE 1. Fiber spinning apparatus. Schematic drawing of vessel and spinneret (a), and overview of the apparatus (b).

TABLE I. Dielectric Constant of Sol-Gel Derived PZT and Nb-PZT Fibers<sup>a)</sup>

| Ceramic | Heat Treatment<br>Temp.[°C]/Time [min.] | Dielectric Constant<br>(% error) |
|---------|---|----------------------------------|
| PZT     | 750/10                                  | 670 (15)                         |
| "       | 1250/10                                 | 870 (10)                         |
| Nb-PZT  | 750/10                                  | 1250 (15)                        |
| "       | 1250/10                                 | 1100 (15)                        |

a) Fiber : Average diameter of 30  $\mu\text{m}$ .

piezoelectric properties. The level of remanent polarization ( $P_r$ ) of the fibers was 37  $\mu\text{C}/\text{cm}^2$  and coercive field ( $E_r$ ) was 19  $\text{kV}/\text{cm}^2$ .

### Mechanical Properties

Preliminary data for the tensile strength of PZT fibers fired at 750°C and 1250°C determined using the pull test were 36 MPa and 40 MPa, respectively. Tensile strengths of ~55 MPa were found for Nb-PZT fibers. This higher value may be attributed to its smaller and more uniform grain size. Finer diameter fibers tended to give larger tensile strength values, though more data with different diameter samples is required to confirm this. Tensile strength values for bulk PZT ceramics reported in the literature is on the order of ~76 MPa<sup>11</sup>, with modulus of rupture using 3-point flexure is in the range of 10 to 40 MPa<sup>12</sup>. Therefore, the fiber tensile strength found for the fibers in this work is considered to be in a similar range as that of the bulk ceramic.

### CONCLUSIONS

Amorphous PZT and Nb-PZT fibers with average diameters of 30  $\mu\text{m}$  have been successfully spun-drawn from sol-gel processed PZT precursor sol using a continuous batch spinning apparatus. The fibers showed pure crystalline perovskite structure after heat treatment at 750°C, and further densification and grain growth were evident after 1250°C firing.

Single fiber dielectric constant and polarization hysteresis measurements were successfully performed using a specially built fixture. Dielectric constant values of the fibers fired at 750°C were lower than that of fibers fired at 1250°C due to porosity and reduced grain size. The dielectric constant of fibers fired at 1250°C were comparable with that of bulk ceramic values. Polarization E-field measurements of Nb-PZT fibers indicated that the level of remanent polarization 37  $\mu\text{C}/\text{cm}^2$ .

Preliminary data for the tensile strength of PZT fibers revealed values similar to that of bulk PZT, though Nb-PZT fiber values were higher than that of pure PZT fibers, probably due to its denser microstructure and smaller, uniform grain size.

### ACKNOWLEDGEMENT

The authors would like to acknowledge the contribution of Professor Hiroshi Iwanaga of Nagasaki University for fiber mechanical measurements. A special thanks to Professor Dan Edie and his group at Clemson University for letting us use their equipment and for their help. Also, the authors wish to thank Drs. L. Eric Cross and Keith Brooks for their help for this project. This project was supported by Office of Naval Research Grant No. N00014-92-1391, program monitor Dr. Lawrence Kabacoff.

## PZT FIBERS--FABRICATION AND PROPERTIES

### REFERENCES

1. E. Crawley and J. deLuis, ACAA Journal, 25, 1373-1385 (1987).
2. N.W. Hagood and A. von Flotow, J. Sound and Vibrations 146, 243-268 (1991).
3. S. Yoshikawa, U. Selvaraj, K.G. Brooks, and S.K. Kurtz, IEEE, 8th International Symposium on Application of Ferroelectrics, Greenville, S.C., Aug. 30 - Sept. 2, 1992, Proceedings, pp. 269-272.
4. D.J. Waller, A. Safari, R. Card, and M.P. O'Toole, J. Am. Ceram. Soc. 73, 3503-3506 (1990).
5. Vinay Seth, U.S. Patent #4,921,328, May 1, 1990.
6. Kuo-Chun Chen, Haixing Zheng, John D. Mackenzie, U.S. Patent #5,072,035, Dec. 10, 1991.
7. U. Selvaraj, A.V. Prasadarao, S. Komarneni, K. Brooks, and S.K. Kurtz, J. Mater. Res., 7, 992-996 (1992).
8. B. Jaffe, W.R. Cook, Jr., and H. Jaffe, Piezoelectric Ceramics, pp. 135-83, Academic Press, New York, 1971.
9. G.J. Hayes, M.S. Thesis, Clemson University (1989).
10. H. Iwanaga, T. Iwasaki, K. Reizen, T. Matsunami, M. Ichihara, and S. Takeuchi, J. Am. Ceram. Soc., 75, 1297-99 (1992).
11. Engineering Report, TP-226, Veritron Piezoelectric Division.
12. R.C. Pohanka, P.L. Smith, and J. Pasternak, Ferroelectrics, 50, 285-291 (1983).

**APPENDIX 48**

## ELECTRORHEOLOGICAL PROPERTIES OF BaTiO<sub>3</sub> SUSPENSIONS

DAVID V. MILLER\*, CLIVE A. RANDALL, AMAR S. BHALLA,  
ROBERT E. NEWNHAM and JAMES H. ADAIR\*\*

Materials Research Laboratory, The Pennsylvania State University

(Received for Publication February 23, 1993)

### ABSTRACT

Electrorheological (ER) fluids based on a silicone oil matrix with a high dielectric constant particulate component, BaTiO<sub>3</sub>, were evaluated. Particle size effects were examined with a commercial BaTiO<sub>3</sub> (0.35µm in size) and a hydrothermally prepared BaTiO<sub>3</sub> powder with an average particle size of 0.07µm. The commercial powder exhibited an ER response to DC fields, but above a critical field strength rheological properties dropped off drastically. The relative magnitude of yield stresses, at field levels below the critical field strength, are comparable with current literature values. Hydrothermally prepared BaTiO<sub>3</sub> powder exhibited minimal ER response to applied DC fields.

Optical microscope studies of dilute suspensions (~1-2 volume percent) were used to correlate fibril formation with ER measurements. Under applied DC fields, turbulent flow dominated above 6.25kV/cm and ER properties diminished. Increased frequency led to an increase in the degree of fibril formation with a maximum level occurring around 60Hz.

In response to AC fields, both types of BaTiO<sub>3</sub> powders showed a strong frequency dependence. Maximum shear stress for a given field strength resulted at about 60Hz. Optical microscopy showed an increase in fibril formation with increased AC field strength (60Hz). Turbulent flow did not appear with increased AC field (60Hz) at all field strengths evaluated (≤20kV/cm). All suspensions exhibited a linear relationship between yield stress and the square of applied electric field, which is characteristic of dipole-dipole interactions.

---

\* Current Address: Loral Vought Systems, Dallas, TX

\*\* Current Address: Materials Science and Engineering, University of Florida,  
Gainesville, FL

---

Communicated by Dr. G. W. Taylor

## 1.0 INTRODUCTION

ER fluids have long been of interest to the automotive industry especially for potential applications as fluid clutches and engine mounts<sup>1-6</sup>. At present, however, ER fluids are limited by insufficient yield stresses, suspension stability, reproducibility as a function of time and temperature, and power consumption considerations. In a recent theoretical paper, Davis pointed out that high dielectric constant particles may be a solution to some of these limitations<sup>7</sup>. Previous theoretical models for ER fluids are based on dipole-dipole electrostatic theory in which the attractive force between adjacent particles, subjected to an electric field, is given by<sup>8-11</sup>:

$$F = \frac{24a^6\epsilon_0 E^2}{R^4} \frac{K_f(K_p - K_f)^2}{(K_p + 2K_f)^2} \quad (1)$$

where,

- a = equivalent particle radius (m)
- r = particle separation distance (m)
- $\epsilon_0$  = permittivity of free space
- E = electric field (V/m)
- $K_f$  = dielectric constant of matrix phase
- $K_p$  = dielectric constant of suspended particulates

This model explains the relationship between yield stress and  $E^2$ , but more recent work shows that the dependence of yield stress ( $\tau_y$ ) on dielectric constant differences between the particle and fluid components are not following equation (1)<sup>7,12,13</sup>.

Based on these observations, the design of new ER fluids with high dielectric constant particles warrants further investigation. This study characterizes fibril formation and yield stress behavior of an ER fluid containing BaTiO<sub>3</sub> particles in silicone oil. BaTiO<sub>3</sub> was chosen for its high dielectric constant, and silicone oil was used because of its high electrical breakdown strength. Dynamic yield stress values were determined by extrapolation of shear stress to zero shear rate with constant applied field. The relative magnitude of yield stress for BaTiO<sub>3</sub> systems is shown to be higher than that predicted by dipole-dipole theory<sup>12</sup>.

## 2.0 EXPERIMENTAL PROCEDURES

### 2.1 Electrorheological (ER) Measurements

The two BaTiO<sub>3</sub> materials evaluated differed in preparation technique and particle size. One system is a coprecipitated, calcined BaTiO<sub>3</sub>† with a mean particle size of

† Grade HPB, TAM Ceramics, Niagara Falls, NY

0.35 $\mu$ m. The other BaTiO<sub>3</sub> powder was produced by hydrothermal synthesis (designated as BT18) and possessed a mean particle size of 700 $\text{\AA}$ <sup>14</sup>. Solid loadings, in silicone oil<sup>\*#</sup>, for the two systems were established from zero field limitations of the viscometer. The useful solid loadings for the commercial powder and BT18 were determined to be 27 and 12.5 volume percent, respectively.

ER measurements were performed in a modified commercial viscometer<sup>†</sup> on suspensions consisting of BaTiO<sub>3</sub> powder and silicone oil using several different loadings. The magnitude and frequency of the applied electric field was controlled with a power supply<sup>‡</sup> and an AC signal generator<sup>±</sup>. Shear rates were varied from 93-4.65sec<sup>-1</sup>. DC field response and upper field limitations were measured at various loadings for two different powders. AC field response was determined up to 18.75kV/cm and frequencies ranging from 10Hz-1kHz for the same suspensions evaluated under DC conditions. An operating frequency of 60Hz was determined optimum for both particle sizes examined, and was used in all AC measurements.

## 2.2 Optical Microscopy Observations

Fibril formation under applied DC and AC fields was observed using an optical microscope. Suspensions were diluted to 1-2 volume percent solids and loaded in a sample cell. The sample cell was connected to the same power supply and AC signal generator used for ER measurements.

After loading a suspension into the sample cell, a pre-selected field was applied, and response of the suspension was observed with a microscope. The response was monitored on a video recorder for later viewing. Fibril formation was observed under both DC and AC fields as a function of frequency.

## 3.0 Results and Discussion

### 3.1 ER Measurements

#### 3.1.1 Zero Field Viscosity

Figure 1 is a plot of shear stress (Pa) as a function of shear rate (sec<sup>-1</sup>) for TAM HPB/silicone oil suspensions at various solids loadings. These data show a steady increase in zero field viscosity with increased solids loading at all shear rates. Pure silicone oil (50mPa·sec) and the 10 volume percent TAM HPB suspension display results characteristic of Newtonian fluids with

\*# SF 96/50 Thomas Scientific

† Brookfield Engineering Labs, Inc., Stoughton, MA

‡ TREK, Model 620A, Medina, NY

± Racal-Dana, High Voltage Sweep Generator - F47, Anaheim, CA

◊ Zeiss Axioskop, Thornwood, NY

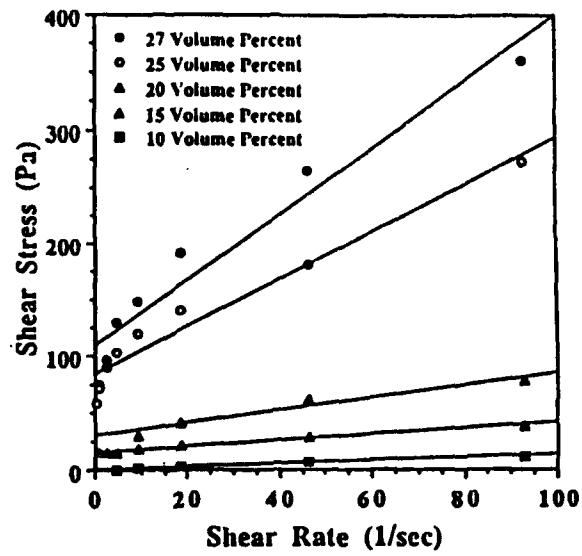


Figure 1 - Shear stress as a function of shear rate for TAM HPB/silicone oil suspensions.

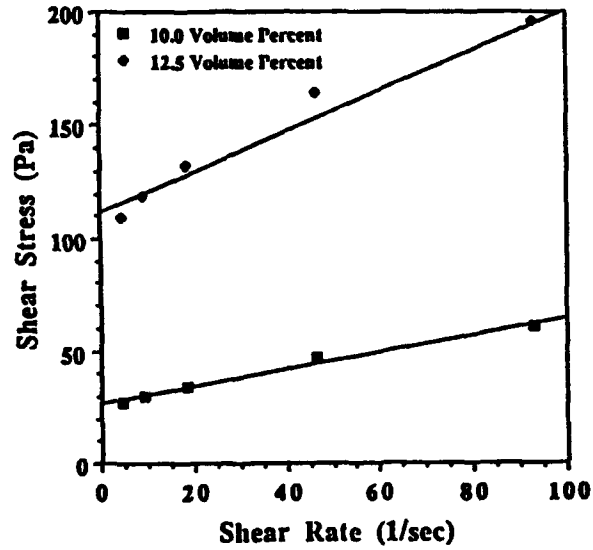


Figure 2 - Shear stress as a function of shear rate for BTH8/silicone oil suspensions.

constant viscosity as a function of shear rate. In contrast, suspensions with solids loadings  $\geq 15$  volume percent exhibited Bingham behavior with a finite yield stress ( $\tau_y$ ) and shear thinning behavior.

Figure 2 shows viscosity as a function of shear stress (Pa) for silicone oil with 10 and 12.5 volume percent BTH8. These data demonstrate that at both solid loadings, there is a large zero field viscosity. This is expected because BTH8 has a much higher surface area than TAM HPB and agglomeration is high at low solids loadings. The curves show that BTH8/silicone oil suspensions at these solids loadings possess Bingham behavior. BTH8/silicone oil suspensions up to 12.5 volume percent solids were examined. Above this loading level, the zero field viscosity was too high to measure rheological behavior.

### 3.1.2 ER Response with DC Fields

Figure 3 shows a linear relationship between  $\tau_y$  and the square of applied DC field (V/cm) at solids loadings from 10 to 25 volume percent. All TAM HPB/silicone oil suspensions demonstrated a well defined ER effect, but a limit for the applied DC field was observed (6.25kV/cm). Above this limit there was a rapid decrease in viscosity back to the zero field level. Suspensions prepared from the hydrothermally prepared powder (BTH8) exhibited a weak ER effect with applied DC field, and the viscosity decreased rapidly at field strengths above 4kV/cm. The underlying reasons for this limiting field behavior will be discussed in detail with respect to the optical microscopy observations.

### 3.1.3 ER Response as a Function of Applied Field Frequency

Figure 4 shows a typical frequency response of TAM HPB and BTH8 suspensions in silicone oil ( $k=2.8$ ). Frequencies were varied from 10Hz-1kHz to establish an optimal frequency for all solids loadings. Optimum frequency varied from 20-100Hz, depending on the powder utilized and operating field. With an operating frequency greater than the optimum frequency, it was difficult to create coherent fibrils between the electrodes. With low frequency AC fields, results similar to applied DC fields were obtained and a maximum applied field strength observed. From these data it was determined that 60Hz should be used in all AC measurements, because maximum viscosity levels were observed around this frequency for all suspensions. Prior work on BaTiO<sub>3</sub> suspensions showed frequency dependent ER response in solvents with high dielectric constant ( $k=12$ ) and high conductivity<sup>12</sup>. Apparent yield stress increased with increasing frequency, and reached a maximum above  $10^3$  Hz.

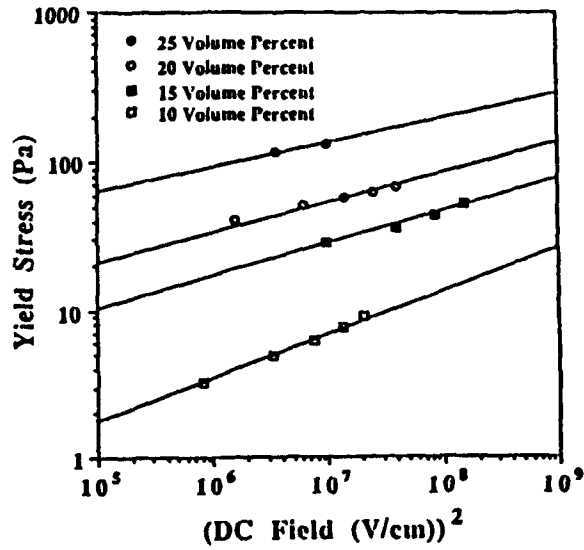
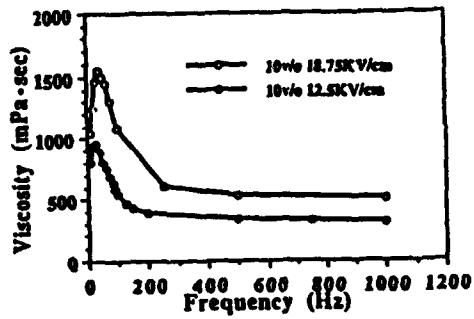


Figure 3 - Yield stress as a function of the square of applied DC field for TAM HPB/ silicone oil suspensions

(a)



(b)

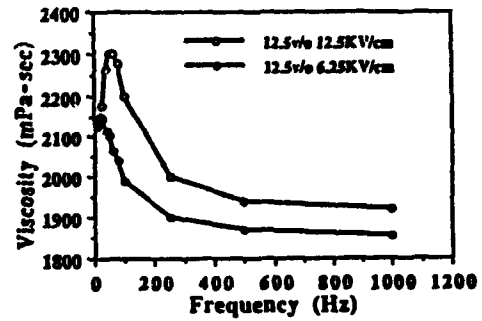


Figure 4 - Viscosity as a function of frequency (Hz) for silicone oil suspensions with (a) 10 volume percent TAM HPB and (b) 12.5 volume percent BTH8.

### 3.1.4 ER Response with Applied AC Field (60 Hz)

Yield stress plotted as a function of  $E^2$  (figure 5) reveals the linear relationship typical of ER fluids. The relative magnitude of yield stress measured here is in good agreement with previous work on BaTiO<sub>3</sub>/dodecane ER fluids evaluated at 400Hz<sup>12</sup>. The yield stresses are greater than those predicted by equation (1), but less than the finite element model developed by Davis<sup>7</sup>. Reasons for these disparities are not fully understood at this time.

### 3.1.5 Particle Size Effects

Figure 6 shows the AC response for BTH8/silicone oil suspensions at two different solid loadings. These results show a trend similar to the commercial powder suspensions of equal solid loadings, but yield stress magnitudes are not as great. These results follow dipole-dipole theory predictions that a decreased particle size will result in a reduced yield stress. This indicates that nanosized particles are not of any particular advantage for enhancing ER properties such as yield stress. Thus, even though nanosized particles may be beneficial to hinder particle settling, if well dispersed, they do not lead to enhanced ER properties in the BaTiO<sub>3</sub>/silicone oil system.

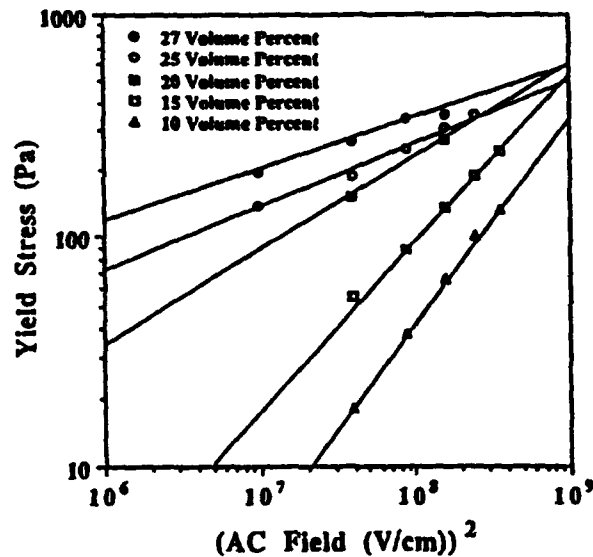


Figure 5 - Yield stress as a function of the square of applied AC field (60 Hz) for TAM HPB/silicone oil suspensions.

THIS  
PAGE  
IS  
MISSING  
IN  
ORIGINAL  
DOCUMENT

148 + 149

Optical microscopy results correlated fibril formation and ER measurements. At high field strengths ( $>6.25\text{kV/cm}$ ), DC or low AC bias ( $<10\text{Hz}$ ), turbulent flow upset fibril formation and reduced the associated ER properties. Fibrils created under an applied AC field ( $60\text{Hz}$ ) did not experience turbulent flow ( $<20\text{kV/cm}$ ).

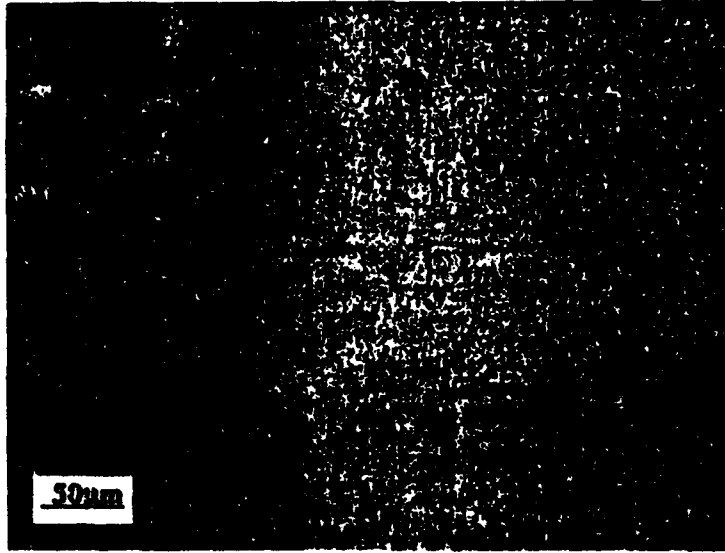


Figure 8 - Optical microscope picture of a TAM IIPB/silicone oil suspension with a  $10\text{kV/cm}$  applied DC field.

## REFERENCES

1. J. D. Carlson, A. F. Sprecher, and H. Conrad (editors), Electrorheological Fluids, Proceedings of the Second International Conference on ER Fluids, Technomic Publishers, Lancaster, PA (1990).
2. D. Scott and J. Yamaguchi, Inter. View., **21** [11] 61-66 (1983).
3. M. Bernuchon, Society of Automotive Engineers Technical Paper No. 840259 (1984).
4. M. Clark, Society of Automotive Engineers Technical Paper No. 851650 (1985).
5. R. Shoureshi, P. L. Graf, and T. L. Houston, Society of Automotive Engineers Technical Paper No. 860549 (1986).
6. T. G. Duclos, D. A. Hodgson, and J. D. Carlson, U.S. Patent No. 4,733,758 (1988).
7. L. C. Davis, Appl. Phys. Lett., **60** [3] 319-321 (1992).
8. A. R. von Hippel, Dielectrics and Waves, John Wiley and Sons, pg. 39 (1954).
9. H. A. Pohl, J. Appl. Phys., **22** [7] 869-71 (1951).
10. H. A. Pohl, J. Appl. Phys., **29** [8] 1182-9 (1958).
11. H. A. Pohl and J. P. Schwar, J. Appl. Phys., **30** [1] 69-73 (1959).
12. T. Garino, D. Adolf and B. Hance, Electrorheological Fluids, Proceedings of the Third International Conference on ER Fluids, R. Tao (editor), World Scientific Publishers, 167-174 (1991).
13. L. F. Evans, I. H. Harness, P. R. Kermod, and J. E. Stangroom, Electrorheological Fluids, Proceedings of the Third International Conference on ER Fluids, R. Tao (editor), World Scientific Publishers, 154-166 (1991).
14. D.V. Miller, C.A. Randall, A.S. Bhalla and J.H. Adair, to be published.
15. C. Bowen, A.S. Bhalla, R.E. Newnham and C.A. Randall, to be published.

**APPENDIX 49**

# Dielectrophoresis: A Means to Assemble Novel Electroceramic Composite Materials

C.A. Randall, C.P. Bowen, T.R. Shrout, A.S. Bhalla, and R.E. Newnham  
Intercollege Materials Research Laboratory  
The Pennsylvania State University  
University Park, PA 16802 U.S.A.

## I. INTRODUCTION

Recent advances in ceramic powder synthesis have led to a wide variety of submicron and micron size particulate materials with controlled stoichiometries, morphologies and size distributions.<sup>(1)</sup> The implementation of these materials into electronic composites, e.g. piezoelectric transducers/sensors, has been restricted owing to inadequate or ineffective assemblage techniques. There is, therefore, an urgent need to develop new assembly methods to engineer composites with controlled connectivity, dimensionality, percolation and anisotropy.<sup>(2)</sup> The use of electric fields and electric field gradients are herein proposed to assemble submicron particulates in a thermoset polymer matrix for various electro-ceramic composite applications.<sup>(3,4,5)</sup>

## II. BACKGROUND

When an electric field is applied to a colloidal suspension, two major phenomena can influence the translational motion of the particles; namely, electrophoresis and dielectrophoresis.<sup>(6)</sup> Electrophoresis involves the translational motion of charged particles in a direction towards the electrode of opposite charge. Dielectrophoresis involves the translational motion of polarized neutral particles under a non-uniform electric field. The translational motion under dielectrophoresis is towards the regions of highest field gradient in the non-uniform field. When particles are chosen with a dielectric constant greater than that of the matrix material, local perturbations to a uniform electric field occurs as shown in Figure 1. The local gradients about these particles give rise to an attraction known as mutual dielectrophoresis. The mutual dielectrophoretic effect destabilizes the initial suspension and induces uniaxial coagulation of the particles into chain-like structures owing to the induced dipole-dipole attractions between the filler particles. Typical chain structures are observed in the optical micrographs, Figure 2b.

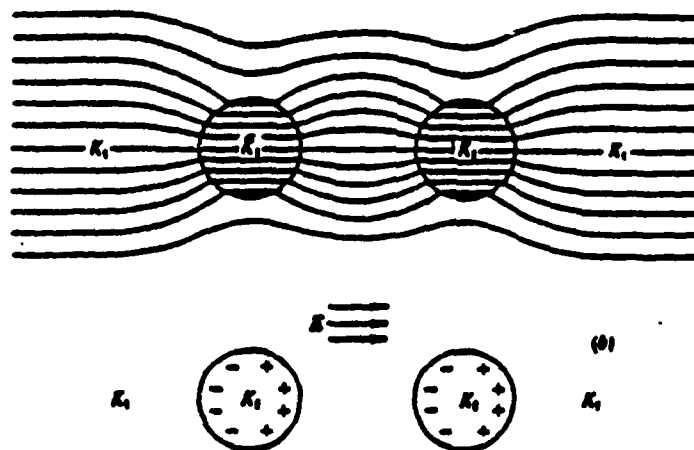
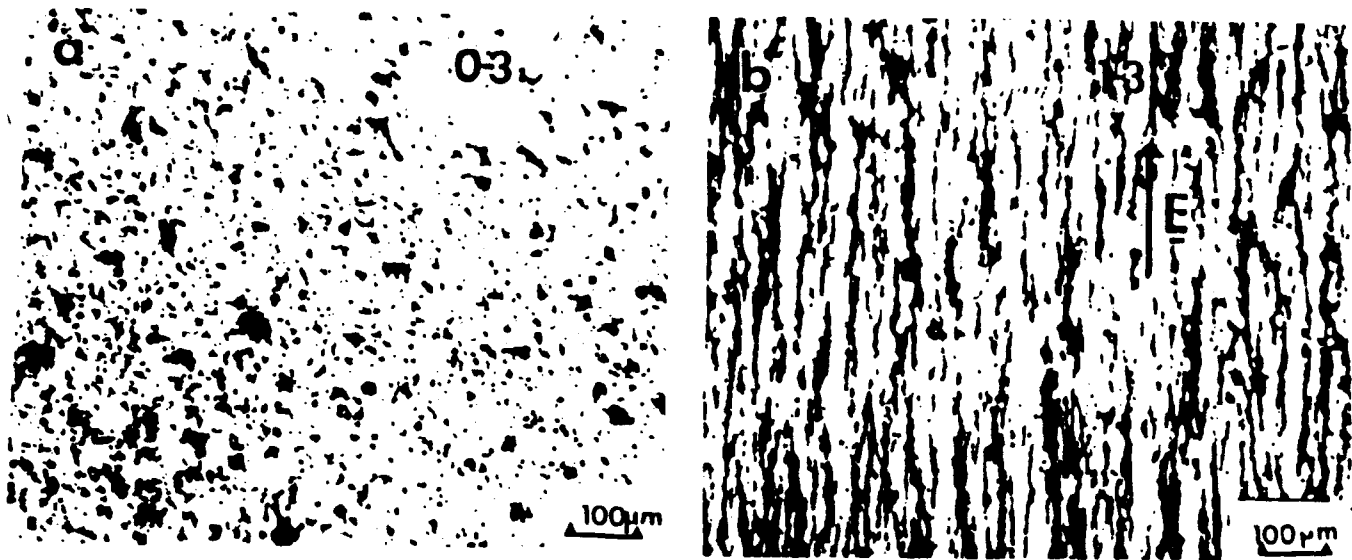


Figure 1. Schematic representation of mutual dielectrophoresis.



**Figure 2a,b.** Shows an optical micrograph of a suspension in a thermoset polymer before and after dielectrophoretic assembly.

### III. COMPOSITES AND CONNECTIVITY

In general, composite properties are strongly dependent on the component material choices, their relative volume fractions and the interconnection or connectivity of those phases. Connectivity describes the spatial distribution of each phase, and this in turn influences the relative degree of series and parallel mixing of properties within the composite. In addition, connectivity influences the dimensionality, percolation and anisotropy of a composite. Two important electroceramic composite connectivities are 0-3 and 1-3 using the Newnham nomenclature.<sup>(2)</sup> The 0-3 connectivity refers to a disperse or self-connected phase in a three-dimensionally continuous matrix, whereas the 1-3 connectivity refers to a one-dimensionally continuous filler in a three-dimensionally continuous matrix.

There exists a variety of processing techniques for the 1-3 connectivity in composites on dimensional scales ranging from 100 $\mu$ m to the macroscopic regime; these include powder injection molding, pick and place and dicing techniques. However, almost no processing techniques exist for composites with fillers of dimension  $\approx$  submicron to micron. The dielectrophoretic assembly technique gives an opportunity to process 1-3 composites on this scale without having to resort to photolithographic methods which rely on slow chemical transformations. In contrast, the dielectrophoretic technique rapidly ( $\geq 1$  millisecond) assembles the particles with electrically induced polarizations.

### IV. DIELECTROPHORETIC ASSEMBLY OF COMPOSITES

Dielectrophoretic assembly of particles requires a suitable dielectric medium which can be solidified under predetermined assembly conditions. These include thermosets, thermoplastics, waxes, gels and glasses. To date, experimentation has focused on thermoset polymers. The general material requirements are listed below:

- (i) Low dielectric constant (K) and loss ( $\tan\delta$ )
- (ii) High breakdown strength
- (iii) High viscosities—suspension stability
- (iv) Fast solidification, i.e. polymerization

Specific details of these requirements and their relation to dielectrophoretic composite assembly can be found in earlier references.<sup>(3,4,7)</sup>

In terms of filler materials, all classes of materials (insulator, semiconductor, metals) have been successfully assembled in thermoset polymers. Limitations of the more conductive fillers, e.g. graphite and aluminum, are that with these material types assembly can only take place below the percolation threshold. When percolation exists, the conductance of the composite inhibits the polarization of fillers.

Key issues that must be addressed in the dielectrophoretic assembly of composites are (1) electrophoresis and (2) the dielectric properties of the polymer. Electrophoresis removes filler from the matrix and transports it onto the electrodes of opposite charge; it can also create chaotic flow within the liquid. Low frequency dielectric properties of an uncured polymer are in some cases (e.g. epoxies) dominated by high space charge polarization mechanisms.<sup>(7,8)</sup> The low frequency dielectric constants dominate and inhibit the local polarization of the filler particles. These two inhibiting effects can be overridden using alternative electric fields; however, this gives rise to an additional variable to optimize.

The optimum frequency for 1-3 assembly can be determined by optical microscopy or through the strength of the interparticle attraction as measured through the electroviscous forces, as discussed by Bowen et al.<sup>(4)</sup> The optimum frequency conditions in various commercial thermoset polymers are summarized in Table I. Once the optimum frequency has been established, the only other processing variables are field strength, particle size, morphology and volume fraction for given material choices. These have to be established for each specific application.

**Table I. Polymers and Suppliers**

|                          | Optimum Frequency<br>(Hz) | Trade Name and Supplier                               |
|--------------------------|---------------------------|---|
| Polyurethane             | 10                        | Hysol-Dexter U50048                                   |
| Silicone elastomer       | 10                        | Sylgard-184, Dow Corning<br>Eccogel, Emerson-Cummings |
| Eccogel epoxy            | 700                       | Eccogel, Emerson-Cummings 1365                        |
| Epon epoxy               | 700                       | EPON 865 shell  |
| Norland optical adhesive | 10                        | Norland-81  |

## V. APPLICATIONS

Many of the electroceramic-polymer composites developed in the mid-seventies and eighties in the U.S.A. and Japan relied on the concepts of connectivity and percolation. Many of these composites, which included non-linear conductors, thermistors, piezoconductors, piezosensors, chemical sensors, etc., can be revisited using dielectrophoretic processing. This is of special interest to the electroceramic composites community, owing to the ever increasing difficulties associated with components miniaturization.

To illustrate the advantages of dielectrophoretic composite assembly, nanoscale BaTiO<sub>3</sub> powders were dispersed in a thermoset polymer and aligned under an alternating electric field. It was found that, using this technique, an anisotropy could be built into the dielectric properties in the composite along the applied field direction. The relative magnitudes between the transverse direction and the field direction scaled approximately 1:10.<sup>(9)</sup> This result indicates that capacitors for multichip package applications in polymer-based substrates can be addressed. Also, capacitive impedance matching in applications such as piezoelectrics can be addressed with dielectrophoresis. The ability to align and assemble other morphologies such as Pb(Zr,Ti)O<sub>3</sub> fibers (~20 μm thick and ~5 mm long) has been shown and has applications for biomedical ultrasonics.

## VI. SUMMARY

Dielectrophoresis has been established as a viable technique for micron/submicron scale assemblage in electroceramic composites. It has been shown to be applicable for a wide range of matrix and filler materials. Techniques have been developed to determine assembly parameters, such as alternating field frequency, which differ for each polymer. The manipulation of the series and parallel mixing through connectivity gives tremendous potential for composite designs in present and future applications, particularly for those "scales" difficult to engineer.

## VII. ACKNOWLEDGEMENTS

This work was sponsored from NEDO grant-in-aid. Many thanks go to Professors L.E. Cross and G.L. Messing for inspirational discussions regarding this topic and to JoAnn Mantz for typing this manuscript.

## VIII. REFERENCES

1. Better Ceramics Through Chemistry Materials, Research Society 32, Editors C.J. Brinker, D.E. Clark, and D.R. Urich (1988).
2. R.E. Newnham, Annual Rev. Mat. Science 16, 47-68 (1986).
3. C.A. Randall, D.V. Miller, J.H. Adair, and A.S. Bhalla, J. Mat. Res. 8, No. 4, 889 (1993).
4. C.P. Bowen, C.A. Randall, A.S. Bhalla, and R.E. Newnham, submitted to J. Mat. Res.
5. C.P. Bowen, T.R. ShROUT, and C.A. Randall, (submitted to J. Intelligent Structures and Materials Systems).
6. H. A. Pohl, J. Appl. Phys. 29, 1182-1189 (1958).
7. C.P. Bowen, C.A. Randall, R.E. Newnham (in progress).
8. D.E. Kranbuehl, S. Delos, P.K. Jue, SAMPE Journal 19 (4) 18-21 (1983).
9. C.A. Randall, S. Miyazaki, K.L. More, A.S. Bhalla, and R.E. Newnham, Mat. Lett. 15, 26-30 (1992).
10. C.A. Randall, C.P. Bowen, T.R. ShROUT, G.L. Messing, and R.E. Newnham, Proceedings of Internal Conference on Electrorheological Fluids, Feldkirch, Austria (1993).

# **THIN FILM FEROELECTRICS**

**APPENDIX 50**

## Origin of Orientation in Sol-Gel-Derived Lead Titanate Films

Keiko Kushida

Central Research Laboratory, Hitachi Ltd., Kokubunji, Tokyo 185, Japan

K. R. Udayakumar,\* S. B. Krupanidhi, and L. Eric Cross\*

Materials Research Laboratory, The Pennsylvania State University, University Park, Pennsylvania 16802

The origin of orientation in sol-gel-derived PbTiO<sub>3</sub> films is investigated in detail. Aging of the solution is found to promote (100) orientation of the films. Characterizing the solution by viscometry indicates that the preferred orientation might be attributable to the change of molecular size in the solution. The substrate also influences the film orientation: more strongly (100)-oriented film forms on Pt-coated Si than on fused quartz. Highly *c*-axis-oriented films with azimuthal orientation are grown on a (100) SrTiO<sub>3</sub> single-crystal disk.

## 1. Introduction

**F**ERROELECTRIC materials having the perovskite structure are of great interest in microelectronics, finding applications in pyroelectric and piezoelectric devices, nonvolatile memories, and optical waveguides. These ferroelectric films should be carefully prepared to utilize their remarkable anisotropy-dependent physical characteristics. Thin-film growth techniques can be advantageous in achieving the ordered state since atomic ordering can be manipulated in the process of film growth.

Fabrication of ferroelectric thin films has usually been accomplished by the sputtering technique, producing oriented or epitaxial films for high-efficiency devices.<sup>1-6</sup> In the last few years, the sol-gel spin-on technique, with its advantages of strict compositional control and low fabrication costs, has been extensively utilized to produce ferroelectric films mainly for memory applications.<sup>7-11</sup> Most of the work has focused on dielectric properties and switching phenomena of relatively thin (<500 nm) films. Consequently, the control of film orientation in the sol-gel process has not been investigated in detail.<sup>12</sup> Moreover, the chemistry of the process, such as the gel structure and its effect upon reaction mechanisms, is not yet fully understood although some attempts have been made to characterize the sol or gel structure.<sup>13-17</sup>

In the present work, the sol-gel spin-on technique has been utilized to produce oriented PbTiO<sub>3</sub> films. The origin of orientation in the film has been investigated in detail to examine the possibility of orientation control. The solution for film fabrication was characterized using viscometry to determine the variation in molecular size, and its effect on the film orientation investigated. Furthermore, the role of the substrate was probed. Finally, epitaxial growth was attempted on SrTiO<sub>3</sub> single crystals.

D. Shanefield—contributing editor

Manuscript No. 196175. Received November 19, 1991; approved December 11, 1992.

\*Member, American Ceramic Society.

## II. Experimental Procedure

## (1) Film Formation

In this work, the solution for film fabrication was prepared by the conventional sol-gel process, with lead acetate trihydrate and titanium isopropoxide as precursors, and 2-methoxyethanol as the solvent.<sup>5-11</sup> Lead acetate trihydrate was dissolved in heated 2-methoxyethanol (70°C) at a 1:26 molar ratio. The solution was distilled at 125°C for 1 h to expel the water of hydration. Upon cooling, a measured amount of titanium isopropoxide was added, followed by refluxing for 2 to 3 h. The solution was then heated until the temperature of the condensing vapor reached that of pure 2-methoxyethanol. In the experiments in which water was added, the molar ratio of water to total metal was maintained at 0.75.<sup>11</sup> Four percent by volume of formamide was added to the solution; formamide is known to be a drying control chemical to prevent cracks in the film. The effect of formamide has been investigated for silica gels,<sup>18,19</sup> and used in PZT films.<sup>20</sup>

Fused quartz, Pt-sputtered (100) Si, and (100) SrTiO<sub>3</sub> single-crystal disks were used as substrates. These substrates were spin-coated with the prepared solution. The rotation speed and the spin time were fixed at 2500 rpm and 35 s, respectively, to ensure that the film thickness was uniform in the substrate and had been saturated during the coating process. Each spin-on layer was 30 nm thick. The samples were heated at 400°C for 15 min for the intermediate pyrolysis step. Films of 180-nm thickness were obtained by repeating the spin-coating and pyrolysis steps 6 times. The films were then annealed in air for crystallization into the perovskite phase.

## (2) Characterization of the Solution by Viscometry

The degree of polymerization in solution was postulated to be the main determinant of orientation characteristics of the films. To test this, the molecular weight,  $M$ , was estimated by viscometry through the Mark-Houwink relation

$$[\eta] = kM^a$$

where  $[\eta]$  is intrinsic viscosity and  $k$  and  $a$  are characteristic constants. As these constants have not been determined for the PbTiO<sub>3</sub> sol-gel process, the relative change was compared between the solutions which bring the difference in orientation of the films.

Intrinsic viscosity  $[\eta]$  was determined from the dynamic viscosity at different concentrations based on the following definition:

$$[\eta] = \lim_{c \rightarrow 0} (\eta - \eta_0)/\eta_0 c$$

where  $\eta$  and  $\eta_0$  are the dynamic viscosities of the solution and pure solvent, respectively, and  $c$  is the concentration of the solution. The dynamic viscosity was measured at 33°C with an Ubbelohde dilution viscometer.

### (3) Characterization of the Crystalline and Dielectric Properties

Each film's crystalline phase was determined by X-ray diffraction. The in-plane orientation was characterized by RHEED (reflection high-energy electron diffraction). The surface morphology and microstructure of the films were observed by scanning electron microscopy.

Dielectric measurements were made with the aid of an impedance analyser using Pt as the top electrode.

## III. Results and Discussion

### (1) Optimization of the Annealing Conditions

Annealing conditions of the  $\text{PbTiO}_3$  films were optimized on Pt-coated Si substrate. X-ray diffraction data showed that the films annealed under a wide range of conditions (450° to 700°C for 0.5 to 8 h) were all single-phase  $\text{PbTiO}_3$ . However, based on the crystallinity, dielectric properties, and surface smoothness, the optimum annealing conditions were determined to be at 500°C for 8 h or 600°C for 2 h. Under these conditions,  $\text{PbTiO}_3$  films with a dielectric constant of 200 and dissipation factor of 0.02 were obtained.

### (2) Aging Effect of the Solution on the Orientation of Films

Through the optimization of annealing conditions, it was found that the age of the solution strongly affected the orientation of films. X-ray diffraction patterns of films made from aged solution (7 months) are dominated by (100) and (200) peaks, except for small peaks of (110) and (211), showing remarkable (100) orientation. On the other hand, films made from fresh solution (2 weeks old) have weak (100) preferred orientation. For comparison, the degree of orientation,  $\alpha = I_{100}/(I_{100} + I_{110})$  was calculated. For the film made from aged solution,  $\alpha$  was 0.88, and  $\alpha$  was 0.56 for the film made from fresh solution. The dependence of orientation on the age of the solution is plotted in Fig. 1, which shows that the film fabricated from aged solution exhibited stronger orientation.

The difference in orientation depending on the nature of additives is evident from the figure. The films made from the solutions containing small amounts of formamide showed lower orientation than those made from the solutions containing water. To examine the effect of formamide and water on the orientation of films, films were fabricated with four kinds of solution. As the results of Table 1 show, the addition of small amounts of formamide was found to suppress the (100) orientation of the films.

In order to explain the aging effect, the solution was modeled as in Fig. 2. When the solution is new, the molecules in the solution are small. As the solution gets older, the molecules in

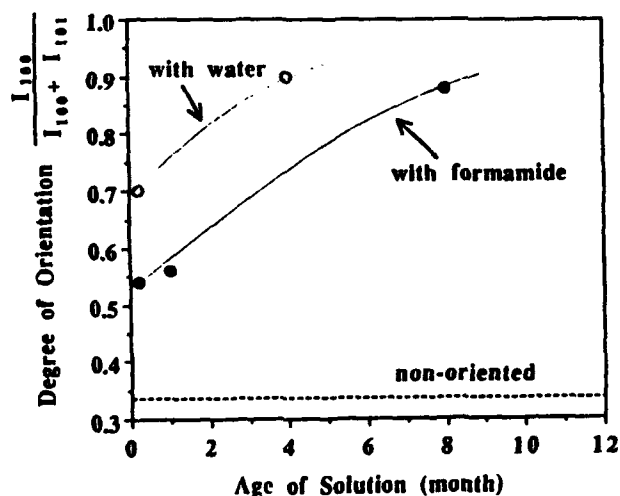


Fig. 1. Degree of orientation  $\alpha = I_{100}/(I_{100} + I_{110})$  vs age of solution.

Table 1. Orientation of the Films Containing Formamide and Water

| Formamide | Water | Degree of (100) orientation, $\alpha$ |
|-----------|-------|---------------------------------------|
| -         | -     | 0.64                                  |
| -         | +     | 0.70                                  |
| +         | -     | 0.54                                  |
| +         | +     | 0.59                                  |

Note: "+" indicates the presence and "-" the absence of the ingredient listed

the solution polymerize. If the polymers make a chainlike or slablike structure, they might be ordered by spinning as shown in Fig. 2. Although the structure of the molecules has not yet been determined precisely, there have been some reports which show the chainlike structure of  $\text{PbTiO}_3$  precursors in the early stage of polymerization.<sup>12,15</sup> This model might be applicable when the degree of polymerization is low, and the three-dimensional linkage has not been completed. To confirm this, the change in molecular size was determined by viscometry.

### (3) Viscometric Measurement of the Solution

The intrinsic viscosity was determined for solutions aged for different periods: three solutions with water (2 weeks, 3 months, and 9 months old), and three solutions with formamide (2 weeks, 3 months, and 8 months old). The change in solution viscosity with time is shown in Fig. 3; the viscosity number of the solution containing formamide is plotted relative to that containing water, assuming that the viscosities are equal at the beginning since the absolute viscosity could not be obtained because of the high viscosity of formamide. As shown in the figure, the viscosity increases with time. The change of viscosity is much greater for the solution containing water, showing the rapid polymerization in the solution. These data agree with the tendency of the orientation changes with time shown in Fig. 1. Therefore, it was concluded that the change in molecular size plausibly explains the orientation in the films.

### (4) Substrate Dependence of Orientation

A strong relation between the film orientation and the viscosity of the solution has been established. However, it is not certain whether the preferred orientation is due only to the solution characteristics or whether it also depends on the substrate. It may be stated that this preferred (100) orientation is advantageous for growing *c*-axis-oriented or epitaxial films. Both to explore the effect of the substrate and to attempt epitaxial growth, films were grown on fused quartz, Pt-coated Si, and (100)  $\text{SrTiO}_3$  disks.

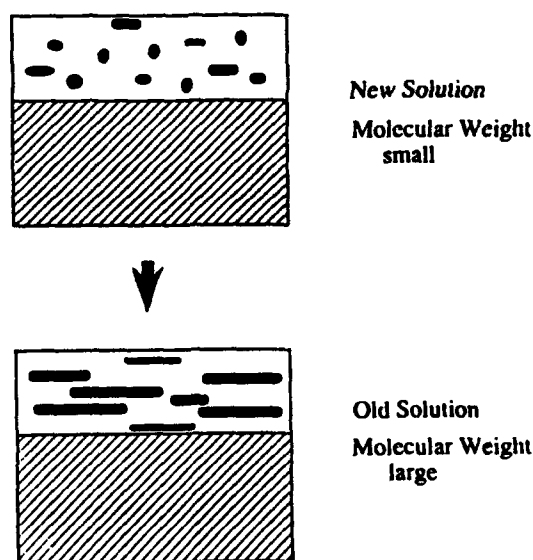


Fig. 2. Model of polymerization in solution.

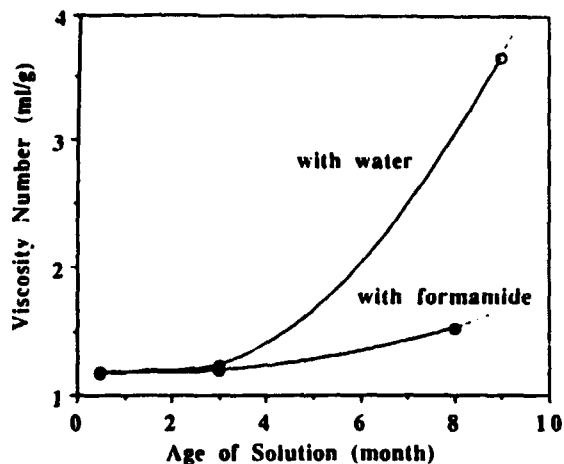


Fig. 3. Change of viscosity with time.

First, the microstructures of well-oriented and slightly oriented films on Pt-coated Si were compared. The cross section of the films was observed by high-resolution SEM. The SEM micrograph of the well-oriented film is shown in Fig. 4. Contrary to expectations, the film did not consist of the pillarlike grains usually observed in strongly oriented films. The grain structure observed suggested that nucleation occurred throughout the film. There was also no big difference in film texture between the well-oriented and slightly oriented films. These facts support the idea that the difference in the orientation may be attributed to the solution characteristics.

Next, the orientations in films on Pt/Si and on fused quartz were compared. The X-ray diffraction patterns of these films are shown in Fig. 5. The film formed on Pt/Si was better crystallized and had much higher orientation than the film on fused quartz. No interaction layer was observed near the interface between fused quartz and PbTiO<sub>3</sub> in the SEM micrograph, indicating that the observed decrease in orientation was due to the crystalline properties of the substrates. The atomic network of the highly (111)-oriented Pt underlayer might enhance crystallinity and (100) orientation. However, the film on the amorphous fused quartz substrate also had the preferred (100) orientation (degree of orientation  $\alpha = 0.52$ ; cf.  $\alpha = 0.3$  for

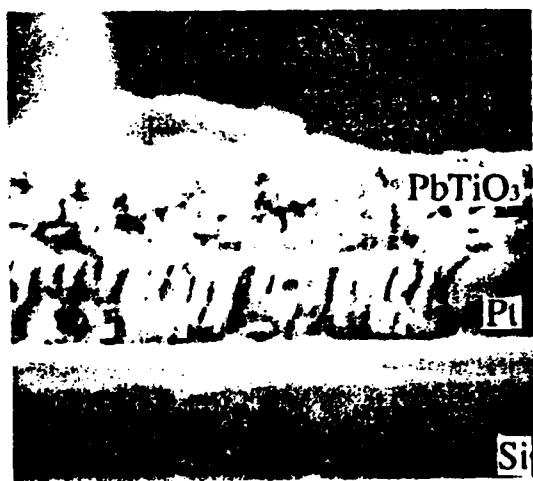


Fig. 4. SEM micrograph, cross section of PbTiO<sub>3</sub> film on Pt-coated Si.

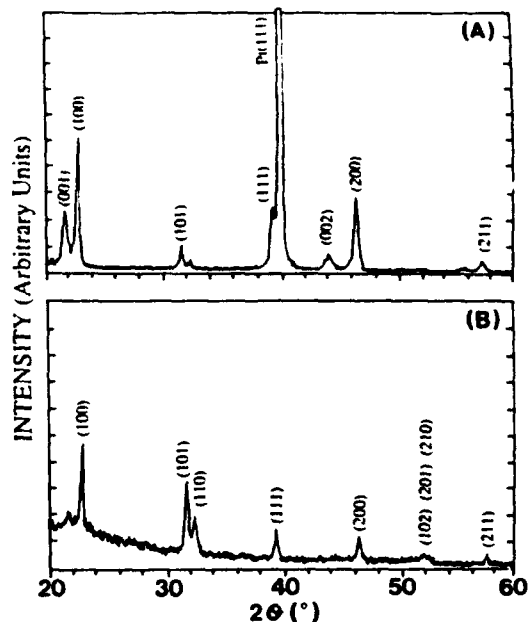


Fig. 5. X-ray diffraction patterns of PbTiO<sub>3</sub> film fabricated on (A) Pt-coated Si and (B) fused quartz.

ceramics). This also agrees with the expected effects of the solution characteristics.

Although the orientation mechanism and the effect of the Pt-coated Si substrate are not fully understood, it is evident that the *a*- or *c*-axis-oriented PbTiO<sub>3</sub> films may be easily formed when an aged solution is used. PbTiO<sub>3</sub> film was fabricated on (100) SrTiO<sub>3</sub> single-crystal disks. In this case, the film was annealed at 700°C for 4 h for epitaxial growth. The X-ray diffraction pattern shows only (00 $l$ ) [ $l = 1, 2, 3$ ] peaks from the PbTiO<sub>3</sub> film (degree of orientation  $\alpha' = I_{00l}/(I_{001} + I_{101}) = 1$ ), indicating the strong *c*-axis orientation of the film. The diffraction intensity is 30 times stronger than that for the film on Pt/Si.

To investigate the growth mode, the RHEED pattern was obtained for this film. Figure 6 shows the RHEED pattern of PbTiO<sub>3</sub> film on SrTiO<sub>3</sub> with the electron beam incident from the [100] direction. The pattern is the reciprocal lattice of the (001) plane; the film has an azimuthal orientation. However, the arch-shaped spots show a moderate degree of orientation near the film surface.

The results presented above show the sol-gel process to be feasible for the fabrication of oriented or epitaxial films when the film thickness is small. For some applications, however, thicker films are required. Fabrication of thicker films and the orientation effects as a function of film thickness must be studied in the future.



Fig. 6. RHEED pattern of PbTiO<sub>3</sub> film on (100) SrTiO<sub>3</sub> disk.

#### IV. Conclusion

The origin of orientation in sol-gel-derived PbTiO<sub>3</sub> films was investigated. Strongly (100)-oriented film was produced when aged solution was spun on a Pt/Si substrate. The solution was characterized by viscometry to estimate the change of molecular size in solution. Polymerization plausibly promoted the (100) orientation of the films. The film orientation also varied with the substrate. More strongly (100)-oriented film formed on Pt-coated Si than on fused quartz. On the SrTiO<sub>3</sub> single-crystal (100) disk, strongly c-axis-oriented films with azimuthal orientation could be grown.

**Acknowledgment:** We thank Dr. Blanco Gordon for a number of helpful discussions on viscometry.

#### References

- \*K. Iijima, Y. Tomita, R. Takayama, and I. Ueda, "Preparation of c-Axis Oriented PbTiO<sub>3</sub> Films and Their Crystallographic, Dielectric, and Piezoelectric Properties," *J. Appl. Phys.*, **60**, 361-67 (1986).
- \*M. Okuyama, T. Ueda, and Y. Hamakawa, "Preparation of Oriented PbTiO<sub>3</sub> Films on Silicon," *Jpn. J. Appl. Phys., Suppl.*, **24-2**, 619-21 (1985).
- \*S. Matsubara, N. Shohata, and M. Mikami, "Epitaxial Growth of PbTiO<sub>3</sub> on MgAl<sub>2</sub>O<sub>4</sub>/Si Substrate," *Jpn. J. Appl. Phys., Suppl.*, **24-3**, 10-12 (1985).
- \*H. Adachi, T. Mitsuyu, O. Yamazaki, and K. Wasa, "Ferroelectric (Pb,Lu)(Zr,Ti)O<sub>3</sub> Epitaxial Thin Films on Sapphire Grown by 4f-Planar Magnetron Sputtering," *J. Appl. Phys.*, **60**, 736-41 (1986).
- \*K. Kushida and H. Takeuchi, "Piezoelectricity of c-Axis Oriented PbTiO<sub>3</sub> Films," *Appl. Phys. Lett.*, **50**, 1800-801 (1987).
- \*H. Takeuchi and K. Kushida, "Lead Titanate Thin Films for Piezoelectric Applications," *Proc. Int. Symp. Appl. Ferroelectr., 7th*, 115-20 (1990).
- \*K. D. Budd, S. K. Dey, and D. A. Payne, "Sol-Gel Processing of PT, PZ, PZT, and PLZT Thin Films," *Br. Ceram. Proc.*, **36**, 107-21 (1985).
- \*S. K. Dey and R. Zuleeg, "Processing and Parameters of Sol-Gel PZT Thin Films for GaAs Memory Applications," *Proc. Symp. Integr. Ferroelectr.*, **1**, 189-94 (1989).
- \*K. R. Udayakumar, J. Chen, S. B. Krupandlu, and L. E. Cross, "Sol-Gel-Derived PZT Thin Films for Switching Applications," *Proc. Int. Symp. Appl. Ferroelectr., 7th*, 741-43 (1990).
- \*K. D. Budd, S. K. Dey, and D. A. Payne, "The Effect of Hydrolysis Conditions on the Characteristics of PbTiO<sub>3</sub> Gels and Thin Films," *Mater. Res. Soc. Symp. Proc.*, **73**, 711-16 (1986).
- \*G. Yi, Z. Wu, and M. Sayer, "Preparation of Pb(Zr,Ti)O<sub>3</sub> Thin Films by Sol-Gel Processing: Electrical, Optical, and Electro-optic Properties," *J. Appl. Phys.*, **64**, 2717-24 (1988).
- \*C. Chen, D. F. Ryder, and W. A. Spurgeon, "Synthesis and Microstructure of Highly Oriented Lead Titanate Thin Films Prepared by a Sol-Gel Method," *J. Am. Ceram. Soc.*, **72**, 1495-98 (1989).
- \*Y. Hayashi and J. B. Blum, "Sol-Gel Derived PbTiO<sub>3</sub>, Part 2, Structural Control of Monolithic Gels," *J. Mater. Sci.*, **22**, 2655-60 (1987).
- \*S. D. Ramamurthi and D. A. Payne, "Structural Investigations of Prehydrolyzed Precursors Used in the Sol-Gel Processing of Lead Titanate," *J. Am. Ceram. Soc.*, **73**, 2547-51 (1990).
- \*T. W. Dekleva, J. M. Hayes, L. E. Cross, and G. L. Geoffroy, "Sol-Gel Processing of Lead Titanate in 2-Methoxyethanol: Investigations into the Nature of the Prehydrolyzed Solutions," *J. Am. Ceram. Soc.*, **71**, C-280-C-282 (1988).
- \*R. A. Lipeles, D. J. Coleman, and M. S. Leung, "Effects of Hydrolysis on Metallo-organic Solution Deposition of PZT Films," *Mater. Res. Soc. Symp. Proc.*, **73**, 665-70 (1986).
- \*K. Kezuka, Y. Hayashi, and T. Yamaguchi, "Synthesis and Characterization of Lead-Titanium Complex Alkoxide," *J. Am. Ceram. Soc.*, **72**, 1660-63 (1989).
- \*G. Ortel and L. Hench, "Effect of Formamide Additive on the Chemistry of Silica Gels, Part I: NMR of Silica Hydrolysis," *J. Non-Cryst. Solids*, **79**, 177-94 (1986).
- \*G. Ortel, L. L. Hench, I. Artaki, J. Jones, and T. W. Zerda, "Effect of Formamide Additives on the Chemistry of Silica Sol-Gels, Part II: Gel Structures," *J. Non-Cryst. Solids*, **105**, 223-31 (1988).
- \*L. E. Sanchez, S. Y. Wu, and I. K. Naik, "Observations of Ferroelectric Polarization Reversal in Sol-Gel Processed Very Thin PZT Films," *Appl. Phys. Lett.*, **56**, 2399-401 (1990). □

**APPENDIX 51**

# Electric field forced phase switching in La-modified lead zirconate titanate stannate thin films

K. G. Brooks, J. Chen, K. R. Udayakumar, and L. E. Cross

Materials Research Laboratory, The Pennsylvania State University, University Park, Pennsylvania 16802

(Received 10 February 1993; accepted for publication 2 October 1993)

Electric field forced antiferroelectric to ferroelectric phase switching has been demonstrated in thin films of  $\text{Pb}_{0.97}\text{La}_{0.02}(\text{Zr},\text{Ti},\text{Sn})\text{O}_3$  perovskites for the first time. Several compositions in the tetragonal antiferroelectric phase field of this system were prepared in thin film form by a sol-gel technique. Forward and reverse switching threshold fields of 27–103 kV/cm and 18–62 kV/cm, respectively, were determined from polarization-electric field hysteresis and incremental capacitance data. Switching times as fast as 300 ns were recorded for one of the antiferroelectric compositions. An electric field induced longitudinal strain of 0.16% was measured for a film of composition  $(\text{Pb}_{0.97}\text{La}_{0.02})(\text{Zr}_{0.60}\text{Ti}_{0.10}\text{Sn}_{0.30})\text{O}_3$  using a laser ultradilatometer. These films are candidate materials for high charge storage integrated capacitors and microelectromechanical devices requiring large nonlinear strain response.

## I. INTRODUCTION

Research in the area of ferroelectric thin films is being driven by the market potential of nonvolatile memory devices.<sup>1-3</sup> Due to the piezoelectric and pyroelectric properties of these thin films, applications are also emerging in the field of microelectromechanical systems (MEMS).<sup>4-6</sup> Ultrasonic micromotors utilizing lead zirconate titanate (PZT) thin films<sup>7,8</sup> and pyroelectric sensors using micro-machined  $\text{PbTiO}_3$  (PT)<sup>9</sup> have been fabricated. Thin film materials capable of large strains are being sought for a range of MEMS applications including micromotors, microvalves, and micropumps. Such devices will be utilized in compact medical, automotive, and space systems. Candidate materials include tetragonal antiferroelectric perovskites in the  $\text{Pb}_{0.97}\text{La}_{0.02}(\text{Zr},\text{Ti},\text{Sn})\text{O}_3$  (PLZTSn) and  $\text{Pb}_{0.99}(\text{Zr},\text{Ti},\text{Sn})_{0.98}\text{Nb}_{0.02}\text{O}_3$  (PZTSnN) systems.

Tetragonal antiferroelectric (AFE) PLZTSn and PZTSnN ceramics of compositional proximity to the morphotropic phase boundary with the rhombohedral ferroelectric phase can be phase switched by application of an electric field from the AFE to FE states. The small free energy difference between the two phases make such switching possible.<sup>10</sup> The large volume difference between the AFE and FE phases dictates that large strains accompany such field induced phase switching.<sup>11</sup> Irreversible or field assisted switching (shape memory effect) occurs when the AFE composition is sufficiently close to the AFE-FE phase boundary that the electric field induced FE phase is metastable, with the free energy difference being less than the reverse switching threshold field energy.<sup>12</sup> The AFE phase can be recovered by thermal annealing or application of a reverse bias field.<sup>13</sup> Reversible or field forced switching occurs in compositions outside the region of metastability.

PLZTSn and PZTSnN ceramics have been investigated for several applications over the past 40 years including energy storage,<sup>14</sup> high strain actuators,<sup>10,13,15,16</sup> and shape memory devices.<sup>17</sup> Recent papers have focused on the thermodynamics of phase switching,<sup>12,15</sup> and transmission electron microscopy investigations of domain structures.<sup>18,19</sup>

Utilization of these ceramics has been limited due to high switching fields, being of the order of the electrical breakdown strength.<sup>14</sup> Degradation of the ceramics under an ac field excitation, with average life cycles of  $\approx 10^7$ , was reported by Pan *et al.*<sup>16</sup>

Synthesis of thin films in the PLZTSn system was motivated by the large strain values reported for the bulk ceramic materials. The largest longitudinal strain reported to date is 0.87% for a bulk ceramic of composition  $(\text{Pb}_{0.97}\text{La}_{0.02})(\text{Zr}_{0.66}\text{Ti}_{0.11}\text{Sn}_{0.23})\text{O}_3$ .<sup>15</sup> Thin films offer the possibility of integrated manufacturing of microsensors, microactuators, and high charge storage capacitors. In this article, we report the synthesis, characterization, polarization-electric field (P-E), and capacitance-voltage (C-V) response of sol-gel derived thin films in the PLZTSn perovskite system. The P-E and C-V data allow delineation of the forward AFE-FE, and reverse FE-AFE, electric field induced switching thresholds. Electric field induced strain and field induced AFE-FE switching speeds are also reported for select compositions.

## II. THIN FILM SYNTHESIS AND COMPOSITION SELECTION

Several compositions in the  $\text{Pb}_{0.97}\text{La}_{0.02}(\text{Zr},\text{Ti},\text{Sn})\text{O}_3$  system were chosen based on an earlier paper which focused on bulk ceramic materials for large displacement transducers.<sup>16</sup> The pertinent area of the  $\text{PbZrO}_3$ - $\text{PbTiO}_3$ - $\text{PbO}:\text{SnO}_2$  ternary phase diagram is shown in Fig. 1; compositions studied are indicated in the figure, and the corresponding chemical formula listed explicitly in Table I. This choice of compositions allowed comparison of phase switching parameters between bulk and thin films.

Thin films of the desired compositions were prepared by the sol-gel spin-on technique. Silicon wafers with titanium bonded platinum electrodes served as substrates. Precursors used for preparation of the sol-gel solutions included lead acetate trihydrate, tin<sup>IV</sup> acetate (anhydrous), lanthanum isopropoxide, zirconium *n*-propoxide, and tita-

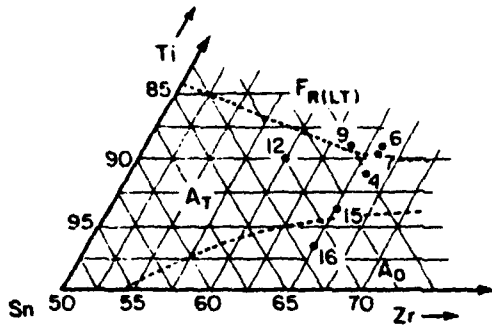


FIG. 1. The  $\text{PbTiO}_3\text{-PbZrO}_3\text{-PbO:SnO}_2$  ternary phase diagram showing the orthorhombic antiferroelectric ( $A_0$ ), tetragonal antiferroelectric ( $A_T$ ), and low temperature rhombohedral ferroelectric ( $F_{R(LT)}$ ) phase fields. Compositions studied are indicated (from Berlincourt, see Ref. 10).

niun isopropoxide. Details of the sol-gel precursor solution synthesis have been described previously,<sup>20</sup> and are summarized in the flow diagram, Fig. 2.

Films were annealed by rapid thermal processing, typically at 700 °C for 20 s, unless noted otherwise. For films annealed under these conditions, only perovskite reflections were observed by grazing angle x-ray diffraction. Films annealed at 600 °C were also phase pure but required extended annealing times to achieve equivalent properties. Films annealed above 750 °C exhibited hysteresis loop degradation which can be attributed to loss of Pb from the film. Film thicknesses were in the range of 0.3–0.4  $\mu\text{m}$ .

Microstructures of the films were characterized by scanning electron microscopy (SEM). The films were found to be very uniform, with microstructures being dependent upon composition. Grain sizes of approximately 0.5  $\mu\text{m}$  were observed for films of composition 4 (Fig. 3). Larger grain sizes, of the order of 1.0  $\mu\text{m}$  were observed for films of compositions 6, 7, and 9.

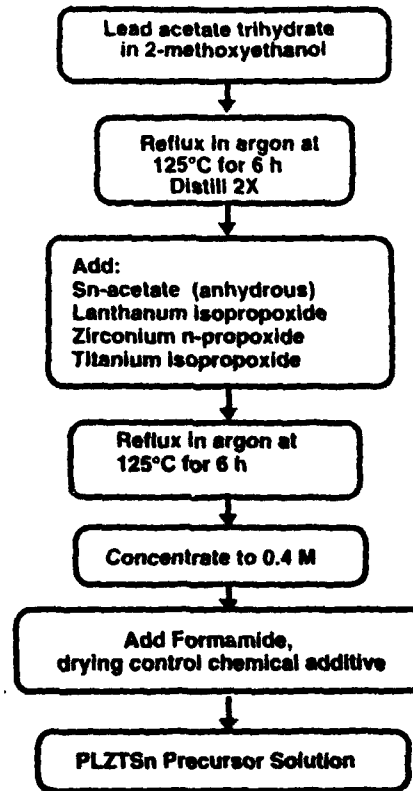


FIG. 2. Flow diagram of the sol-gel synthesis of PLZTSn thin films.

### III. FIELD INDUCED AFE-FE PHASE SWITCHING

#### A. Measurements

Polarization-electric field hysteresis was measured using a modified Sawyer-Tower circuit. Electrical contact with the film surface was achieved with a Hg-probe test fixture. The effective electrode area was  $4.3 \times 10^{-3} \text{ cm}^2$ . Samples were driven with a 10–15 V, 60 Hz signal (10 V  $\approx$  300 kV/cm for film thickness studied). Scanning elec-

TABLE I. Compositions studied and summary of thin film and bulk ceramic electric field induced switching data.

| No. | Composition  | Thin film         |                      |                      |   | Bulk ceramic <sup>a</sup> |                      |   |
|-----|--|-------------------|----------------------|----------------------|---|---------------------------|----------------------|---|
|     |  | $E_{AFF}$ (kV/cm) | $E_{AFE-FE}$ (kV/cm) | $E_{FE-AFE}$ (kV/cm) | $P_{max}$ ( $\mu\text{C}/\text{cm}^2$ ) | $E_{AFF}$ (kV/cm)         | $E_{AFE-FE}$ (kV/cm) | $P_{max}$ ( $\mu\text{C}/\text{cm}^2$ ) |
| 4   | $(\text{Pb}_{0.97}\text{La}_{0.02})(\text{Zr}_{0.66}\text{Ti}_{0.09}\text{Sn}_{0.25})\text{O}_3$   | 300               | 103                  | 53                   | 32                                      | 75                        | 50                   | 43                                      |
| 6   | $(\text{Pb}_{0.97}\text{La}_{0.02})(\text{Zr}_{0.66}\text{Ti}_{0.11}\text{Sn}_{0.23})\text{O}_3$   | 300               | 85 <sup>b</sup>      | 23 <sup>c</sup>      | 33                                      | 46                        | 21                   | 40                                      |
| 7   | $(\text{Pb}_{0.97}\text{La}_{0.02})(\text{Zr}_{0.66}\text{Ti}_{0.109}\text{Sn}_{0.235})\text{O}_3$ | 300               | 81 <sup>b</sup>      | 47 <sup>c</sup>      | 26                                      | 58                        | 22                   | 36                                      |
| 9   | $(\text{Pb}_{0.97}\text{La}_{0.02})(\text{Zr}_{0.64}\text{Ti}_{0.11}\text{Sn}_{0.25})\text{O}_3$   | 300               | 27 <sup>b</sup>      | ... <sup>d</sup>     | 11                                      | 60                        | 24                   | 36                                      |
| 12  | $(\text{Pb}_{0.97}\text{La}_{0.02})(\text{Zr}_{0.60}\text{Ti}_{0.16}\text{Sn}_{0.20})\text{O}_3$   | 200               | 44                   | 18                   | 26                                      | 59                        | 49                   | 32                                      |
|     |  | 300               | 40                   | 20                   | 28                                      |                           |                      |   |
| 15  | $(\text{Pb}_{0.97}\text{La}_{0.02})(\text{Zr}_{0.65}\text{Ti}_{0.07}\text{Sn}_{0.28})\text{O}_3$   | 200               | 89                   | 62                   | 21                                      |                           |                      |   |
|     |  | 300               | 87                   | 59                   | 24                                      |                           |                      |   |
|     |  | 400               | 87                   | 54                   | 26                                      |                           |                      |   |
| 16  | $(\text{Pb}_{0.97}\text{La}_{0.02})(\text{Zr}_{0.65}\text{Ti}_{0.058}\text{Sn}_{0.312})\text{O}_3$ | 800               | 233                  | 134                  | 31                                      |                           |                      |   |

<sup>a</sup>Data from Ref. 14.

<sup>b</sup>Determined from C-V data, initial cycle.

<sup>c</sup>Determined from C-V data.

<sup>d</sup>Metastable FE phase formation.

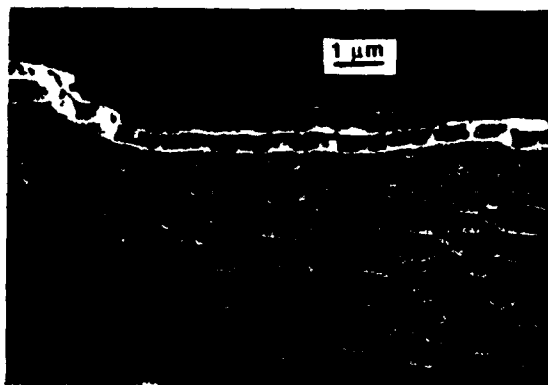


FIG. 3. Typical SEM microstructure of PLZTSn thin films. Shown above is the photomicrograph of a film of composition 4 annealed at 700 °C for 20 s.

tron microscopy was used to determine film thickness. All measurements described were carried out at 25 °C.

Capacitance data as a function of slowly varying bias field was collected with a computer interfaced impedance analyzer (HP 4192A). Sputtered Au electrodes approximately 1000 Å thick and  $2.8 \times 10^{-3} \text{ cm}^2$  in area were used. Capacitance was determined using a 10 mV, 10 kHz test signal. Under these conditions, the dielectric loss was always less than 0.08. The dc bias was slowly stepped through 0.2 V increments in a cyclic manner between -10 and +10 V.

Electric field induced strain was measured using a laser interferometer with a film surface displacement resolution of  $10^{-2} \text{ Å}$ .<sup>21</sup> Phase switching was induced with a 500 Hz electric field of varying magnitude and under different bias conditions.

The switching current was measured as a function of time by the square pulse technique. The signal pick-up resistor was 5 Ω to reduce the RC constant. A parallel resistor of 50 Ω was used to reduce the signal reflection during the measurements.

## B. Results and discussion

Dynamic polarization-electric field (P-E) hysteresis curves were recorded for all the compositions, and the switching field data tabulated in Table I. The P-E traces for compositions 12 and 16, exemplifying phase switching, are shown in Fig. 4. Forward switching (AFE-FE) and backward switching (FE-AFE) fields were determined by taking the intersections of two lines representing the steepest and flattest sections of the hysteresis loops. For compositions in close proximity to the AFE-FE phase boundary (6,7,9), switching threshold fields could not be determined from P-E hysteresis data. The remanence observed for these boundary compositions indicates that some fraction of the film is retained in the FE state at zero field. The switching data obtained is summarized in Table I. For films of composition 15, switching parameters were investigated as a function of applied field. The forward switch-

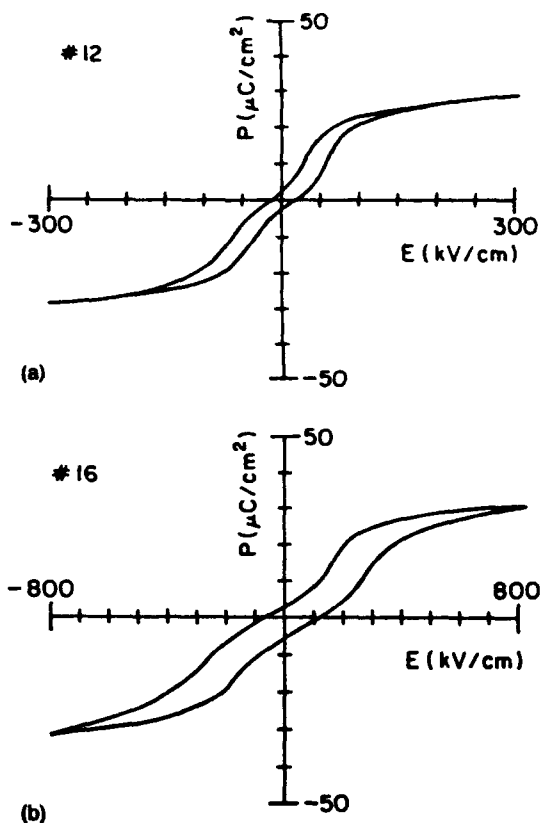


FIG. 4. Polarization-electric field hysteresis loop for thin films of composition (a) 12, (b) 16. Forward switching (AFE-FE) and backward switching (FE-AFE) fields were determined by taking the intersections of two lines representing the steepest and flattest sections of the hysteresis loops.

ing threshold was constant as a function of increasing field from 200 to 400 kV/cm. However, the reverse switching threshold was found to decrease and the maximum polarization increase as applied field increased. The ability to switch films of composition 16, which lies in the orthorhombic AFE phase field, was an interesting result. The forward switching threshold of 233 kV/cm under an applied field of 800 kV/cm is indicative of the large free energy difference between this and the FE phase.

Phase switching thresholds can also be derived from capacitance as a function of slowly varying bias field. The relationship between the P-E hysteresis and  $C-V$  data is shown schematically in Fig. 5. Phase switching thresholds can be estimated from the  $C-V$  curves by defining switching as the bias at maximum capacitance. This definition, however, yields forward and reverse thresholds slightly larger than those obtained from analogous P-E hysteresis data. The incremental capacitance data for compositions 12 and 16 is shown in Fig. 6 (compare with the corresponding P-E curves of Fig. 4). This data made it possible to measure the threshold fields when the P-E curves were ambiguous, particularly in the case of boundary compositions (6,7,9). In the case of composition 9, only forward switching could be positively determined. The P-E and  $C-V$  data indicate that a metastable FE phase is induced upon application of field to the virgin sample, and is re-

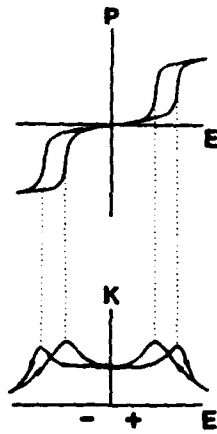
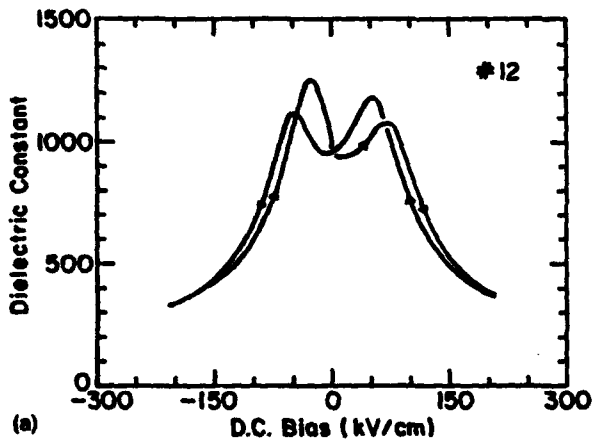


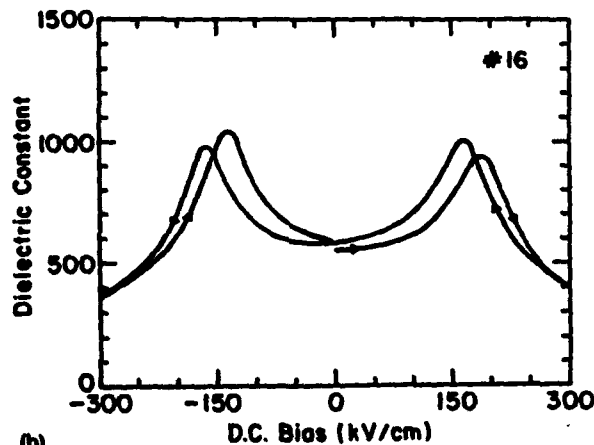
FIG. 5. Schematic illustration of the relationship between P-E hysteresis loop and incremental C-V data.

tained to a large extent after field removal. In fact, metastable ferroelectric phase may be predominantly present in boundary compositions 6,7,9; the absence of initial P-E curves on these compositions makes this a distinct possibility.

In all of the thin films studied, the data suggests the coexistence of FE and AFE phases, by the observed rema-



(a)



(b)

FIG. 6. Incremental capacitance data for films of composition (a) 12 and (b) 16.

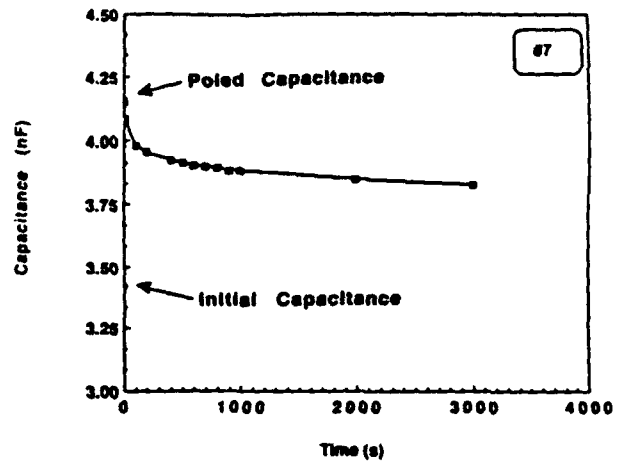


FIG. 7. Capacitance decay of poled film (composition 7).

nence in the P-E data (all cases), and the broadening of the capacitance maximum peaks in the C-V data, (6,7,9). Graef<sup>19</sup> observed the coexistence of AFE and FE domains in the same grain by transmission electron microscopy of PLSnZT bulk ceramic materials of composition  $(\text{Pb}_{0.97}\text{La}_{0.02})(\text{Zr}_{0.55}\text{Sn}_{0.35}\text{Ti}_{0.10})\text{O}_3$  (compare to composition 12). Similar observations were described by Zhiming *et al.*<sup>18</sup> for ceramics of composition  $\text{Pb}_{0.99}[(\text{Zr}_{1-x}\text{Sn}_x)_{1-x}\text{Ti}_x]_{0.98}\text{Nb}_{0.02}\text{O}_3$ ; it was suggested that the AFE-FE phase boundary is not distinct, but can rather be defined as the composition where the volume of coexisting AFE and FE phases are equal. The observation of forward switching by C-V analysis of film composition 6, which is compositionally in the FE phase field, provides the first supporting evidence to this conclusion. Further research on these phase switchable thin films, especially high resolution electron microscopy (HREM), is necessary to prove the coexistence of AFE and FE domains in the same grain.

Berlincourt<sup>11</sup> determined that a lateral contraction of 0.02% occurs due to alignment of the AFE phase when ceramics of composition  $\text{Pb}_{0.99}(\text{Zr},\text{Ti},\text{Sn})_{0.98}\text{Nb}_{0.02}\text{O}_3$  are poled; a similar phenomenon is observed in PLZTSn ceramics. Such a lateral contraction in thin films would produce an effective tensile stress due to substrate clamping and should favor the larger volume FE phase, assuming no other stresses. This could lead to metastable FE phase formation, i.e., a stress stabilized shape memory phenomenon. Such an effect might contribute to the retention of some fraction of FE phase in all compositions studied. This would offer one explanation for the remanence observed in all of the P-E measurements.

Zhiming *et al.*<sup>18</sup> observed that the piezoelectric coefficient  $d_{33}$  and remanent polarization  $P_r$  of poled (induced metastable FE phase) ceramics of composition  $\text{Pb}_{0.99}\text{Nb}_{0.02}[(\text{Zr}_{0.82}\text{Sn}_{0.18})_{0.968}\text{Ti}_{0.032}]_{0.98}\text{O}_3$  decrease with time, disappearing after about a year. Similar phenomena were observed in thin films described here. Figure 7 represents the time dependence of capacitance in virgin samples of composition 7 which have been poled with a 300 kV/cm

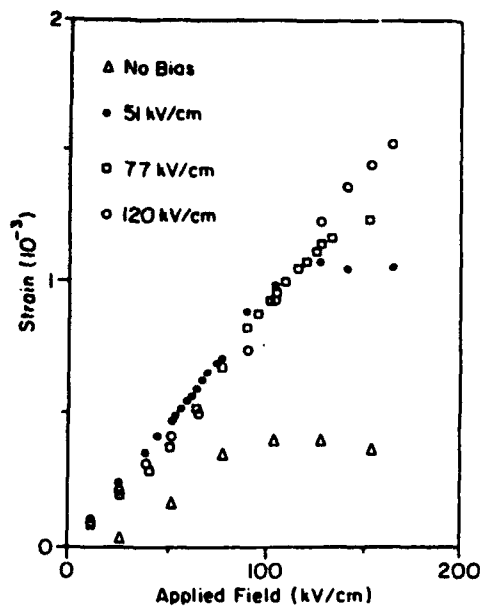


FIG. 8. Field induced strain for a film of composition 12 as a function of field and applied bias.

field. It is observed that the poled capacitance (FE phase) decays with time. This suggests that the FE domains shrink at the expense of AFE domains, with aging. We suggest that some volume of FE phase will be retained, however, due to stress effects in the thin films.

In Table I, switching data for bulk ceramics of identical compositions to those studied for the thin films is reproduced for comparison purposes.<sup>16</sup> In most cases (compositions 4, 6, 7), the forward switching threshold fields were significantly larger for the thin films when compared with the ceramics; the maximum polarization values in the films were lower than in the corresponding bulk materials.

Electric field induced longitudinal strain data for a film of composition 12 is presented in Fig. 8. The strain was observed to increase with increasing ac and dc bias fields. The measurement technique employed allowed only discrete strain measurements. The maximum strain achieved was 0.16%; for a bulk ceramic of the same composition, a value of 0.42% has been reported.<sup>16</sup> For these experiments, the function generator used had a maximum internal bias of approximately 5 V (which corresponds to the highest bias applied to 120 kV/cm), and a maximum  $V_{rms}$  of 4.65 V (which corresponds to the maximum applied field of 160 kV/cm). The data indicates that further increase of the  $V_{rms}$  and bias field would increase the observed strain. This assumption is supported by the increased polarization values observed in the film of composition 15 as the field was increased from 200 to 400 kV/cm, as discussed above.

For microactuator applications, apart from the field induced polarization and strain, the parameter of interest is the switching speed of phase transition between the antiferroelectric and ferroelectric phases. Figure 9 illustrates the switching current as a function of time for a film of composition 4; the film was  $0.43 \mu\text{m}$  thick, with an electrode area of  $250 \times 250 \mu\text{m}^2$ . The switching time is less

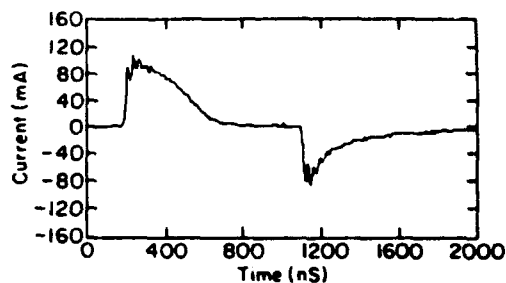


FIG. 9. Switching behavior of PLZTsn thin film of composition 4. The switching speed of the film is about 300 ns.

than 300 ns for forward switching which is shorter than the  $2 \mu\text{s}$  switching time reported for the bulk ceramic of equivalent composition.<sup>22</sup> The backward switching time was found to be of the same magnitude as the forward switching time. The switching time of phase transition is influenced by the grain size, stress, and defects in the material. Thin films are characterized by smaller grain sizes in general and lower level of defects than the bulk ceramic which can possibly explain the faster switching speed in the films. Furthermore, thin films have a large surface area resulting in faster heat dissipation during the field induced phase transition; this aids in preventing the acceleration of fatigue which is a major problem in the reliability of antiferroelectric ceramic devices.

#### IV. SUMMARY

Thin films of antiferroelectric PLZTsn, which exhibit electric field induced AFE-FE phase switching, have been prepared by the sol-gel spin-on technique. Switching voltages (typically less than 4 V) and threshold fields of these films were in a range that permit its utility in micromechanical devices; strains of 0.16% have been measured in these films. The fast response of the films was manifest in the observed switching speed of 300 ns.

<sup>1</sup>D. Bondurant and F. Gnadinger, *IEEE Spectrum*, 30 (1989).

<sup>2</sup>W. A. Geideman, *IEEE Trans. Ultrasonics, Ferroelectrics and Frequency Control* 38, 704 (1991).

<sup>3</sup>J. F. Scott and C. A. Paz de Araujo, *Science* 246, 1400 (1989).

<sup>4</sup>J. Chen, K. R. Udayakumar, K. G. Brooks, and L. E. Cross, *Mater. Res. Soc. Symp. Proc.* 243, 361 (1992).

<sup>5</sup>K. G. Brooks, K. R. Udayakumar, J. Chen, U. Selvaraj, and L. E. Cross, *Mater. Res. Soc. Symp. Proc.* 276, 11 (1992).

<sup>6</sup>S. W. Wenzel and R. M. White, *IEEE Trans. Electron Devices* 35, 735 (1988).

<sup>7</sup>A. M. Flynn, L. S. Tavrow, S. F. Bart, R. A. Brooks, D. J. Ehrlich, K. R. Udayakumar, and L. E. Cross, *J. Microelectromechanical Systems* 1, 44 (1992).

<sup>8</sup>K. R. Udayakumar, J. Chen, K. G. Brooks, L. E. Cross, A. M. Flynn, and D. J. Ehrlich, *Mater. Res. Soc. Symp. Proc.* 243, 49 (1992).

<sup>9</sup>D. L. Polla, C. Ye, and T. Tamagawa, *Appl. Phys. Lett.* 59, 3539 (1991).

<sup>10</sup>D. Berlincourt, *IEEE Trans. Sonics Ultrason.* SU-13, 116 (1966).

<sup>11</sup>D. Berlincourt, H. H. A. Krueger, and B. Jaffe, *J. Phys. Chem. Solids* 25, 659 (1964).

<sup>12</sup>P. Yang and D. A. Payne, *J. Appl. Phys.* 71, 1361 (1992).

- <sup>11</sup> D. Jaffe, *Proc. Inst. Radio Engineers* **49**, 1264 (1961).
- <sup>14</sup> W. Y. Pan, C. Q. Dam, Q. M. Zhang, and L. E. Cross, *J. Appl. Phys.* **66**, 6014 (1989).
- <sup>15</sup> Y. Sugawara and K. Uchino, in *Proceedings of the 7th IEEE International Symposium on Applications of Ferroelectrics*, edited by S. B. Krupanidhi and S. K. Kurtz (IEEE, New York, 1991), pp. 328-329.
- <sup>16</sup> W. Y. Pan, Q. M. Zhang, A. S. Bhalla, and L. E. Cross, *J. Am. Ceram. Soc.* **72**, 571 (1989).
- <sup>17</sup> A. Furata, K. Oh, and K. Uchino, in *Proceedings of the 7th IEEE International Symposium on Applications of Ferroelectrics*, edited by S. B. Krupanidhi and S. K. Kurtz (IEEE, New York, 1991), pp. 528-529.
- <sup>18</sup> C. Zhiming, L. Jingyu, and W. Yongling, *Ferroelectrics* **101**, 225 (1990).
- <sup>19</sup> M. De Graef, J. S. Speck, D. R. Clarke, and D. Dimos, *Mater. Res. Soc. Symp. Proc.* **243**, 1 (1992).
- <sup>20</sup> K. G. Brooks, J. Chen, K. R. Udayakumar, and L. Eric Cross, *Mater. Res. Soc. Symp. Proc.* **243**, 443 (1992).
- <sup>21</sup> Q. M. Zhang, W. Y. Pan, and L. E. Cross, *J. Appl. Phys.* **63**, 2492 (1988).
- <sup>22</sup> W. Y. Pan, W. Y. Gu, and L. E. Cross, *Ferroelectrics* **99**, 185 (1989).

**APPENDIX 52**

## MEASUREMENTS OF DIELECTRIC CONSTANT AND QUALITY FACTOR OF $\text{Ba}(\text{Mg}_{1/3}\text{Ta}_{2/3})\text{O}_3$ AT X BAND FREQUENCIES

JYH SHEEN, RUYAN GUO, A. S. BHALLA, AND L. E. CROSS

Materials Research Laboratory, The Pennsylvania State University,  
University Park, Pennsylvania 16802, U.S.A.

(Received for Publication June 25, 1993)

**ABSTRACT** Dielectric properties of  $\text{Ba}(\text{Mg}_{1/3}\text{Ta}_{2/3})\text{O}_3$  in forms of ceramic, single crystal fiber, and polyethylene composite at microwave frequencies were measured. The dielectric constants 23.33, 24.30, and 26.50 and the quality factors 8,050, 6,430, and larger than 2,000 at 10 GHz were measured for the ceramic, hot pressed ceramic and the fiber respectively. The powder was studied by forming composites of  $\text{Ba}(\text{Mg}_{1/3}\text{Ta}_{2/3})\text{O}_3$  - Polyethylene. It is found that the experimental dielectric constant values at X band frequencies fit reasonably well to the logarithmic mixture rule. A newly reported mixing equation by Wakino et al. was studied by comparing with our experimental results.

### I. INTRODUCTION

The  $\text{A}(\text{B}'_{1/3}\text{B}''_{2/3})\text{O}_3$  ( $\text{A}=\text{Ba}^{2+}, \text{Sr}^{2+}$ ,  $\text{B}'=\text{Mg}^{2+}, \text{Zn}^{2+}, \text{Mn}^{2+}$ ,  $\text{B}''=\text{Nb}^{5+}, \text{Ta}^{5+}$ ) perovskite compounds have been reported for the application of microwave dielectric resonator [1]. These materials have dielectric constants 22 to 41 and low dielectric losses.  $\text{Ba}(\text{Mg}_{1/3}\text{Ta}_{2/3})\text{O}_3$  (BMT) is one of the perovskite compounds which has been reported with dielectric constant about 25 and Q values 5,000 to 30,000 at 10 GHz [2-4] (Table 1). The single crystal of BMT is recently identified to be one of the potential substrate materials for high Tc superconducting thin film at microwave applications [5]. It is cubic with a lattice constant  $a=0.4088\text{nm}$  comparing to the YBCO superconductor  $a=0.3820\text{nm}$ ,  $b=0.3892\text{nm}$ . The dielectric constant 25 is suitable for many microwave device applications. Its very low loss makes it a good candidate for substrate and support structure for superconductor antenna [6].

Communicated by Dr. G. W. Taylor

TABLE 1 Reported Microwave Dielectric Properties of BMT Ceramics.

| f(GHz) | $\epsilon'$ | Q            | Ref. |
|--------|-------------|--------------|------|
| 10     | 25.4        | 5,000-30,000 | [2]  |
| 10.5   | 25          | 16,800       | [3]  |
| 7      | 25          | 10,200       | [4]  |

In this paper, we report the dielectric properties of BMT samples prepared in various forms at microwave frequencies. Dielectric constants and quality factors of the ceramic, hot pressed ceramic, and single crystal fiber of BMT were systematically studied using different microwave measurement techniques.

The dielectric constants of 0:3 composite samples, xBMT: (1-x)Polyethylene (PE) made by various volume percentages of PE and BMT powders were measured at X band frequencies. The experimental results were then compared with the logarithmic mixture rule and a newly reported mixing equation by Wakino et al. [7]. It is found that the experimental data fit reasonably well with the logarithmic rule and Wakino's equation. By extrapolating the measured values of dielectric constant, the dielectric constant of pure BMT are also estimated.

## II EXPERIMENT

### (1) Sample Preparation

#### (a) Ceramic Sample

Ceramic specimens of BMT were prepared by solid state reaction using conventional techniques. Weighing from high purity magnesium oxide(3N5), tantalum penta oxide(4N), and barium carbonate(grade 1), the starting powders were mixed, ball milled, dried, and ground. Well mixed fine powders were calcined in an alumina crucible at 1,500°C for three hours. Calcined BMT powder was characterized by XRD to confirm the single phase(Hexagonal,  $a=0.5773\text{nm}$ ,  $c=$

0.7094nm). The powder with added nonaqueous binder were pressed using a hydraulic uniaxial press into circular pellets. The binder was burned out at 550°C for about 3 hours. The binder-free green pellets were sintered at temperature between 1,600 to 1,670°C for various soaking time. Well sintered sample with high density and fully ordered hexagonal perovskite phase were produced.

The hot pressed BMT ceramic sample was provided by Dr. W. Wersing of the Siemens Company. The ceramic sample was prepared essentially using the similar process with additional grain growth and densification by means of hydrostatic pressing at elevated temperatures.

#### (b) Single Crystal Fiber

The laser heated pedestal growth technique was used to grow the BMT single crystal fiber [5]. A molten zone was formed on the BMT feed rod by a  $\text{CO}_2$  laser and supported by the surface tension. A seed crystal was placed in contact with the molten zone and the fiber was grown by pulling out of the molten zone with the feedrod moving simultaneously into the molten zone. The pulling and feed rates were controlled in range of 0.5 to 1 mm/min with relative 1:2 reduction ratio. Both the feed rod(0.7mm $\times$ 0.7mm in cross section) and the seed rod(0.35mm $\times$ 0.35mm in cross section) were cut from the ceramic pellet. A [112] oriented as grown BMT single crystal fiber with diameter 0.48 mm was used for measurement.

#### (c) Composite Sample

The ordered and single phase BMT ceramic powder and high purity and low density(0.915 g/cm<sup>3</sup>) PE powder with reported dielectric constant 2.25 and quality factor 2,500 at 10 GHz [8] were used for preparing the composite samples. Suitable amounts of PE and BMT powders were mixed using alcohol as a solvent with  $\text{ZrO}_2$  balls in a plastic jar by ball milling for more than 10 hours. After the well mixed suspension was stirred and evaporated to almost dry state, it was then baked in at 80°C in an oven for 4 to 5 hours to obtain the complete dried powder mixture. The mixture was then pressed using a steel die at a temperature of 125°C(the melting point of PE is 115°C) and under a pressure  $\sim$ 7,000 lb/in<sup>2</sup> to make slab samples.

## (2) Mixture Rules for the Composite Samples

A series of studies on the mixture rules are available in the literature [9]. The logarithmic mixture rule is one of the most suitable mixing rules. The logarithmic mixture rule applies well in the case of high dielectric constant phase dispersed in a low dielectric constant matrix which is adequate in the present case of BMT dispersed in the PE matrix. In addition, the logarithmic mixture has the advantage of having a very simple relation for deriving the extrapolated dielectric constant values from the measured results. Recently, Wakino et al. [7] reported a new mixing equation,

$$\epsilon_r^{(V_1-V_0)} = V_1 \epsilon_{r1}^{(V_1-V_0)} + V_2 \epsilon_{r2}^{(V_1-V_0)} \quad (1)$$

where  $\epsilon_r$ ,  $\epsilon_{r1}$ , and  $\epsilon_{r2}$  are dielectric constants of composite, materials 1 and 2 and  $V_1$  and  $V_2$  are the volume fractions of materials 1 and 2 respectively. The  $V_0$  is about 0.35. For  $V_1=V_0$ , this equation is the same as the logarithmic mixture rule. They claimed that this new equation is by far the best among the other equations reported till now.

In this paper, the logarithmic and the new mixture rules are used to compare with our measured dielectric constant values of composite samples. The predicted dielectric constant of BMT by extrapolating the dielectric constants of various composite compounds is also given. We found our measured data fit well to the logarithmic rule and to the new reported equation. The predicted dielectric constant of BMT by using the log rule to extrapolate the measured values to 100% BMT volume percentage is -23.

Because the surface conditions (roughness and porosity) of the composite samples could not be precisely controlled the quality factors ( $Q = 1/\tan\delta$ ) of the samples are not of very precise values. The estimation of  $Q$  values by this powder mixing method is not adequate without solving the surface condition problems.

### (3) Measurement Methods

The dielectric constant of the two BMT ceramic samples were measured by the Hakki and Coleman post resonance technique [10] and the quality factor was measured by a cavity resonator transmission method [11]. The dielectric properties of fiber were measured by the cavity perturbation technique [12,13]. The dielectric constants of composite samples were measured by the cavity perturbation technique and the S11 and S21 transmission and reflection method [14]. Since the bad surface conditions of the composite samples as mentioned before, two different methods were used to ensure accurate results.

## III. EXPERIMENTAL RESULTS AND DISCUSSIONS

### (1) Ceramic and Fiber Samples

The dielectric constants and quality factors of the BMT ceramic and fiber samples are listed in table 2. The fiber sample has the highest dielectric constant followed by the hot pressed ceramic and the ceramic samples. However, the ceramic sample has a higher quality factor than that of the hot pressed sample. This agrees with the results on BMT reported by K. Matsumoto et al. [2]. They found the dielectric constant increases with increasing the relative density but the quality factor does not always increase with increasing relative density. Quality factors of both ceramic samples agree with the reported values. The quality factor of BMT fiber is higher than the capability that our perturbation method can measure where the highest Q value can be accurately measured is about 2,000 [13].

TABLE 2 Dielectric Properties of BMT at 10 GHz.

|                     | $\epsilon'$ | Q       |
|---------------------|-------------|---------|
| Ceramic             | 23.33       | 8,050   |
| Hot pressed ceramic | 24.30       | 6,430   |
| Fiber               | 26.50       | > 2,000 |

## (2) Composite Samples

The dielectric constants of composite samples with various volume percentages were measured by the S11 & S21 technique and the cavity perturbation technique. Good agreement between the measured results obtained from these two techniques was desired to ensure correct measurement results. Fig.1 shows the results measured by the S11 & S21 technique at X band frequencies. Table3 shows the average dielectric constant values at X band frequencies plotted in Fig.1 and the results measured by the perturbation technique at 10 GHz. The measurement results by the two techniques have differences <5%. The average dielectric constant value by these two methods was used for extrapolation on estimating the dielectric constant of pure BMT. In Fig.2, the measured results are compared with the Wakino's equation, and the logarithmic rule. It was found the measured results fit well to the logarithmic rule and to the equation (1). By using the logarithmic mixture rule, the extrapolately estimated dielectric constant value of pure BMT ceramic is ~23. Comparing to the reported dielectric constant ~25 on BMT [2-4], the difference is 8%. However, if we compare this value with the values of table2, the differences are 1.4% and 5.3% respectively.

TABLE 3 Dielectric Constants of the BMT-PE Composite Samples.

| Volume %  | $\epsilon'$ |              |
|-----------|-------------|--------------|
|           | S11 & S21   | Perturbation |
| 100% PE   | 2.25        | 2.29         |
| 9.05% BMT | 3.09        | 3.16         |
| 19.3% BMT | 4.10        | 4.01         |
| 37.5% BMT | 6.09        | 5.91         |
| 58.1% BMT | 8.53        | 8.48         |

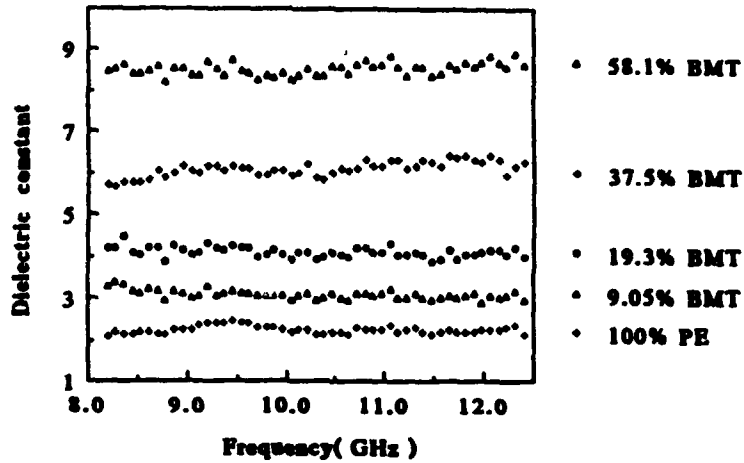


FIGURE 1 Dielectric Constants of BMT-PE Composites Measured by the S11 and S21 Technique.

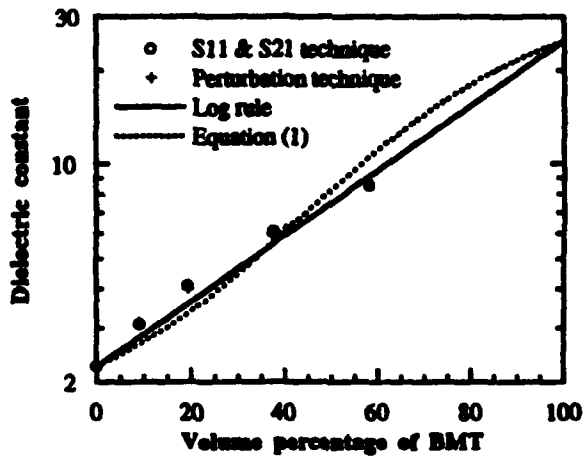


FIGURE 2 Comparison of Experimental Data and Theoretical Expressions.

## VI. CONCLUSION

The dielectric properties of BMT of various forms are reported in this paper. Due to the moderate dielectric constant and very low loss value in this material, it is a very attractive material for various microwave applications. Our measurements on the dielectric properties of ceramic samples are close to the reported values. Single crystal fiber has shown higher dielectric constant value than that of ceramic samples.

Dielectric constant of composite materials with various mixture volume percentages of BMT and PE have been investigated in X band frequencies. We found our measured results agree with the new reported equation and with the logarithmic rule. With the estimation on the dielectric constant of 100% volume percentage BMT by the logarithmic mixture rule, this powder mixture method gave a reasonable prediction on the dielectric constant of BMT ceramic at X band frequencies.

## ACKNOWLEDGEMENTS:

The authors like to thank Dr. C.J. Peng for his help during the preparation of composite samples and Dr. W. Wersing, Siemens Company, for supplying the hot pressed ceramic sample. This work was supported by the Defense Advanced Research Projects Agency under the contract # DN 00014-90-J-4140.

## REFERENCES:

- [1] S. Nomura, Ferroelectrics, **49**, 61 (1983).
- [2] K. Matsumoto, T. Hiuga, K. Takata, and H. Ichimura, IEEE 1986 6th Inter. Sym. on Appl. of Ferroelectrics, 118.
- [3] S. Nomura, K. Toyama, and, K. Kaneta, Jpn. J. Appl. Phys., **21**, 624 (1982).
- [4] H. Tamura, T. Konoike, Y. Sakabe, and K. Wakino, Commun. Am. Ceram. Soc., **C59** (1984).
- [5] Ruyan Guo, A.S. Bhalla, and L.E. Cross, To be published.
- [6] R.J. Dinger and D.J. White, IEEE Trans. Antennas Propagat., **38**, 1313 (1990).
- [7] K. Wakino, T. Okada, N. Yoshida, and K. Tomono, Reported at the Am. Ceram. Soc. Meeting, Cincinnati, Ohio, Apr. 1993.
- [8] D.M. Pozar, "Microwave Engineering," (Addison Wesley, New York, 1990), p.715.

- [9] W.R. Tinga, W.A.G. Voss, and D.F. Blossey, I. Appl. Phys., **44**, 3897 (1973).
- [10] Y. Kobayashi, and M. Katoh, IEEE Trans. Microwave Theory Tech., **MTT-33**, 586 (1985).
- [11] H. Tamura, H. Hatsumoto, and K. Wakino, Jpn. J. Appl. Phys., **28**, Suppl. 28-2, 21 (1989).
- [12] ASTM D 2520-86, 210 (1986).
- [13] D.C. Dube, M.T. Lanagan, J.H. Kim, and S.J. Jang, " I. Appl. Phys., **63**, 2466 (1988).
- [14] Hewlett-Packard, Product Note 8510-3.

**GRADUATING STUDENTS  
IN THE PROGRAM**

**APPENDIX 53**

The Pennsylvania State University  
The Graduate School

**STRUCTURAL AND THERMODYNAMIC INVESTIGATION  
OF THE FERROELECTRIC PHASE TRANSITION  
IN LANTHANA-SUBSTITUTED LEAD TITANATE**

A Thesis in  
Solid State Science

by  
George Andrew Rossetti, Jr.

Submitted in Partial Fulfillment  
of the Requirements  
for the Degree of

Doctor of Philosophy  
May 1993

## ABSTRACT

The structural and thermodynamic properties of the perovskite-structured solid solution between lead titanate and the defect compound lanthanum titanate have been investigated. The end member lead titanate is representative of a large family of oxygen octahedra ferroelectrics that undergo discontinuous phase transitions from a centrosymmetric cubic prototype ( $Pm\bar{3}m$ ) to a tetragonal ferroelectric phase ( $P4mm$ ) of the type commonly characterized by the condensation of a Brillouin zone-center polar lattice vibrational mode. The aliovalent substitution of lanthanum (III) for lead (II) induces tricritical-like behavior and diffuses the phase transition.

To better understand these changes in phase transition behavior, a series of well crystallized, chemically derived powder specimens were prepared. The temperature variation of the order parameter (spontaneous polarization) through the transition was measured indirectly by diffraction methods via the coupling to the spontaneous elastic strain. These data were combined with calorimetric data and used to estimate the renormalization of the relevant parameters of the thermodynamic potential as a function of the extent of lanthanum doping within the quasi-homogeneous approximation of the Landau-Devonshire theory. In addition, detailed structural information was obtained on selected compositions using X-ray line profile analysis, transmission electron microscopy, and powder neutron methods.

The results suggested that a systematic complication of the ferroelectric domain structure was responsible for the anomalous dielectric behavior. The role played by composition fluctuations, heterophase fluctuations, extended defects, and/or additional lattice instabilities appeared to be secondary. When interpreted within the theoretical framework of the Landau-Devonshire formalism, the breakdown of the conventional first-order phase transition behavior was primarily associated with changes in the elastic contributions to the thermodynamic potential.

**APPENDIX 54**

The Pennsylvania State University  
The Graduate School  
Department of Electrical and Computer Engineering

**ELECTRICAL AND ELECTROMECHANICAL PROPERTIES OF  
FERROELECTRIC THIN FILMS FOR MICROELECTROMECHANICAL  
APPLICATIONS**

**A Thesis in  
Electrical Engineering**

**by  
Jiayu Chen**

**Submitted in Partial Fulfillment  
of the Requirements  
for the degree of**

**Doctor of Philosophy**

**August 1993**

between the electrodes and ferroelectric thin films played an important role in electrical properties at high frequencies.

Piezoelectric and electrostrictive properties of ferroelectric thin films were studied systematically first time. According to the characteristics of field induced strain, the films can be divided into three groups: normal ferroelectric type (PZT), ferroelectric relaxor type (90PMN10PT), and antiferroelectric type (PLSZT); each of them has its own advantages for micromechanical device applications. PZT (52/48) thin films has a large piezoelectric coefficient:  $d_{33}$  is 215 (pC/N) at d.c. bias field of 75 kV/cm;  $d_{31}$  is -100 (pC/N). Electromechanical coupling factor  $k_{eff}$  was in the range of 0.15-0.49. The field induced piezoelectricity in 90PMN10PT thin films is tunable by d.c. bias field,  $d_{33}$  coefficients vary from 27 (pC/N) to 256 (pC/N). Electrostrictive coefficients were  $M_{11}=3.5 \times 10^{-16} \text{ m}^2/\text{V}^2$  and  $Q_{11}=1.2 \times 10^{-2} \text{ m}^2/\text{C}^2$  respectively. The piezoelectric characteristics of antiferroelectric thin films (PLSZT) was also controlled by electric fields. When the fields are smaller than the phase switching field, the film is in the "off" (antiferroelectric) state; when the fields are larger than the phase switching field, the film generates a large field induced strain. The largest piezoelectric coefficient  $d_{33}$  is about 200 (pC/N) and this value can be enhanced 35 times near a resonant frequency.

Finally, a cantilever type microactuator was designed, and the calculated parameters showed that the ferroelectric thin film actuator has great promise.

## Abstract

Ferroelectric thin films have various potential applications in electronic devices. This thesis investigated the dielectric, electrical and electromechanical properties of lead based ferroelectric thin films and their potential applications in microelectronic and micromechanical devices, such as nonvolatile random access memories, dynamic random access memories, and microactuators.

Dielectric and ferroelectric properties of thin films in the lead zirconate-lead titanate (PZT) solid solution have been studied. X-ray diffraction and ESEM *in situ* study on the sol/gel thin film growth process revealed that the ferroelectric thin films crystallized rapidly and that rapid thermal processing could improve the quality of the films. The dielectric constants and remanent polarization of the films reached a maximum near the morphotropic phase boundary composition; the values were 1300 and  $35 \mu\text{C}/\text{cm}^2$  respectively. Lead zirconate film has antiferroelectric characteristics and lead titanate had a fairly high remanent polarization of  $22 \mu\text{C}/\text{cm}^2$  with a large coercive field of 90 kV/cm.

Ferroelectric relaxor composition of lead magnesium niobate-lead titanate (PMN-PT) thin films were also successfully fabricated by the sol/gel technique. Thin films with composition 90PMN10PT had dielectric constant as high as 6300 at room temperature which is the highest value that has been reported in ferroelectric thin films.

Electrical conduction and dielectric breakdown mechanism of these films have been studied. Dielectric breakdown field was as high as 2 MV/cm and leakage current was as low as  $10^{-9} \text{ A}/\text{cm}^2$  in PZT thin films. With some simplifying assumptions, the space charge model fit fairly well in PZT thin films. Charge injection is one of the main factors which causes initial dielectric breakdown of the films. Interfacial layers

**APPENDIX 55**

**The Pennsylvania State University**

**The Graduate School**

**Materials Program**

**THE DIELECTRIC, PIEZOELECTRIC, AND PYROELECTRIC PROPERTIES  
OF LEAD ZIRCONATE - LEAD ZINC NIOBATE - LEAD TITANATE  
CERAMICS**

**A Thesis in**

**Materials**

**by**

**Edward F. Alberta**

**Submitted in Partial Fulfillment  
of the Requirements  
for the Degree of**

**Master of Science**

**May 1994**

## ABSTRACT

As sensor and transducer technology advances there is an increasing need for smart materials. When evaluating materials for smart applications, the weak field dependence of the dielectric and piezoelectric constants can be effective guides. Earlier studies in the solid solution system of the relaxor ferroelectric  $\text{Pb}(\text{Mg}_{1/3}\text{Nb}_{2/3})\text{O}_3$  [PMN] and the ferroelectric  $\text{PbTiO}_3$  [PT] have shown strong weak-field induced piezoelectric effect. Antiferroelectric materials have also been shown to exhibit this desired non-linear response. It was for this reason that the solid solution of the ferroelectric PT, and the antiferroelectric  $\text{PbZrO}_3$  [PZ] and the relaxor  $\text{Pb}(\text{Zn}_{1/3}\text{Nb}_{2/3})\text{O}_3$  [PZN] has been chosen to be explored for possible use as a smart sensor material under weak DC fields.

Solid solutions containing PZ have been widely studied in the past due to the antiferroelectric to ferroelectric phase transition and the existence of morphotropic phase boundaries. The systems to be studied in this thesis are (x)PZ - (y)PZN [PZZN] and (x)PZ - (y)PZN - (z)PT [PZNT]. These systems have been shown to possess a room temperature morphotropic phase boundary between the orthorhombic antiferroelectric and rhombohedral ferroelectric phases near  $x \sim 93\%$  PZ. They also look promising for piezoelectric and pyroelectric applications due to the large pyroelectric figures of merit  $F_V = 0.31 \times 10^{-10} \text{ C}\cdot\text{cm}/\text{J}$  and  $F_D = 0.35 \times 10^{-8} \text{ C}\cdot\text{cm}/\text{J}$ , low coercive fields of 8 to 10 kV/cm, large piezoelectric coupling coefficients such as  $k_{15} \sim 50\%$  and remanent polarizations on the order of 25 to 30  $\mu\text{C}/\text{cm}^2$ .

This thesis has explored the dielectric, piezoelectric and pyroelectric properties of PZZN and PZNT as a function of electrical bias. The focus was on those compositions near the antiferroelectric - ferroelectric morphotropic phase boundary. In addition, a phase diagram based on the properties measured has been created.

Electrical bias was shown to decrease the dielectric constant of the ferroelectric phases. It was also found to increase the dielectric constant for the antiferroelectric phase. Of the piezoelectric coefficients studied,  $d_{31}$ ,  $k_{31}$  and  $k_p$  showed little if any variation with electric field. For comparison, piezoelectric measurements were also made on a PZT-5A sample. This sample showed an increase in  $d_{31}$  with increasing bias.

A typical room temperature dielectric constant was about 350 and the loss factor was found to be 2%. The ferroelectric phases showed remanent polarizations of  $30 \mu\text{C}/\text{cm}^2$ . The piezoelectric coefficients  $d'_{31}$  and  $d''_{31}$  were found to be 6-7 pC/N and 0.35-0.45 pC/N. The piezoelectric coupling factor  $k_{31}$  was found to be less than 10%.

Large thermal hysteresis was found in the lower temperature phase transitions. However, the Curie point was found to vary by only 1 to 2°C. In compositions with  $z > 93.0$  mol% PZ the ferroelectric phase was found to be stable at room temperature if poled at a sufficiently high temperature. Those compositions with  $z = 93.0$  mol% PZ and greater were found to be easily poled at room temperature.